A COMBINED FEEDBACK CONTROLLER DESIGN FOR ACTIVE VIBRATION SUPPRESSION

A Dissertation
Presented to
The Academic Faculty

by

Pavithra Manghaipathy

In Partial Fulfillment
of the Requirements for the Degree
Masters Thesis in the
School Of Aerospace Engineering

Georgia Institute of Technology
May 2018

A COMBINED FEEDBACK CONTROLLER DESIGN FOR ACTIVE VIBRATION SUPPRESSION

Approved by:

Dr. Sathyanaraya Hanagud, Advisor
School of Aerospace Engineering
Georgia Institute of Technology

Dr. Eric Feron
School of Aerospace Engineering
Georgia Institute of Technology

Dr. George Kardomateas
School of Aerospace Engineering
Georgia Institute of Technology

Date Approved: April 23, 2018

ACKNOWLEDGEMENTS

I would sincerely like to thank my advisor Dr. Sathyanaraya Hanagud, for all his support, time and guidance throughout this research. His valuable knowledge and direction helped me focus and understand a lot of the concepts and see the potential uses of the data. I would also like to thank Dr. Eric Feron for teaching me the bases for control theory in the frequency domain. I would like to extend my thanks to Dr. George Kardomateas for his course and teaching me about modelling dynamic structures. Lastly and most importantly, I would like to sincerely thank my parents for their constant love and support without which I would not be where I am today.

TABLE OF CONTENTS

LIST OF TABLES

LIST OF FIGURES

SUMMARY

To prevent failure due to fatigue, especially in high-performance aircraft, there is a significant amount of interest in vibration suppression methods with a special focus on active vibration control methods. This thesis demonstrates vibration controller designs, by using a combination of acceleration & positive position feedback (PPF), acceleration & velocity feedback and positive position feedback (PPF) & velocity feedback, along with smart actuators based on piezoelectric stacks in order to address the issue. While several feedback and controller methods exist, this previously unexplored design was chosen to emphasize the effects of two types of combined feedback over a single feedback. Noting the work by Caughey & Goh (1983) and Fanson (1984) for the controller design process, this thesis aims to perform a stability analysis and expand on the use of the method designed by Hanagud & de Noyer (1998); a control method which uses a single specified closed frequency and a preset closed loop damping ratio to control the damping. Therefore, the new research presented in this thesis includes the following:

Study combinations of two feedbacks (Acceleration & Velocity, Position & Velocity and Acceleration & Position) to design controllers that yield a single closed loop frequency for specified closed loop damping ratio and a new solution technique of equating coefficients of the transfer function denominator.

Modifying the design to include frequencies other than the single closed loop frequency by a perturbation method. The perturbation is about a single closed loop frequency ωf.

Search for a design that uses minimum energy required by the controller to suppress and control vibrations.

Search for the best combination; Acceleration & Velocity, Position & Velocity or Acceleration & Position Feedback design.

1. INTRODUCTION

It is known that vibrations can cause fatigue damage in high-performance aircraft. For example, there is a growing need for advanced vibration suppression to prevent buffet induced damage. While there have been significant efforts to study vibrations, the knowledge of these vibration studies is being used to design methods of suppressing vibration and increasing the lifespan of vehicles through active control. For example, in a study of tail buffet and fatigue cracks, Hanagud et. al [1] presented a design of a smart structure based actuator for vibration suppression. This was done after analyzing that buffet induced vibration of a vertical tail of a high-performance aircraft, F-15, that significantly increased maintenance costs of the twin vertical tail assembly. When considering space structures, Omidi et. Al [2] also pointed out that the most severe disturbances arise from resonant excitations. Omidi also noted that suppression of resonant modes affects the frequency response and lower the amplitude peak in the entire frequency domain. From those observations, it is clear that one can consider single and multi-mode vibration suppression methods. Therefore, with more understanding of vibration modes and sources in aerospace systems, vibration suppression methods offer a way to increase the life-span, decrease maintenance efforts and allow certain aircraft to meet the high maneuverability and performance requirements.

With a growing need for vibration suppression in aerospace systems to avoid failure due to fatigue, there is currently a significant amount of focus on vibration control techniques for various classes of aircraft. First it is necessary to model the systems and evaluate natural frequencies, responses and design the control system. Aerospace structures can be treated as distributed parameter systems which imply that the structures contain a large number of nodes and controllers are chosen

to include important nodes within the bandwidth. As mentioned previously in Omidi et al. [2], choosing multi-modal or a single resonant mode both provide solutions for vibration suppression. One assumption for computational purposes is the use of Euler Bernoulli beam for bending which implies neglecting shear deformation effects and rotary inertia effects. With the equations of motions for multiple nodes, the vibration of the elements can be modeled, and this applies to a wide variety of systems. Sweigert and Forward's work [3] in the Journal of Spacecraft researched the effects of piezoelectric based electronic damping and observed the amplitudes of various modes on a cylindrical mast. While the focus was on the observation of how the amplitudes of modal vibration behave and how modes can combine to change the damping ratio, a key outcome from this study of modes was the idea of increasing damping by understanding different modes based on an analytical model and damping loop analyses.

2. BACKGROUND

2.1. Passive Controllers

Vibration suppression techniques include both passive and active control. Mostly used passive vibration reduction is of two main types; absorber and damper. A passive absorber is added to the system to apply an equal and opposite force by the absorber itself. However, this method only works for very specific frequencies. The latter method, either by fluid damping, viscoelastic materials or tuned mass dampers as listed by Knipe [4] operates attenuating a damping force. Most have used systems with a damping coefficient in the range of 0.01 to 0.03. To implement and design passive vibration suppression methods, to increase the damping ratio by an order of magnitude. However, no such passive control material exists to facilitate this. A comparison of the two techniques performed by Wang [5] ; Bernstien [6] states that passive control is typically used for sound energy applications due to its impact range. Therefore while passive control methods have been used for successfully in the past, they have small operating ranges and limitations on efficiency due to the material properties at different frequencies and temperatures as demonstrated by Nashie et. Al in 1985. Since passive methods involve adding changes to the structure which in turn affects the dynamics and overall operation & maintenance cost and does not meet the required damping levels to be applied to high-performance of vehicles. With the F-15 aircraft, Bayon de Noyer [7] and even Roberts [8] note that passive technique to improve the response for the F-15 consisted of reinforcing the fin assembly with patches.

2.2. Active Controllers

One of the active vibration control includes feedback control such as position, velocity or acceleration wherein the selected quantities are measured and fed back. An early exploration of active vibration control was first started in the 1980s. At the time, the new idea for the specific application in airframes had an H_∞ controller for higher harmonic control action. The work paved the way for further intensive studies on the method and feasibility, one such example was by Hanagud and Obal [9] focused more on the active control design and implementation of the piezoelectrics and control architecture based on feedback. Hanagud and Babu [10] also started the work on smart structures in airframe vibration control through the use of piezoceramic sensors after the first known application of piezoceramics in vibration suppression by Olsen [11].

There are several controller techniques available for active structural vibration control as seen through the review by Alkhatib and Golnaraghi [12] where the process for designing an active control system is examined in significant detail. There are several controller types to choose from and a few recent examples are listed as follows; such as the PID feedback controller (Prasad and Hanagud [13], Khot et al [14]), Velocity feedback control (Aoki et al [15]), H_∞ and H_2 output feedback control (Hanagud, Obal and Calise [9], Zhang et al [16] & Iorga, Baruh, Ursu [17] and Gosh et al [18] respectively), Acceleration feedback and sliding mode variable structure control (Z-c Qiu et al. [19]), LQR control with an IMSC base (Bhattacharya et al [20]) and Adaptive Control (for example using two PID controllers as proposed by Ma and Ghasemi-Nejhad [21]). With a focus on specifically distributed-parameter system control for aerospace structures, Bailey and Hubbard [22] used a cantilever beam model with a PVF (Polyvinyl fluoride) active damper

mounted on the side and observed transverse vibrations. It was noted that one could achieve linear or non-linear damping using either constant-gain or constant-amplitude controllers respectively.

As stated by Chee et al [23], the most common mathematical models when it comes to piezoelectric actuators are linear yet, there still needs to be more work for various configurations, analytical models and for the development of robust control algorithms for both linear and nonlinear models. However, there is still a focus to master linear system and therefore a review of the various papers discussing the matter shows that Positive Position Feedback (PPF) seems to be the chosen controller for current endeavors in vibration control.

A big advantage that has been mentioned by both Fanson, Goh and Caughey [24] and Wang [5] when it comes to PPF, is the lack of sensitivity to spillover. This implies that it is a better fit for higher frequencies as also explored by Periera et al's stability analysis [25] and additionally does not destabilize with finite actuator dynamics. In addition, PPF is independent of controller damping ratio and requirements include low system frequency gain and resonant frequencies as stated by Mahmoodi et al [26]. Mahmoodi et al [26] also proposed a modified PPF Method (MPPF) to improve efficiency and prevent instability due to spillover, by implementing a resonant controller using collocated control systems. The method consisted of two parallel compensators; a second order filter for small damping and a first order for transient disturbances that make up an acceleration feedback [27]. The proposed PPF controller by Caughey and Fanson [24] based on modal displacement signals, maximizes damping of the concerned frequency range while maintaining stability.

As listed above there are several actuators and sensors that can be used for vibration suppression. The working of the actuators can be simply described as delivering a force proportional to a voltage

input. With the feedback, the voltage that needs to be supplied to counteract the vibrations' force will be fed into the actuator which imparts an appropriate amount of force. From Fanson [24] and Wang [5], it is clear from the above-listed sources that piezoelectric actuators and sensors are preferred due to their longevity, range of operating conditions, fast settling time and low power consumption. Bayon De Noyer [1] also discusses the Offset Piezoceramic Stack Actuator (OPSA) to increase damping ratio, with the corresponding cantilever beam FEM model and brings about the effect of placement of the actuators. Additionally, a report by Ezratty [28], uses the models to compare different cases of piezoelectric layers and stacks with different offsets. Added to the actuator position and details, several papers also compare single and multi-degree of freedom vibration suppression systems using piezoceramic actuators and there are different PPF design procedures that can be explored [27]. While a lot of the information on the placement of said actuators comes from the FEM analysis and the like, some papers like Gosh et al [18] hint at the use of H_2-robust control when it comes to determining the optimum location of said actuator.

One issue that does arise ,however with active control is that energy is required to power the actuators. While piezoelectric actuators due to their inherent distributed nature are a perfect for the active control problem as noted by Gennaro [29], energy consumption and the general stability of the overall control scheme if one takes into account the loss of accuracy when measuring and estimating values from sensors, for example, angular velocity is not available for direct measurement and the estimation inherently carries uncertainty. However, piezoceramics are, from a design perspective, a fruitful choice for actuators and sensors due to their light weight, mechanical simplicity, efficient electric to mechanical energy conversion and large useable bandwidth as noted by Serafi et. Al [30]

3. SCOPE OF THESIS

Therefore, the present scope of active control using piezoelectric and piezoceramic materials have been studied from various from modelling techniques, control algorithms, analysis and optimization methods and performance analysis. Focusing on linear control, an area that has not been explored is the question of combining feedback controls, specifically combination acceleration and position feedback, velocity and acceleration feedback and velocity and position feedback. The main areas covered in this thesis are as follows:

1. Study combinations of two feedbacks (Acceleration & Velocity, Position & Velocity and Acceleration & Position) to design controllers that yield single closed loop frequency for specified closed loop damping ratio and a new solution technique of equating coefficients.
2. Modifying the design to include frequencies other than the single closed loop frequency by the perturbation method, perturbing about a single closed loop frequency ωf.
3. Search for a design that uses minimum energy required by the controller to suppress and control vibrations
4. Search for the best combination; Acceleration & Velocity, Position & Velocity or Acceleration & Position.

4. DYNAMICS AND CONTROLS

The following sections go into detail how the beam was modeled and the compensator and control system was designed for system response simulation.

In this thesis, we consider flexural (bending) vibrations of linear elastic beams with n modes and is here restricted to Euler-Bernoulli beam. Initially, we consider a simply supported beam and later the model can be extended to other boundary conditions. Thus the differential equation is

$$\frac{\partial^2}{\partial x^2}\left(EI\frac{\partial^2 v}{\partial x^2}\right)+m\frac{\partial^2 v}{\partial t^2}=q(x,t) \tag{4.1}$$

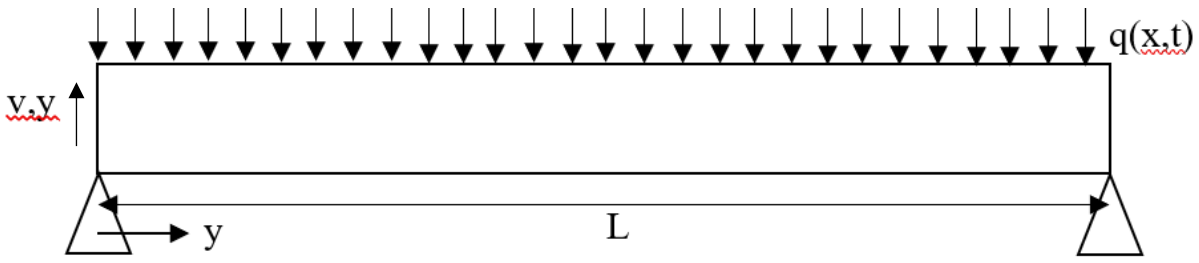

Figure 1: Uniform Beam

First, considering free vibrations, with q=0 resulting in modes and frequencies, with a constant E we have;

$$EI\frac{\partial^4 v}{\partial x^4}+m\frac{\partial^2 v}{\partial t^2}=0 \tag{4.2}$$

With m=ρA;

$$v = \phi(x)e^{i\omega t} \tag{4.3}$$

$$EI\frac{d^4\phi}{dx^4} - m\omega^2\phi = 0 \tag{4.4}$$

And taking $\frac{m\omega^2}{EI} = a^4$ we have

$$\frac{d^4\phi}{dx^4} - a^4\phi = 0 \tag{4.5}$$

This gives

$$\phi(x) = A_1 \sin ax + A_2 \cos ax + A_3 \sinh ax + A_4 \cosh ax \tag{4.6}$$

Applying a simply supported beams boundary conditions gives

$$\phi(x) = A_1 \sin\frac{n\pi x}{L} \tag{4.7}$$

Therefore $a = a_n = \frac{n\pi}{L}$

$$a^4 = \frac{n^4\pi^4}{L^4} = \frac{m{\omega_n}^2}{EI} \tag{4.8}$$

$${\omega_n}^2 = \frac{n^4\pi^4 EI}{mL^4} \tag{4.9}$$

Next, for forced vibrations, we can expand:

$$v(x,t) = \sum_{n=1}^{\infty} \xi_n(t) \sin\frac{n\pi x}{L} \tag{4.10}$$

And with the differential equation

$$EI\frac{\partial^4 v}{\partial x^4} + m\frac{\partial^2 v}{\partial t^2} = q(x,t) \tag{4.11}$$

We obtain the following from 10 and 11

$$\sum_{n=1}^{\infty} EI\xi_n \frac{n^4\pi^4}{L^4} \sin\frac{n\pi x}{L} + \sum_{n=1}^{\infty} m\ddot{\xi}_n \sin\frac{n\pi x}{L} = q(x,t) \tag{4.12}$$

By multiplying the above equation by $\sin\frac{j\pi x}{L}dx$ and integrating from x=0 to x=L, we have

$$\frac{n^4\pi^4 EI}{L^4}\frac{L}{2}\,\xi_j + m\frac{L}{2}\,\ddot{\xi}_j = \int_0^L q(x,t)\sin\frac{j\pi x}{L}dx \tag{4.13}$$

By denoting

$$\frac{2}{L}\int_0^L q(x,t)\sin\frac{j\pi x}{L}dx \;= Q_j(t) \tag{4.14}$$

And using

$$\frac{n^4\pi^4 EI}{L^4} = {\omega_j}^2$$

Which means we can re-write the previous equation as follows

$$\ddot{\xi}_j + {\omega_j}^2\xi_j = Q_j(t)$$

Now, for a one degree of freedom approximation, with subscript s to denote the structure that is controlled and using ξ_s for ξ_j

$$\ddot{\xi}_s + {\omega_s}^2 \xi_s = \frac{Q_s(t)}{m}$$

By adding a modal damping and dropping subscript j to s, we obtain

$$\ddot{\xi} + 2\zeta_s \omega_s \dot{\xi} + \omega_s^2 \xi = Q_0(t) \tag{4.15}$$

It should be noted that similar equations can be obtained for other boundary conditions.

4.1. ACCELERATION AND POSITIVE POSITION FEEDBACK

4.1.1. Formulation of Positive Position Feedback (PPF) Controller

For a Positive Position Feedback we get

$$\ddot{\xi} + 2\zeta_s \omega_s \dot{\xi} + \omega_s^2 \xi = Q_1 + g{\omega_c}^2 \eta \tag{4.1.1.1}$$

And the compensator

$$\ddot{\eta} + 2\zeta_c \omega_c \dot{\eta} + \omega_c^2 \eta = {\omega_s}^2 \xi \tag{4.1.1.2}$$

This results in the following transfer function

$$\frac{\xi(s)}{Q_1(s)} = \frac{[s^2 + 2\zeta_c\omega_c s + \omega_c^2]}{[s^2 + 2\zeta_s\omega_s s + \omega_s^2][s^2 + 2\zeta_c\omega_c s + \omega_c^2] - g\omega_s^2\omega_c^2} \quad (4.1.1.3)$$

Goh, Fanson and Caughey had only considered the positive position feedback (hereon referred to as PPF). Then they equated D(s) to two closed loop eigenvalues i.e. for a closed loop solution, the characteristic equation in Laplace domain was as follows

$$\begin{aligned} D(s) &= [s^2 + 2\zeta_s\omega_s s + \omega_s^2][s^2 + 2\zeta_c\omega_c s + \omega_c^2] + abg\omega_c^2(\alpha s^2 + (1-\alpha)\omega_s s) \\ &= (s^2 + 2\zeta_{f1}\omega_{f1} s + \omega_{f1}^2)(s^2 + 2\zeta_{f2}\omega_{f2} s + \omega_{f2}^2) \end{aligned} \quad (4.1.1.3.4)$$

Our objective is also to design for a selected closed loop damping ratio. Then $\zeta_{f1} = \zeta_{sp}$ (known) and this means that we have 6 unknowns in the equation which are $\zeta_c, \omega_c, \omega_{f1}, \omega_{f2}\ and\ g$. This means we have 6 unknowns and 4 equations that we obtain from equating the coefficients of s^3, s^2, s^1 and s^0 which again calls for the need of a solution by iteration similar to the procedure used by Goh, Fanson and Caughey.

Then we modify the procedure and reduce the number of unknowns to 4 by exploring the possibility of seeking two coincident closed loop eigenvalues. This, we equate to:

$$D(s) = (s^2 + 2\zeta_f\omega_f s + \omega_f^2)^2 \quad (4.1.1.3.5)$$

Then ζ_f+ω_f, are coincident closed loop frequencies with specific $\zeta_{f1} = \zeta_{sp}$.Comparing the coefficients for the different powers of s in the equations gives rise to the following equalities:

$$\mathbf{S^3:}\ \mathbf{2}(\boldsymbol{\zeta_c\omega_c + \zeta_s\omega_s}) = \mathbf{4}\boldsymbol{\zeta_f\omega_f} \quad (4.1.1.3.6)$$

$$\mathbf{S^2:}\ \boldsymbol{\omega_c^2 + 4\zeta_c\zeta_s\omega_c\omega_s + \omega_s^2 = 2\omega_f^2 + 4{\zeta_f}^2\omega_f^2} \quad (4.1.1.3.7)$$

$$\mathbf{S^1:}\ \boldsymbol{2\omega_c\omega_s(\zeta_s\omega_c + \zeta_c\omega_s) = 4\zeta_f{\omega_f}^3} \quad (4.1.1.3.8)$$

$$\mathbf{S^0:}\ \boldsymbol{-(-1+g){\omega_c}^2{\omega_s}^2 = {\omega_f}^4} \quad (4.1.1.3.9)$$

Applying the Routh-Hurwitz to determine the stability of the system the following conditions can be obtained for $D = a_0s^4 + a_1s^3 + a_2s^2 + a_3s^1 + a_4s^0$

$$\frac{a_1a_2 - a_0a_3}{a_1} > 0$$

$$\frac{a_1a_2a_3 - a_0{a_3}^2 - {a_1}^2a_4}{a_1a_2 - a_0a_3} > 0$$

To obtain the required variables from the given input; comparing the coefficients for the different powers of s gives rise to the following equalities:

Using ζs=0.01 and for values of ζf from 0.1 to 0.9, values for ζc, ω_f/ω_s, ω_c/ω_s and gain g were found from Mathematica.

Table 1: PPF Feedback Data for ζc, wc/ws and g for different ζf

ζf	ζc	ω_c/ω_s	g	ω_f/ω_s	Settling Time (s)
0.1	0.18684	1.017874	0.031332	1.000900137	6.8016
0.2	0.363976	1.073589	0.125772	1.00190191	3.1911
0.3	0.50928	1.161921	0.250649	1.0029046	2.1104
0.4	0.621425	1.276303	0.376455	1.003907839	1.4388
0.5	0.705319	1.410585	0.487476	1.004912347	1.1195
0.6	0.767475	1.559792	0.57916	1.005918041	1.0606
0.7	0.813687	1.720187	0.652595	1.006924358	0.8662
0.8	0.84841	1.889052	0.710774	1.000900137	0.7916
0.9	0.874863	2.06443	0.756857	1.00190191	0.7591

4.1.1.2. Step Input Response

The step responses for ζf =0.1 and 0.9 are shown in the plots below and one can note that the response moves from about 9 oscillations to an overdamped scenario.

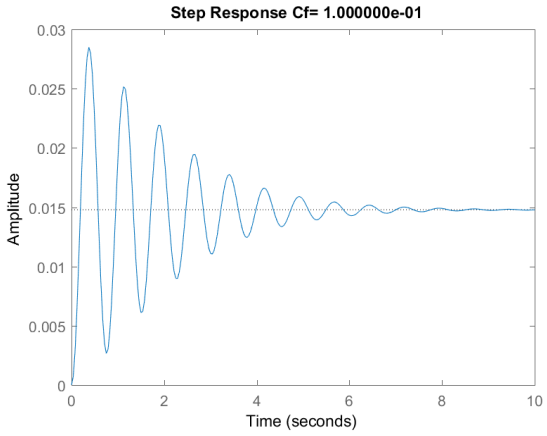

Figure 2: PPF Feedback Step Response for ζf=0.1

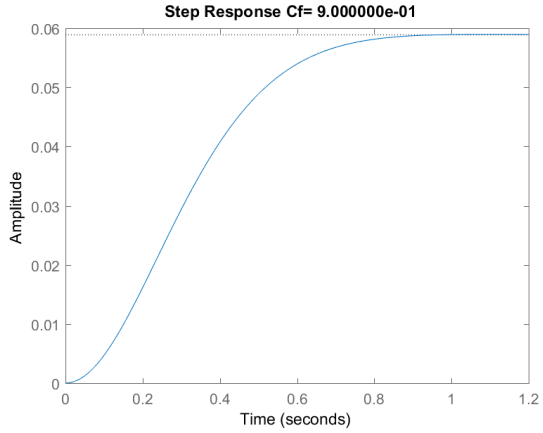

Figure 3: PPF Feedback Step Response for ζf=0.9

4.1.1.3. Step Input Response

To properly study the stability from a frequency domain perspective, the the bode plots for the transfer function were plotted and the following table has data for the gain margin and phase margin for the various cases listed.

Table 2: Gain and Phase Margins for Different ζf

ζf	Gain Margin (dB)	Phase Margin
0.1	Inf	Inf
0.2	Inf	Inf
0.3	Inf	Inf
0.4	Inf	Inf
0.5	Inf	Inf
0.6	Inf	Inf
0.7	Inf	Inf
0.8	Inf	Inf
0.9	Inf	Inf

The gain margin and phase margin were obtained using Matlab's 'margin()' function and checked by hand as well and the infinite nature points towards the systems inherent stability. This means that a system with infinite gain and phase margin is robust and the margin to change and still remain with stable solutions is infinity.

4.1.1.4.Perturbations from coincident closed loop frequency

For ζf=0.2; the following sections display the data for the closed loop solutions with perturbations i.e. the closed loop transfer function has the denominator:

$$D(s) = (s^2 + 2\zeta_f(\omega_f + \delta)s + (\omega_f + \delta)^2)^2 \quad (4.1.1.4.1)$$

$$\mathbf{S^3: \pm 4\zeta_f\delta + 4\zeta_f\omega_f} \quad (4.1.1.4.2)$$

$$\mathbf{S^2: 2\delta^2 + 4\zeta_f^2\delta^2 \pm 4\delta\omega_f \pm 8\zeta_f^2\delta\omega_f + 2\omega_f^2 + 4\zeta_f^2\omega_f^2} \quad (4.1.1.4.3)$$

$$\mathbf{S^1: \pm 4\zeta_f\delta^3 + 12\zeta_f\delta^2\omega_f \pm 12\zeta_f\delta\omega_f^2 + 4\zeta_f\omega_s^3} \quad (4.1.1.4.4)$$

$$\mathbf{S^0}: \boldsymbol{\delta^4 \pm 4\delta^3\omega_f + 6\delta^2\omega_f^2 \pm 4\delta\omega_f^3 + \omega_f^4} \quad (4.1.1.4.5)$$

The solutions are perturbed from the ωf=8.372494 values and the following table displays the controller parameters we obtain from solving the equations, the settling times in seconds and the gain and phase margins of the resulting step response and bode plots respectively.

Table 3: PPF Feedback Values for Different Perturbations

δ	Variables (Positive δ)				Variables (Negative δ)			
	ω_c/ω_s	g	ζc	Settling Time(s)	ω_c/ω_s	g	ζc	Settling Time (s)
0	1.0736	0.1258	0.3640	3.1912	1.0736	0.1258	0.3640	3.1911
0.1	1.0975	0.1228	0.3604	3.5771	1.0494	0.1280	0.3678	3.1381
0.2	1.1212	0.1190	0.3571	3.6629	1.0250	0.1293	0.3719	3.4328
0.3	1.1446	0.1146	0.3539	4.0690	1.0003	0.1297	0.3763	3.7650
0.4	1.1679	0.1096	0.3510	4.7947	0.9753	0.1290	0.3810	4.1192
0.5	1.1909	0.1040	0.3482	5.2171	0.9499	0.1271	0.3862	4.8012

From the above data it seems as though adding negative perturbations is a more favorable design for the PPF controller. However, the controller energy required should be studied before any judgements are made.

4.1.1.5. Energy Analysis

The energy dissipated for the cases with different ζf are shown in the table below after they were calculated for each cycle using the equivalent damping formula $-\pi\omega C_{eq}X_p^2$. It should be noted however that the calculations are an estimate since they were performed by hand and therefore the uncertainty and probability of errors in determining the amplitude and number of peaks (for larger cases) need to be taken into account. The errors due to determining the amplitude of the responses can be attributed to results' behaviour. However, there is a steady rise in energy dissipated as

damping increases which makes intuitive sense since to damp faster, more energy would be required.

Table 4: Controller Energy Required for PPF Feedback with Different Perturbations

δ	Energy Required (Positive δ)	Energy Required (Negative δ)
0	12.28245	12.28257
0.1	10.6607	12.26578
0.2	10.50745	12.36969
0.3	9.760871	14.12837
0.4	9.218997	15.41703
0.5	8.885114	16.95767

Therefore while negative perturbations may cause slightly higher damping and smaller settling times, since it requires more energy, the best possible design choice for the PPF controller is the case with a positive perturbation of 0.5.

4.1.2. Formulation of Acceleration Feedback Controller

We have the compensator

$$\ddot{\eta} + 2\zeta_c\omega_c\dot{\eta} + \omega_c^2\eta = b\ddot{\xi} \tag{4.1.2.1}$$

This results in the following transfer function

$$\frac{\xi(s)}{Q_1(s)} = \frac{[s^2 + 2\zeta_c\omega_c s + \omega_c^2]}{[s^2 + 2\zeta_s\omega_s s + \omega_s^2][s^2 + 2\zeta_c\omega_c s + \omega_c^2] + ag\omega_c^2(bs^2)} \tag{4.1.2.2}$$

To obtain the required variables from the given input; comparing the coefficients for the different powers of s gives rise to the following equalities:

$$S^3: 2(\zeta_c\omega_c + \zeta_s\omega_s) = 4\zeta_f\omega_f \quad (4.1.2.3)$$

$$S^2: (1 + abg)\omega_c^2 + 4\zeta_c\zeta_s\omega_c\omega_s + \omega_s^2 = 2\omega_f^2 + 4{\zeta_f}^2\omega_f^2 \quad (4.1.2.4)$$

$$S^1: \omega_c\omega_s(2\zeta_s\omega_c + 2\zeta_c\omega_s) = 4\zeta_f{\omega_f}^3 \quad (4.1.2.5)$$

$$S^0: {\omega_c}^2{\omega_s}^2 = {\omega_f}^4 \quad (4.1.2.6)$$

The values were calculated using Mathematica are listed below in Table 5. It can be noted that if the acceleration was taken as a negative feedback, all the values remain the same and the signs of the gain g change implying that for stable solutions the feedback has to be positive.

Table 5: Acceleration Feedback Data for ζc, ωc/ωs and g for different ζf

ζf	ζc	ω_c/ω_s	g	Settling Time (s)
0.1	0.19	1	0.0324	6.8016
0.2	0.39	1	0.1444	3.1911
0.3	0.59	1	0.3364	2.1104
0.4	0.79	1	0.6084	1.4388
0.5	0.99	1	0.9604	1.1195
0.6	1.19	1	1.3924	1.0606
0.7	1.39	1	1.9044	6.8292
0.8	1.59	1	2.4964	3.4736
0.9	1.79	1	3.1684	2.3439

The data above shows the acceleration feedback's unique behavior with ωc/ωs equaling 1 for all closed loop damping rations.

4.1.2.2. Step Input Response

The step responses for ζf=0.1 and 0.9 individually are shown below from Figure 4 and Figure 5 and the plots are followed by a plot showing all the step responses in Figure 6.

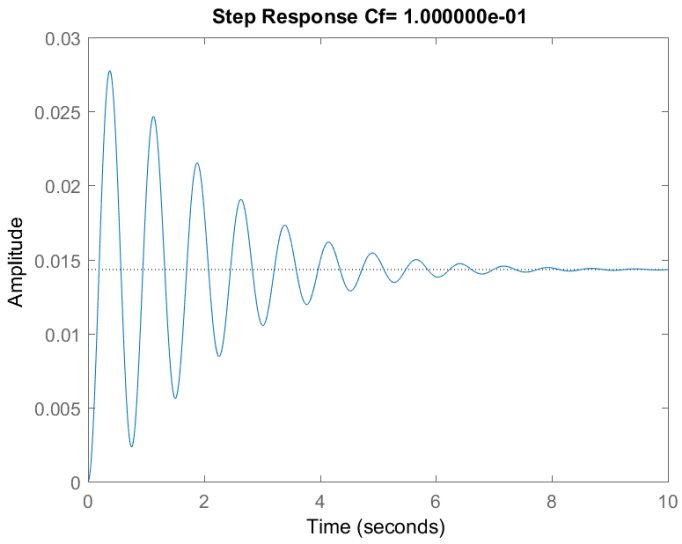

Figure 4: Acceleration Feedback Step Response for ζf=0.1

The plot above illustrated a system that settles completely under 10 seconds and although it has 9 oscillations, i.e. peaks, the image below in Figure 5 shows a single peak and damping within about a second.

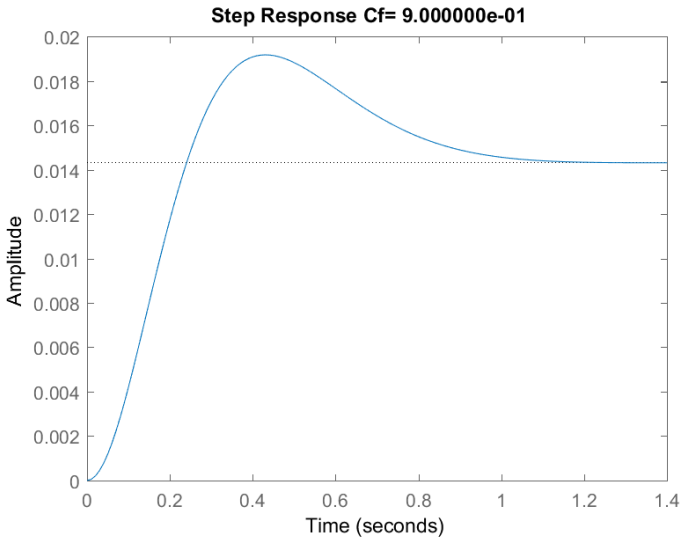

Figure 5: Acceleration Feedback Step Response for ζf=0.9

The curves in Figure 6 illustrate the step responses for various damping ratios.

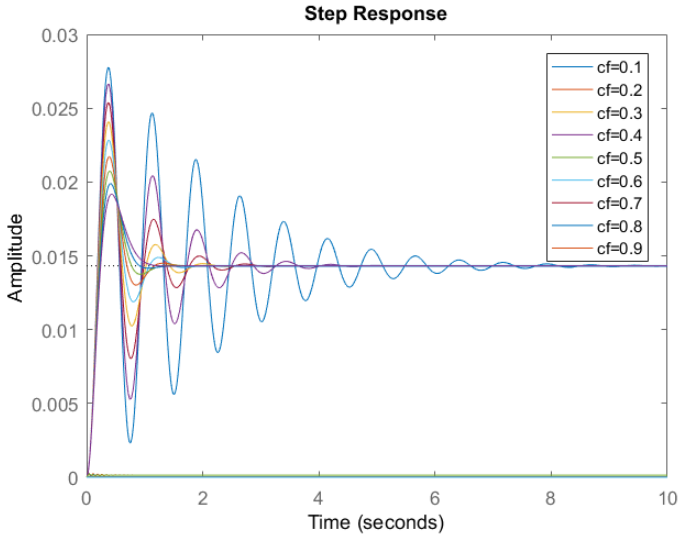

Figure 6: Combined acceleration feedback step response

4.1.2.3.Bode Plots

The bode plots for different closed loop damping ratios were run and the gain and phase margins obtained are listed below in Table 6.

Table 6: Gain and Phase Margins for Different ζf

ζf	Gain Margin (dB)	Phase Margin
0.1	Inf	Inf
0.2	Inf	Inf
0.3	Inf	Inf
0.4	Inf	Inf
0.5	Inf	Inf
0.6	Inf	Inf
0.7	Inf	Inf
0.8	Inf	Inf
0.9	Inf	Inf

Since all the bode plots show infinite gain and phase margin, the bode plots all have similar shapes with only a minor shift as seen below in Figure 7 and Figure 8 for plots with closed loop damping ratio 0.1 and 0.9. The change can be viewed as the peak decreasing which is an expected change.

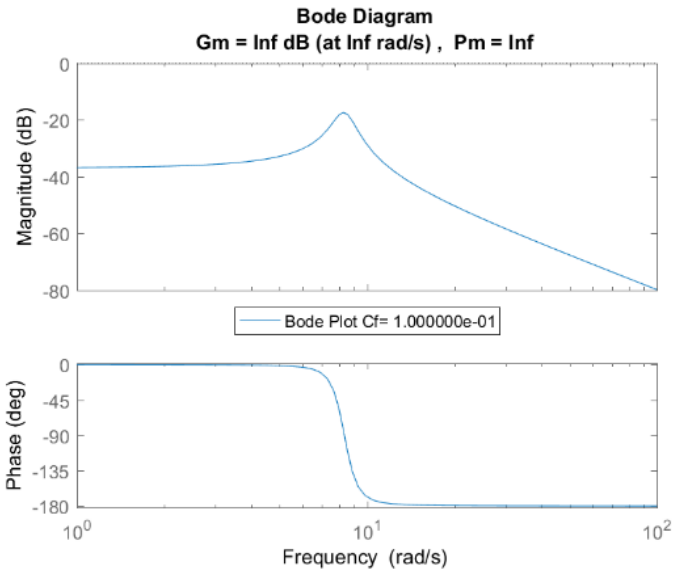

Figure 7: Acceleration Feedback Step Response for ζf=0.1

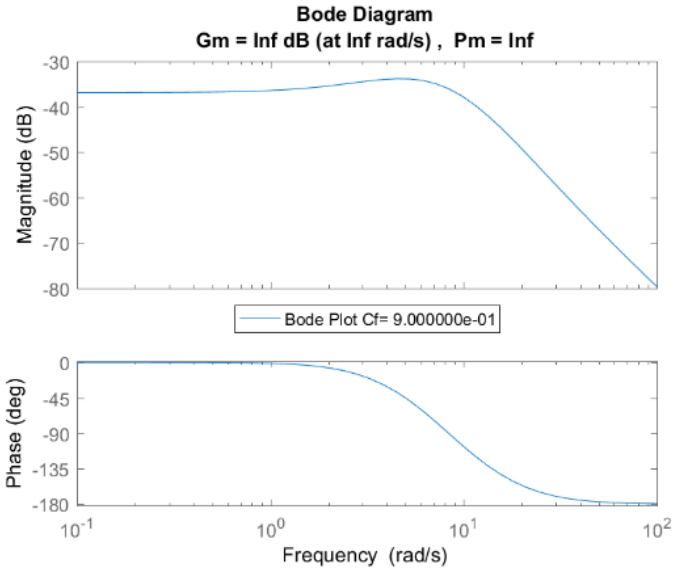

Figure 8: Acceleration Feedback Step Response for ζf=0.9

4.1.2.4. Perturbations

Perturbing the solutions from ωf= 8.3566 we obtain values listed in Table 7.

Table 7: Acceleration Feedback Values for Different Perturbations

δ	ω_c/ω_s	g	ζc	Settling Time (s)	Gain Margin	Phase Margin
0	1.0000	0.1444	0.3900	8.3566	3.4736	Inf
0.1	1.0241	0.1681	0.3855	8.4566	2.8978	Inf
0.2	1.0484	0.1910	0.3811	8.5566	3.3295	Inf
0.3	1.0731	0.2130	0.3768	8.6566	3.4501	Inf
0.4	1.0980	0.2344	0.3726	8.7566	3.5348	Inf
0.5	1.1232	0.2550	0.3685	8.8566	3.6044	Inf

4.1.2.5. Energy Analysis

The controller energy required was calculated for perturbations from a fixed ωf= 8.3566 for a closed loop damping ratio of 0.2.

Table 8: Controller Energy Required for Acceleration Feedback with perturbations

δ	Energy Required
0	0.851123
0.1	0.830212
0.2	0.892351
0.3	0.913331
0.4	0.934554
0.5	0.956021

From the above data it is clear that for acceleration feedback, the ideal case with least controller energy required is with a 0.1 perturbation.

4.1.3. Formulation of Velocity Feedback Controller

We have the compensator

$$\ddot{\eta} + 2\zeta_c\omega_c\dot{\eta} + \omega_c^2\eta = b\omega_s\dot{\xi} \tag{4.1.3.1}$$

This results in the following transfer function

$$\frac{\xi(s)}{Q_1(s)} = \frac{[s^2 + 2\zeta_c\omega_c s + \omega_c^2]}{[s^2 + 2\zeta_s\omega_s s + \omega_s^2][s^2 + 2\zeta_c\omega_c s + \omega_c^2] + ag\omega_c^2(b\omega_s s)} \tag{4.1.3.2}$$

To obtain the required variables from the given input; comparing the coefficients for the different powers of s gives rise to the following equalities:

$$\mathbf{S^3:}\ \boldsymbol{2(\zeta_c\omega_c + \zeta_s\omega_s) = 4\zeta_f\omega_f} \tag{4.1.3.3}$$

$$\mathbf{S^2:}\ \boldsymbol{\omega_c^2 + 4\zeta_c\zeta_s\omega_c\omega_s + \omega_s^2 = 2\omega_f^2 + 4{\zeta_f}^2\omega_f^2} \tag{4.1.3.4}$$

$$\mathbf{S^1:}\ \boldsymbol{\omega_c\omega_s(2\zeta_s\omega_c + abg\omega_c + 2\zeta_c\omega_s) = 4\zeta_f{\omega_f}^3} \tag{4.1.3.5}$$

$$\mathbf{S^0:}\ \boldsymbol{{\omega_c}^2{\omega_s}^2 = {\omega_f}^4} \tag{4.1.3.6}$$

The values were calculated using Mathematica are listed below in Table 5. It can be noted that if the acceleration was taken as a negative feedback, all the values remain the same and the signs of the gain g change implying that for stable solutions the feedback has to be positive.

Table 9: Velocity Feedback Data for ζc, ωc/ωs and g for different ζf

ζf	ζc	ωc/ωs	g	ωf/ωs	Settling Time (s)
0.1	0.2067	0.8370	-0.0766	0.9149	0.2067
	0.1743	1.1990	0.0545	1.0950	0.1743
0.2	0.4677	0.6882	-0.4147	0.8296	0.4677
	0.3238	1.4640	0.1989	1.2100	0.3238
0.3	0.7786	0.5679	-1.1698	0.7536	0.7786
	0.4440	1.7806	0.3806	1.3344	0.4440
0.4	1.1445	0.4710	-2.5486	0.6863	1.1445
	0.5404	2.1542	0.5684	1.4677	0.5404
0.5	1.5696	0.3931	-4.8165	0.6269	1.5696
	0.6176	2.5891	0.7459	1.6091	0.6176
0.6	2.0576	0.3303	-8.3027	0.5747	2.0576
	0.6795	3.0891	0.9056	1.7576	0.6795
0.7	2.6116	0.2797	-13.4031	0.5288	2.6116
	0.7293	3.6574	1.0453	1.9124	0.7293
0.8	3.2340	0.2385	-20.5827	0.4884	3.2340
	0.7696	4.2965	1.1656	2.0728	0.7696
0.9	3.9267	0.2050	-30.3774	0.4528	3.9267
	0.8023	5.0082	1.2682	2.2379	0.8023

The data above shows the acceleration feedback's unique behavior with ωc/ωs equaling 1 for all closed loop damping rations.

4.1.3.2. Step Input Response

The step responses for ζf=0.1 and 0.9 individually are shown below in Figure 9 parts a through d, shown together to compare easily, and the plots are followed by figures showing all the step responses. The increase in closed loop damping expectedly reduces the number of oscillations however for the case of positive gain g, the system becomes overdamped while the negative gain case results in a single peak.

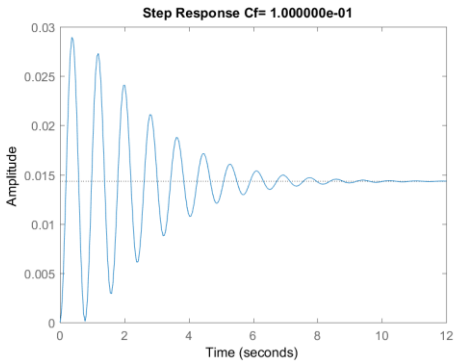

Figure 9a: Velocity Feedback Step Response for ζf=0.1 g<0

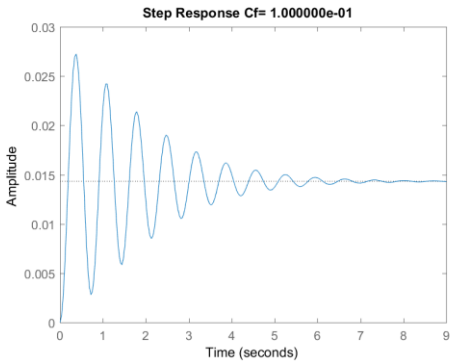

Figure 9b: Velocity Feedback Step Response for ζf=0.1 g>0

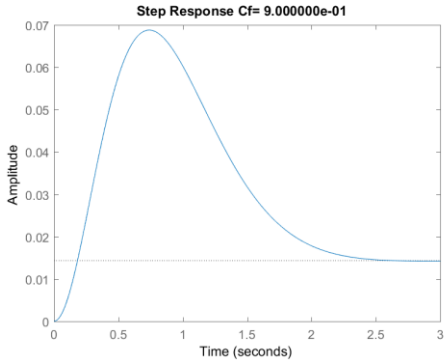

Figure 9c: Velocity Feedback Step Response for ζf=0.9 g<0

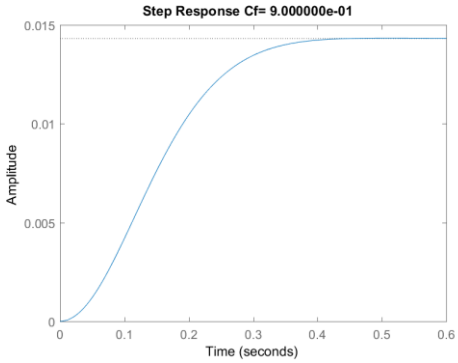

Figure 9d: Velocity Feedback Step Response for ζf=0.9 g>0

The images from Figure 9a to 9d illustrate the differences between changing the damping ratio for positive and negative gains.

The combined step responses can be visualized using the figures below in Figure 10 and Figure 11.

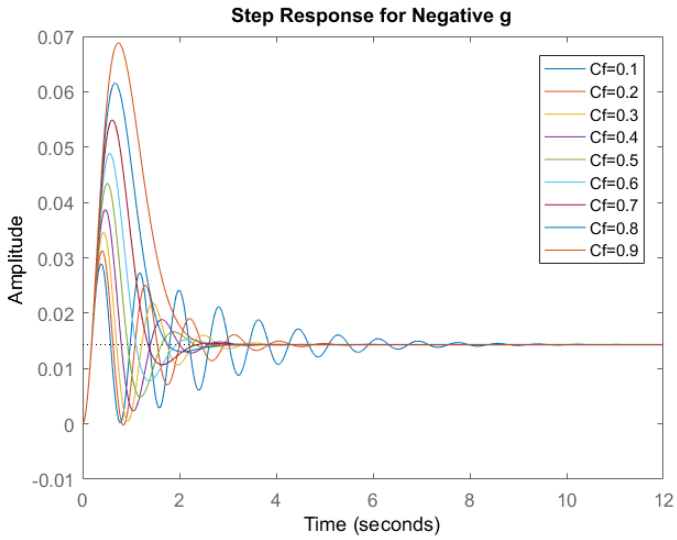

Figure 10: Velocity feedback step response for negative g

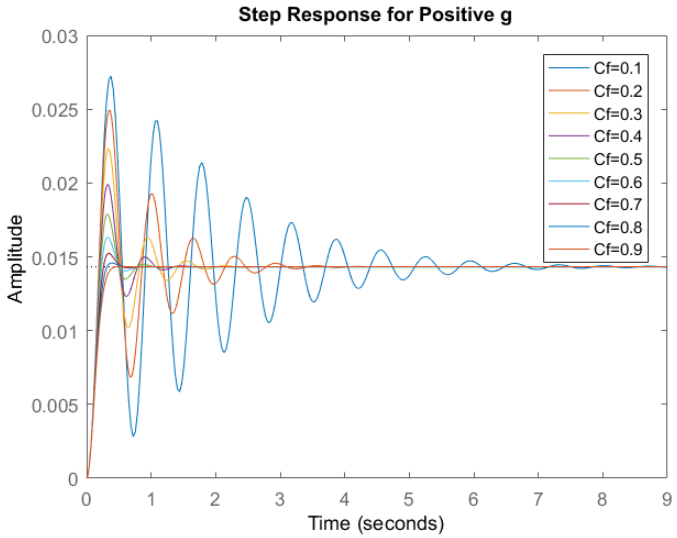

Figure 11: Velocity feedback step response for positive g

4.1.3.3. Bode Plots

The bode plots for different closed loop damping ratios were run and the gain and phase margins obtained are listed below in Table 10.

Table 10: Gain and Phase Margins for Different ζf

ζf	Gain Margin dB	Phase Margin
0.1	Inf	Inf
	27.02999	Inf
0.2	Inf	Inf
	34.84058	Inf
0.3	Inf	Inf
	40.67	Inf
0.4	Inf	Inf
	45.53664	Inf
0.5	Inf	Inf
	49.82119	Inf
0.6	Inf	Inf
	53.6546	Inf
0.7	Inf	Inf
	57.16302	Inf
0.8	Inf	Inf
	60.40004	Inf
0.9	Inf	Inf
	63.40514	Inf

Since all the bode plots show infinite gain and phase margin, the bode plots all have similar shapes with only a minor shift as seen below for plots with closed loop damping ratio 0.1 and 0.9.

The images below from Figure 12a to d illustrate the bode plots for different damping ratios with positive and negative gain g. It can be noted that the positive g cases show non-infinite gain margins. As mentioned previously, since infinite gain margins allude to inherent stability and provide a robust design, this analysis helps with the choice of g which would preferably be negative.

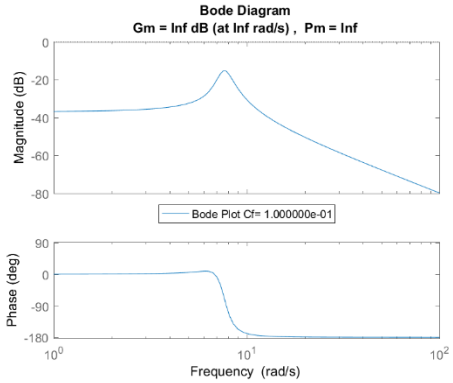

Figure 12a: Velocity Feedback Bode Plot for ζf=0.1 g<0

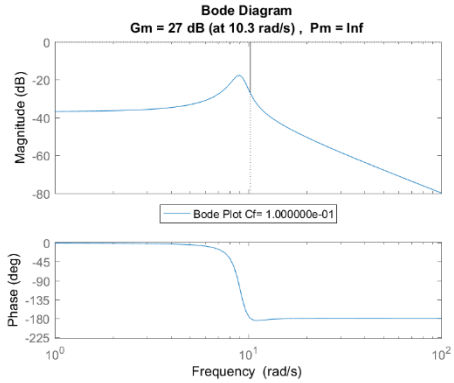

Figure 12b: Velocity Feedback Bode Plot for ζf=0.1 g>0

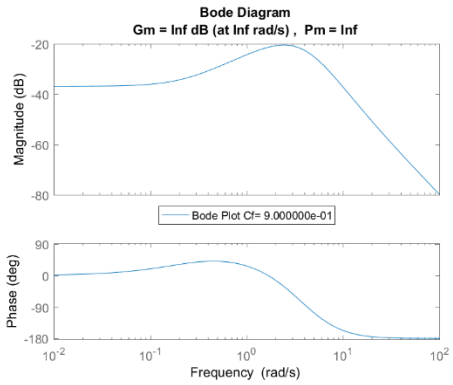

Figure 12c: Velocity Feedback Bode Plot for ζf=0.9 g<0

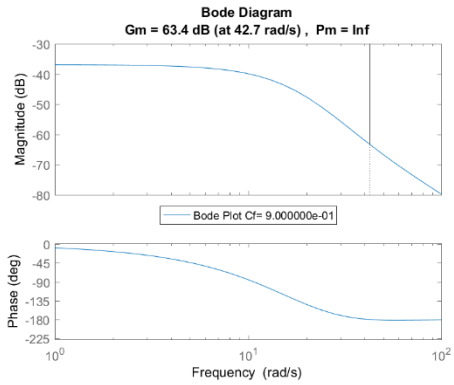

Figure 12d: Velocity Feedback Bode Plot for ζf=0.9 g>0

Therefore, while the step response shows better damping for positive gains, the fact that the gain margins are too large and that the infinite gain margins offer a more robust stability, the negative gain g cases should be considered for future designs.

4.1.3.4. Perturbations

Perturbing the solutions from ωf= 8.3566 we obtain values listed in Table 7.

Table 11: Velocity Feedback Values for Different Perturbations

δ	ω_c/ω_s	g	ζc	ω_f/ω_s	Settling Time (s)	Gain Margin	Phase Margin
0	0.68818	-0.41474	0.46765	6.93233	4.56867	Inf	Inf
0.1	0.70817	-0.37187	0.46120	7.03233	5.39658	Inf	Inf
0.2	0.72846	-0.33171	0.45493	7.13233	6.23242	Inf	Inf
0.3	0.74903	-0.29407	0.44883	7.23233	7.43805	Inf	Inf
0.4	0.76988	-0.25878	0.44289	7.33233	9.02460	Inf	Inf
0.5	0.79103	-0.22567	0.43710	7.43233	10.60978	Inf	Inf

It is important to note that the gains were chosen as per the previous section's conclusion on the negative gain g cases offering the most practical solution.

4.1.3.5. Energy Analysis

The controller energy required was calculated for perturbations from a fixed ωf= 5.7508 for a closed loop damping ratio of 0.2.

Table 12: Controller Energy Required for Velocity Feedback only with perturbations

δ	AP
0	0.032701
0.1	0.033651
0.2	0.034615
0.3	0.071184
0.4	0.032844
0.5	0.032267

From the above data it is clear that for acceleration feedback, the ideal case with least controller energy required is with a 0.5 perturbation.

4.1.4. Formulation of Combined Acceleration and Positive Position Feedback (PPF) Controller

We discuss the formulation of the vibration controller for the one D.O.F mode. First a compensator is introduced; the compensator receives an input from the output of the structural system of equations. Then the compensator sends a signal of $bg{\omega_c}^2\eta$ to the control actuator on the structure giving rise to a 2 D. O.F control equation as below

$$\ddot{\xi} + 2\zeta_s\omega_s\dot{\xi} + \omega_s^2\xi = Q_1 - bg{\omega_c}^2\eta \tag{4.1.4.1}$$

And the compensator with compensator gain 'a'

$$\ddot{\eta} + 2\zeta_c\omega_c\dot{\eta} + \omega_c^2\eta = (1-\alpha)a\ddot{\xi} + a\alpha\omega_s^2\xi \tag{4.1.4.2}$$

Therefore, when α=1, we have PPF feedback and when $\alpha = 0$ we have the acceleration feedback. This gives rise to a combination of acceleration and PPF feedback at other times and results in the following transfer function of $\frac{\xi(s)}{Q_1(s)}$

$$\frac{\xi(s)}{Q_1(s)} = \frac{[s^2 + 2\zeta_c\omega_c s + \omega_c^2]}{[s^2 + 2\zeta_s\omega_s s + \omega_s^2][s^2 + 2\zeta_c\omega_c s + \omega_c^2] - abg\omega_c^2((1-\alpha)s^2 + \alpha\omega_s^2)} \tag{4.1.4.3}$$

Which results in the following equations when comparing coefficients (where a is the controller gain).

$$\mathbf{S^3:}\ \mathbf{2(\zeta_c\omega_c + \zeta_s\omega_s) = 4\zeta_f\omega_f} \tag{4.1.4.4}$$

$$\mathbf{S^2:}\ \mathbf{(1 + abg(-1+\alpha))\omega_c^2 + 4\zeta_c\zeta_s\omega_c\omega_s + \omega_s^2 = 2\omega_f^2 + 4{\zeta_f}^2\omega_f^2} \tag{4.1.4.5}$$

$$\mathbf{S^1:}\ \boldsymbol{\omega_c\omega_s(2\zeta_s\omega_c + 2\zeta_c\omega_s) = 4\zeta_f\omega_f{}^3} \tag{4.1.4.6}$$

$$\mathbf{S^0:}\ \boldsymbol{(1 - abg\alpha)\omega_c{}^2\omega_s{}^2 = \omega_f{}^4} \tag{4.1.4.7}$$

Which gives the following criteria for stability

$$g > \frac{-\zeta_c\omega_c{}^3 - 4\zeta_c^2\zeta_s\omega_c^2\omega_s - 4\zeta_c\zeta_s^2\omega_c\omega_s^2 - \zeta_s\omega_s{}^3}{ab(-1+\alpha)\omega_c{}^2(\zeta_c\omega_c + \zeta_s\omega_s)} \tag{4.1.4.8}$$

$$g > \frac{-\zeta_c\zeta_s\omega_c{}^4 - 4\zeta_c^2\zeta_s^2\omega_c^3\omega_s + 2\zeta_c\zeta_s\omega_c^2\omega_s^2 - 4\zeta_s\zeta_c^3\omega_c^2\omega_s^2 - 4\zeta_c\zeta_s^3\omega_c^2\omega_s^2 - 4\zeta_c^2\zeta_s^2\omega_c\omega_s^3 - \zeta_s\zeta_c\omega_s{}^4}{ab\omega_c(\zeta_c\omega_c + \zeta_s\omega_s)(-\zeta_s\omega_c^2 + \alpha\zeta_s\omega_c^2 - \zeta_c\omega_c\omega_s + 2\alpha\zeta_c\omega_c\omega_s + \alpha\zeta_s\omega_s^2)} \tag{4.1.4.9}$$

With the initial condition of ζs =0.01, the equations were solved in Mathematica to get the controller parameters and the closed loop frequency for different values of ζf at different values of the ratio α. The following table lists the values of ζc, $^{\omega_f}/_{\omega_s}$, $^{\omega_c}/_{\omega_s}$, g and the settling time of the unit step response in seconds for different ζf, all at α=0.5 since it provides a way to observe how the different required closed loop damping ratio affects all the design elements.

Table 13: Acceleration & PPF Feedback Data for ζc, wc/ws and g for different ζf and α=0.5

ζf	ζc	$^{\omega_f}/_{\omega_s}$	$^{\omega_c}/_{\omega_s}$	g	Settling time (s)
0.1	0.09	1.09	2.31	1.46	7.136
0.2	0.1	1.21	4.84	1.82	3.402
0.3	0.1	1.33	7.97	1.9	1.733
0.4	0.1	1.47	11.68	1.93	1.113
0.5	0.1	1.61	16.02	1.95	0.764
0.6	0.1	1.76	21.01	1.96	0.656
0.7	0.1	1.91	26.69	1.96	0.567
0.8	0.1	2.07	33.08	1.97	0.579
0.9	0.1	2.24	40.19	1.97	0.450

It should be noted that for the equations to be solved efficiently, the ratios to the structure's frequency were taken, i.e. ω_f/ω_s and ω_c/ω_s. Then a specific value of ωs was taken to be 1.33 Hz based on a first mode estimate. An increased closed loop system frequency can be observed with favorable results though it should be noted that the controller values of ωc would be significantly high. The behavior of the controller damping ratio ζc can be attributed to the ratio α=0.5 since plain acceleration feedback also displays similar behaviour in certain situations.

4.1.4.2. Step Input Responses

The step responses for α=0.5 ζf =0.1, 0.2, 0.3 and 0.9 are shown below in Figure 13 through Figure 16.

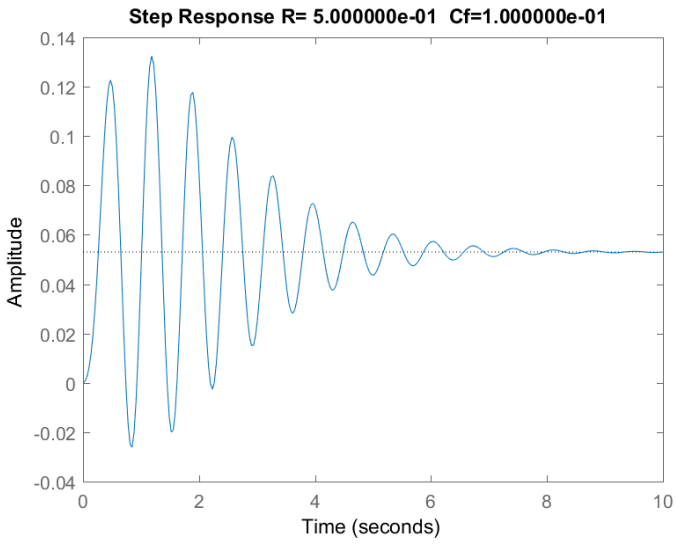

Figure 13: Acceleration & PPF Feedback Step Response for ζf=0.1

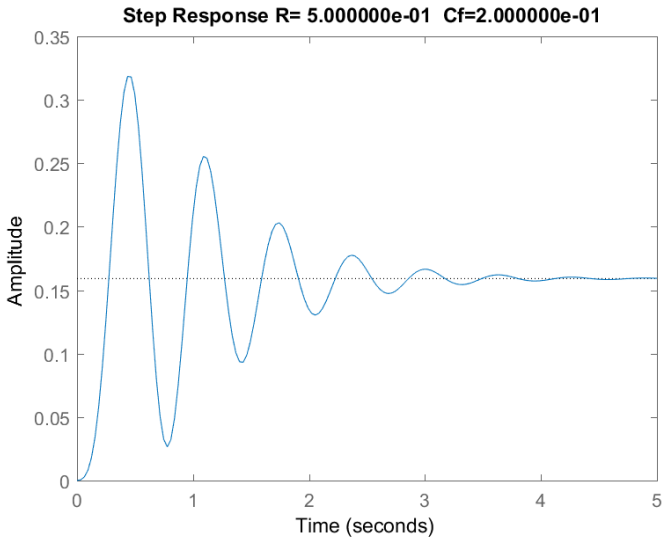

Figure 14: Acceleration & PPF Feedback Step Response for ζf=0.2

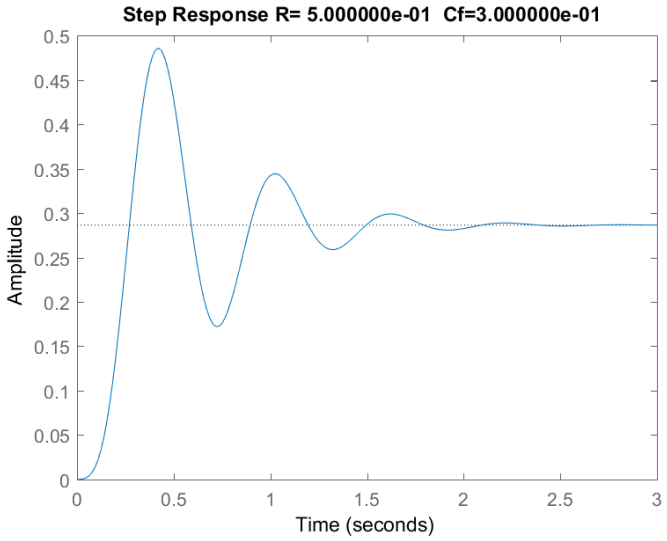

Figure 15: Acceleration & PPF Feedback Step Response for ζf=0.3

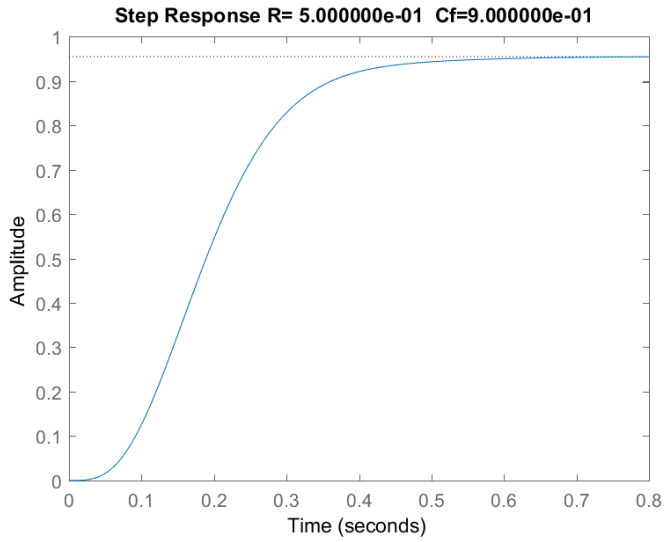

Figure 16: Acceleration & PPF Feedback Step Response for ζf=0.9

It can be clearly noted that the increased damping quite significantly decreases settling time and even the change from 0.1 to 0.2 causes the system to get damped in about half the time with 1/3rd of the oscillations. Now, in order to observe how the ratio α, affects the step responses, the following Table 14 lists the values for ζf=0.2.

Table 14: Acceleration & PPF Feedback Data for ζc, ωf/ωs, ωc/ωs and g for different α with ζf=0.2

α	ζc	ω_f/ω_s	ω_c/ω_s	g	Settling Time (s)
0.1	0.39	1	0.99	-0.18	3.49044
0.2	0.4	1	0.97	-0.25	3.488526
0.3	0.41	1	0.94	-0.41	3.474544
0.4	0.46	1	0.84	-1.02	3.511353
0.5	0.1	1.21	4.84	1.82	3.402157
0.6	0.32	1.01	1.21	0.5	3.233963
0.7	0.35	1	1.13	0.29	3.209912
0.8	0.36	1	1.1	0.2	3.209284
0.9	0.36	1	1.08	0.15	3.498037

The step responses for the above listed cases for α=0.1 and 0.9 are shown below in Figure 17 and Figure 18.

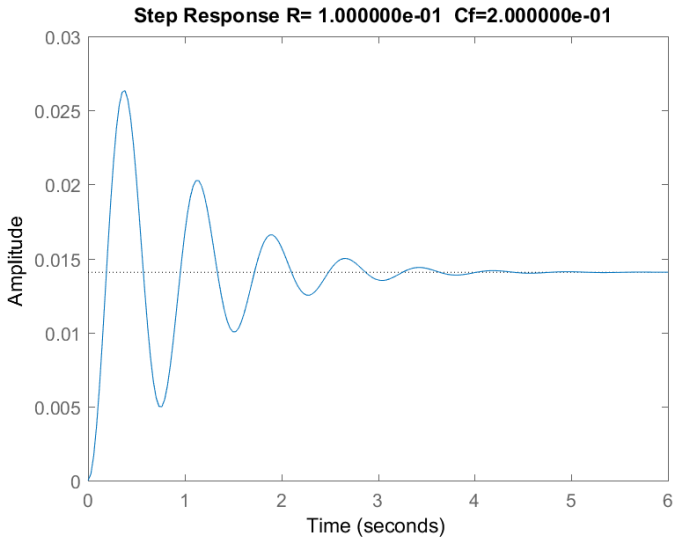

Figure 17: Acceleration & PPF Feedback Step Response for ζf=0.2 and α=0.1

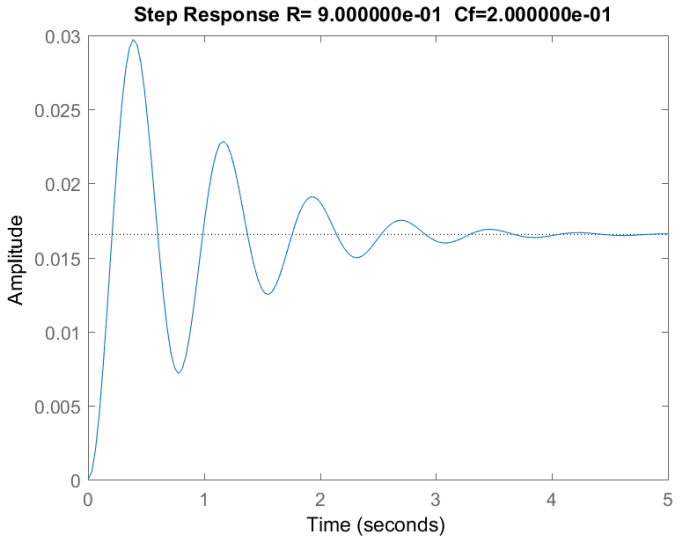

Figure 18: Acceleration & PPF Feedback Step Response for ζf=0.2 and α=0.9

It can be observed that there isn't a significant difference in the settling times or the number of peaks in the step response. It can be noted that the gains required shift from negative to positive as

the ratio increases, this implies that as the PPF feedback increases, the gain required shifts sign which is reflective of the behaviour of controller with only PPF feedback.

4.1.4.3. Bode Plots

As per the previous section, keeping α=0.5, the bode plots for different closed loop damping ratios were run and the gain and phase margins obtained are listed below in Table 15.

Table 15: Gain and Phase Margins for Different ζf

ζf	Gain Margin (dB)	Phase Margin
0.1	-0.06816	-1.92508
0.2	0.372526	16.83422
0.3	2.316655	Inf
0.4	4.298304	Inf
0.5	4.763132	Inf
0.6	5.874266	Inf
0.7	9.072164	Inf
0.8	8.35368	Inf
0.9	10.64812	Inf

At an initial glance, the Gain Margins fall within the reasonable range for the order of system at hand being less about 20 dB and the infinite Phase margin points towards robustness. With the case for ζf=0.2 however the phase margin is low and should preferably be at least 30 degrees. The negative values however imply that the system is unstable at that value.

The bode plots for cases of interest are shown below from Figure 19 through Figure 22.

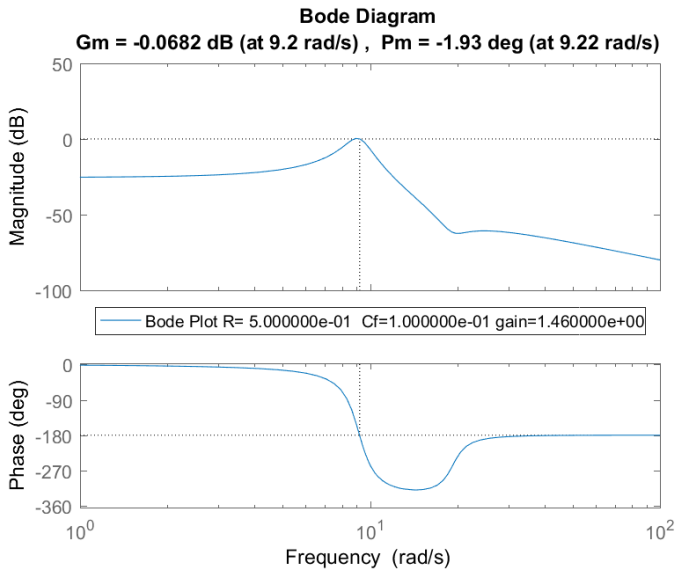

Figure 19: Acceleration & PPF Feedback Bode Plot for ζf=0.1

The case above with negative gain and phase margin clearly shows an unstable system and while the bode plot below in Figure 20 has positive margins, the gain margin is smaller than the ideal.

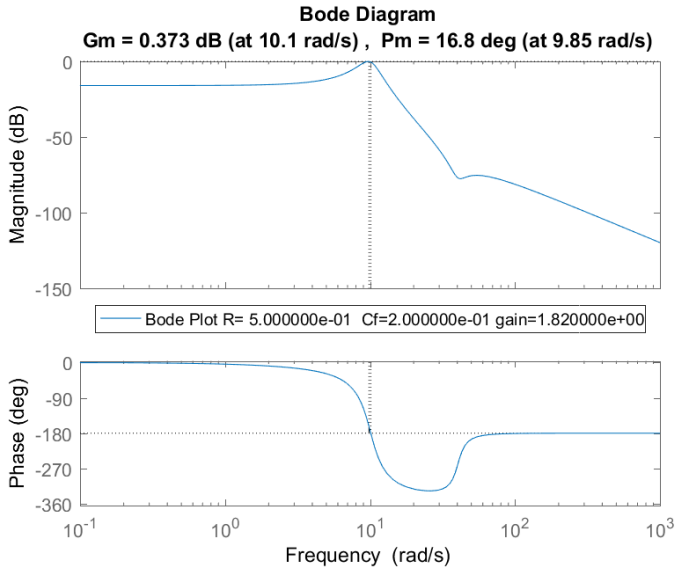

Figure 20: Acceleration & PPF Feedback Bode Plot for ζf=0.2

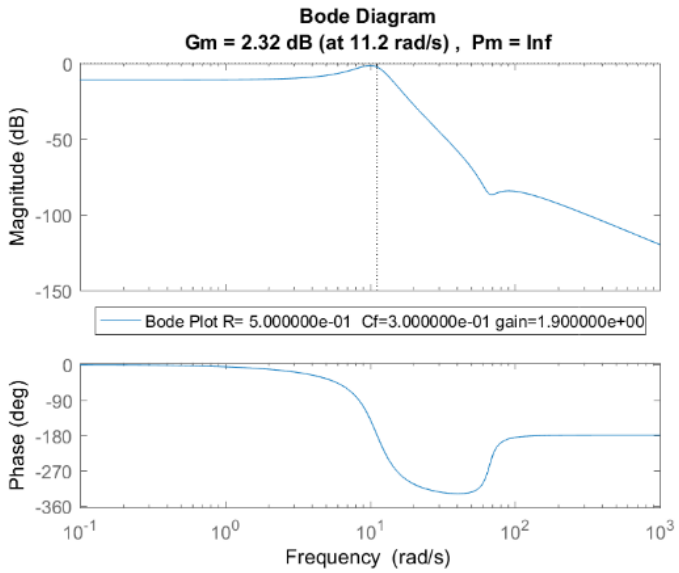

Figure 21: Acceleration & PPF Feedback Bode Plot for ζf=0.3

The gain margin for the case shown below in Figure 22 shows a gain margin within the ideal range and for the case above, a suggestion would be to add a proportional gain to increase the gain margin.

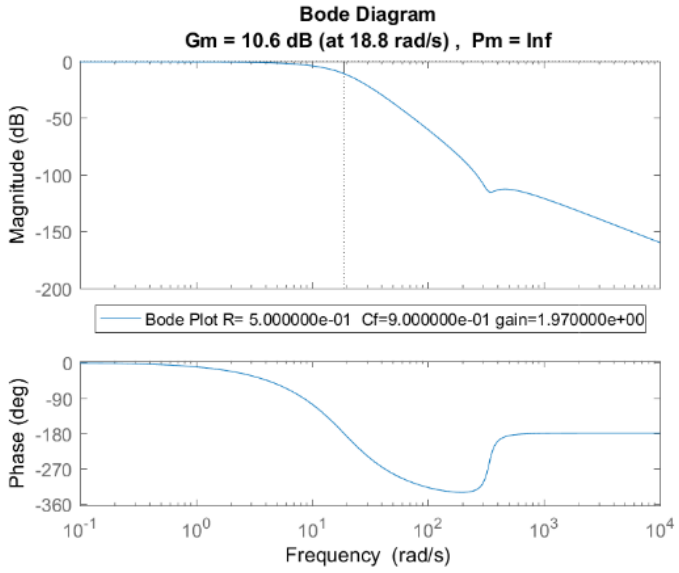

Figure 22: Acceleration & PPF Feedback Bode Plot for ζf=0.9

Now, with ζf=0.2, the values for different values of ratio α are shown below in Table 16.

Table 16: Gain and Phase Margins for Different α and ζf=0.2

α	Gain Margin (dB)	Phase Margin
0.1	Inf	Inf
0.2	Inf	Inf
0.3	Inf	Inf
0.4	Inf	Inf
0.5	0.372526	16.83422
0.6	32.27918	Inf
0.7	Inf	Inf
0.8	Inf	Inf
0.9	Inf	Inf

From the data presented above, most of the cases reflect robust controller designs with infinite gain and phase margins showcasing the inherent stability of the system. For α=0.5 and 0.6 however, the positive values still allude to a stable system however for practicality only the 0.5 would need to have a proportional gain added. Adding any other gain would compromise the stability of the system though the performance of the system on it's own displays favourable responses.

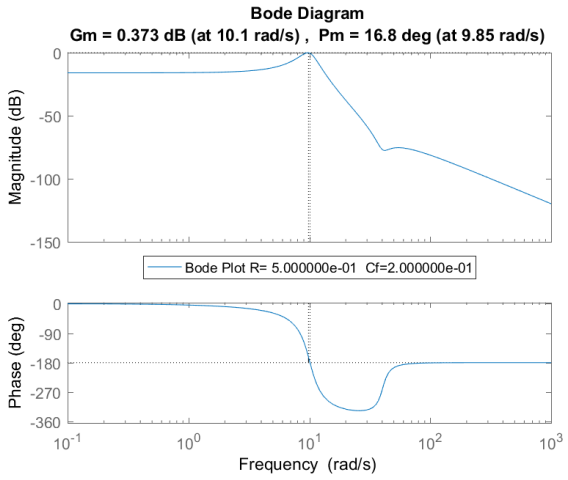

Figure 23: Acceleration & PPF Feedback Bode Plot for ζf=0.2 and α=0.5

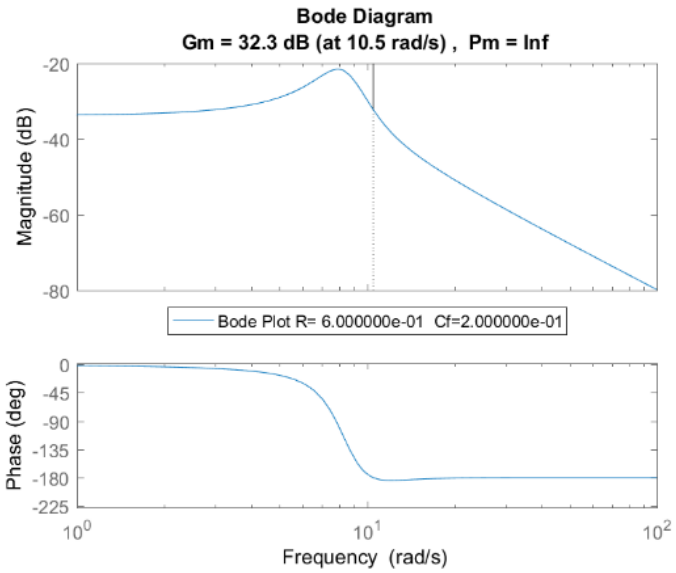

Figure 24: Acceleration & PPF Feedback Bode Plot for ζf=0.2 and α=0.6

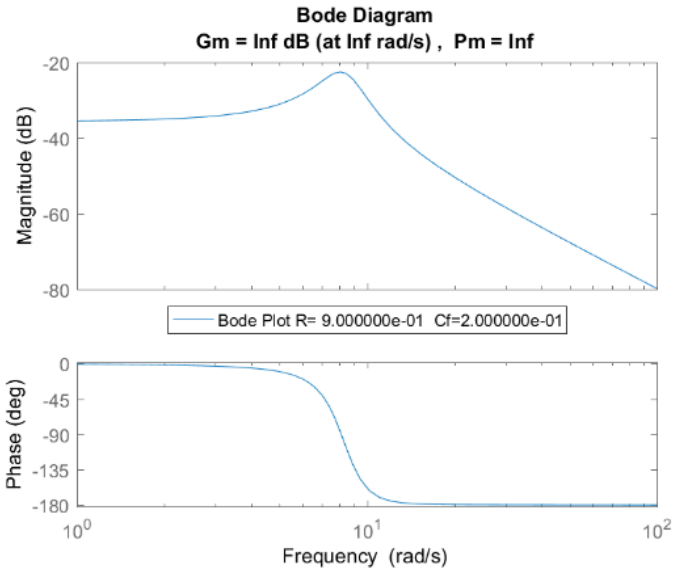

Figure 25: Acceleration & PPF Feedback Bode Plot for ζf=0.2 and α=0.9

4.1.4.4.Perturbations from coincident closed loop frequency

For ζf=0.2; the following sections display the data for the closed loop solutions with perturbations from ωf to (ωf +δ) The solutions are perturbed from the ωf=10.069 values and the following table

displays the controller parameters we obtain from solving the equations, the settling times in seconds and the gain and phase margins of the resulting step response and bode plots respectively.

Table 17: Acceleration & PPF Feedback Values for Different Perturbations

δ	ω_c/ω_s	g	ζc	Settling Time (s)	Gain Margin	Phase Margin
0	4.7735	1.8149	0.0989	4.5042	35.7004	Inf
0.1	4.9410	1.8203	0.0965	4.6497	37.7786	Inf
0.2	5.1071	1.8251	0.0943	4.7866	39.6612	Inf
0.3	5.2720	1.8294	0.0923	4.9162	41.4233	Inf
0.4	5.4358	1.8332	0.0904	5.0359	42.9706	Inf
0.5	5.5986	1.8367	0.0886	5.1538	44.3571	Inf

It is the clear the system remains stable albeit with high gain margins and it can be noted that higher perturbations lead to higher settling time meaning the optimal solution is the non-perturbed case.

4.1.4.5. Energy Analysis

The energy dissipated for the cases with different ζf are shown in the table below after they were calculated for each cycle using the equivalent damping formula $-\pi\omega C_{eq}X_p^2$.

Table 18: Energy Dissipated by the system

ζf	Energy Dissipated
0.1	-0.2247
0.2	-1.72125
0.3	-4.74097
0.4	-8.4115
0.5	-11.2621
0.6	-17.7416
0.7	-21.355
0.8	-43.475

In order to find the optimal solution for this type of feedback, one must look at the energy required, i.e. the energy from the controller. For the most optimal solution, from the previous sections, α=0.8, offers the smallest settling time for ζf=0.2. However, we are interested in how much energy the controller requires therefore, for a required closed loop damping ratio of 0.2, with different α the compensator $\ddot{\eta} + 2\zeta_c\omega_c\dot{\eta} + \omega_c^2\eta = (1-\alpha)a\ddot{\xi} + a\alpha\omega_s^2\xi$ has the following energy requirement. Note that the cases with 'NaN' represent values that are Not Available due to the response being unstable.

Table 19: Controller Energy Required for Different α

α	Energy Required
0.1	**0.415848**
0.2	0.674834
0.3	1.443654
0.4	3.517051
0.5	5.908508
0.6	2.817024
0.7	4.672384
0.8	6.598122
0.9	9.299874

For the least energy required, we consider α=0.1. Adding Perturbations the following values are obtained:

Table 20: Controller Energy Required for α=0.1 with perturbations

δ	Energy Required
0	**0.46176**
0.1	1.459495
0.2	2.149146
0.3	4.084385
0.4	4.191573
0.5	6.823103

Therefore, for a required damping ratio of 0.2, the acceleration and velocity feedback requires an α of 0.1 i.e. a dominant of Acceleration feedback, with no perturbation for the most optimal controller with parameters:

$$\omega_c/\omega_s = 0.99,\ g=-0.18,\ \zeta c=0.39$$

4.2. COMBINED ACCELERATION AND VELOCITY

4.2.1. Formulation of Acceleration and Velocity Feedback Controller

We discuss the formulation of the vibration controller for the one D.O.F mode. First a compensator is introduced; the compensator receives an input from the output of the structural system of equations. Then the compensator sends a signal to the control actuator on the structure giving rise to a 2 D. O.F control equation as below

$$\ddot{\xi} + 2\zeta_s\omega_s\dot{\xi} + \omega_s^2\xi = Q_1 - bg{\omega_c}^2\eta \tag{4.2.1.1}$$

And the compensator

$$\ddot{\eta} + 2\zeta_c\omega_c\dot{\eta} + \omega_c^2\eta = a\alpha\ddot{\xi} + (1-\alpha)\omega_s a\dot{\xi} \tag{4.2.1.2}$$

Therefore, when α=1, we have acceleration feedback and when $\alpha = 0$ we get velocity feedback. This gives rise to a combination of acceleration and velocity feedback at other times and results in the following transfer function

$$\frac{\xi(s)}{Q_1(s)} = \frac{[s^2 + 2\zeta_c\omega_c s + \omega_c^2]}{[s^2 + 2\zeta_s\omega_s s + \omega_s^2][s^2 + 2\zeta_c\omega_c s + \omega_c^2] + abg\omega_c^2(\alpha s^2 + (1-\alpha)\omega_s s)} \quad (4.2.1.3)$$

Comparing the coefficients for the different powers of s for the above and required closed loop transfer function gives rise to the following equalities:

S^3: $\boldsymbol{2(\zeta_c\omega_c + \zeta_s\omega_s) = 4\zeta_f\omega_f}$ (4.2.1.4)

S^2: $\boldsymbol{(1 + ab\alpha g)\omega_c^2 + 4\zeta_c\zeta_s\omega_c\omega_s + \omega_s^2 = 2\omega_f^2 + 4\zeta_f{}^2\omega_f^2}$ (4.2.1.5)

S^1: $\boldsymbol{\omega_c\omega_s(2\zeta_s\omega_c + ab(1-\alpha)g\omega_c + 2\zeta_c\omega_s) = 4\zeta_f\omega_f{}^3}$ (4.2.1.6)

S^0: $\boldsymbol{\omega_c{}^2\omega_s{}^2 = \omega_f{}^2}$ (4.2.1.7)

The equations were put into Mathematica and the following values were obtained. Table 21 lists the values that were obtained and as seen with the velocity only feedback, there are 2 possible solutions for each ζf with positive and negative g values.

Table 21: Acceleration + Velocity Feedback Data for ζc, wc/ws and g for different ζf

ζf	ζc	ω_f/ω_s	ω_c/ω_s	g	Settling time (s)
0.1	0.2323	0.8077	0.6524	-0.4739	9.7238
	0.1834	1.0382	1.0780	0.0501	6.2985
0.2	0.5964	0.6447	0.4157	-3.2970	5.9184
	0.3610	1.0824	1.1716	0.2056	2.9577
0.3	1.1068	0.5249	0.2755	-11.5348	4.5520
	0.5239	1.1282	1.2729	0.4408	1.8706
0.4	1.7791	0.4368	0.1908	-30.0110	4.5178
	0.6732	1.1758	1.3825	0.7339	1.2105
0.5	2.6223	0.3711	0.1377	-65.4396	3.7091
	0.8097	1.2250	1.5006	1.0671	0.8879
0.6	3.6415	0.3210	0.1030	-126.4613	4.2375
	0.9344	1.2758	1.6277	1.4260	0.8496
0.7	4.8393	0.2820	0.0795	-223.6484	3.9886
	1.0484	1.3282	1.7642	1.7992	0.6009
0.8	6.2174	0.2509	0.0630	-369.5040	4.4411
	1.1524	1.3822	1.9104	2.1776	0.6045
0.9	7.7768	0.2258	0.0510	-578.4598	4.4924
	1.2472	1.4376	2.0667	2.5544	0.5213

The cases above are stable according to Routh Hurwitz criteria and both positive and negative gains yield stable solutions and the differences between them will be examined further in this chapter.

4.2.2. Step Input Responses

The step responses for cases ζf=0.1 and 0.9 with both positive and negative gains are shown below from Figure 26 through Figure 29.

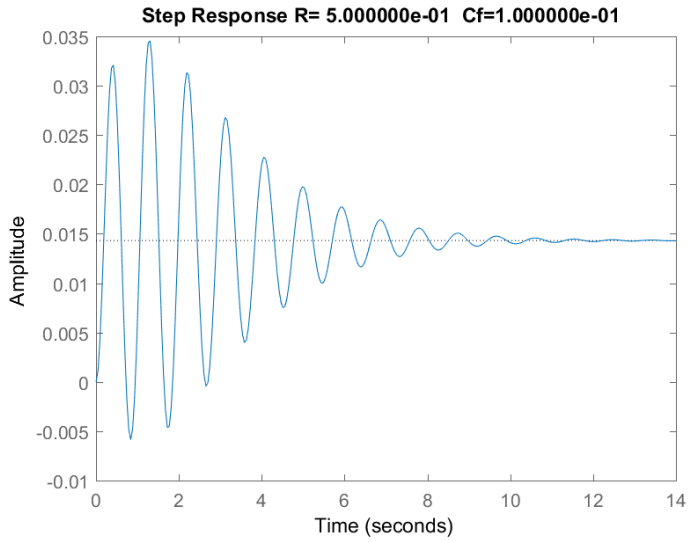

Figure 26: Acceleration & Velocity Feedback Step Response for ζf=0.1 g<0

It can be noted that as the damping ratio increases, the step response goes from about 11 oscillation peaks to an almost overdamped case.

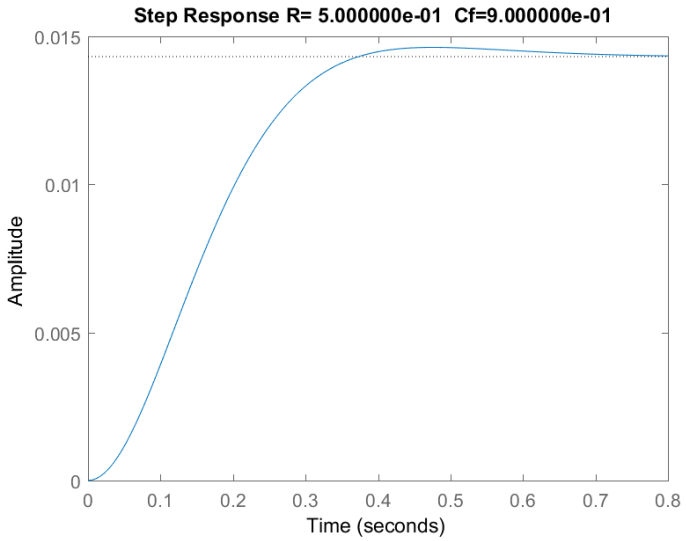

Figure 27: Acceleration & Velocity Feedback Step Response for ζf=0.9 g<0

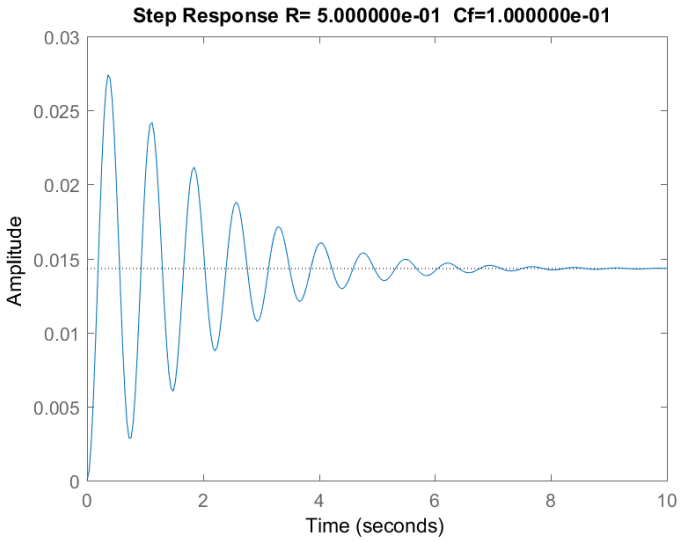

Figure 28: Acceleration & Velocity Feedback Step Response for ζf=0.1 g>0

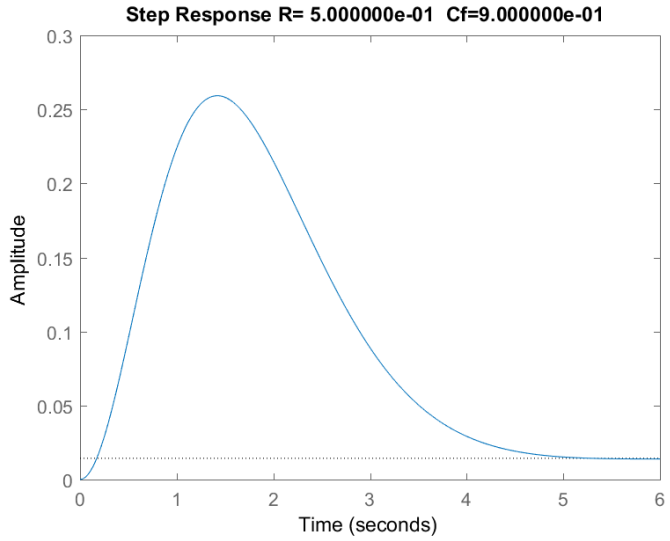

Figure 29: Acceleration & Velocity Feedback Step Response for ζf=0.9 g>0

In order to observe the step responses more clearly, the response plots for negative and positive g were separated plotted below in Figure 30 and Figure 31 respectively.

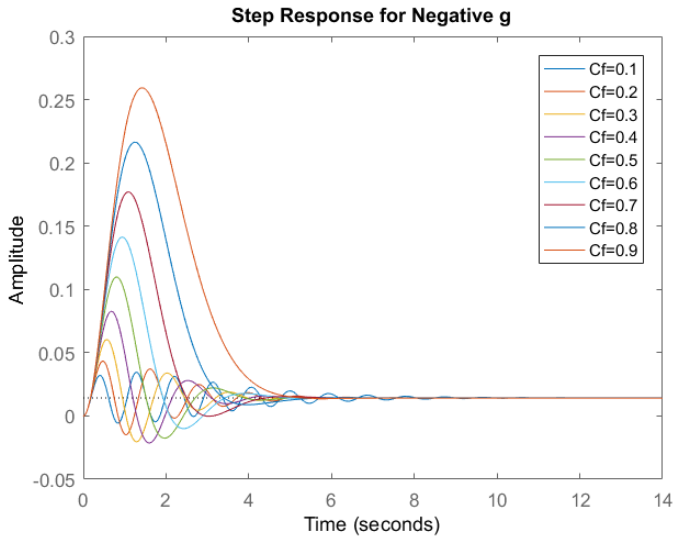

Figure 30: Acceleration & Velocity feedback step response for negative g

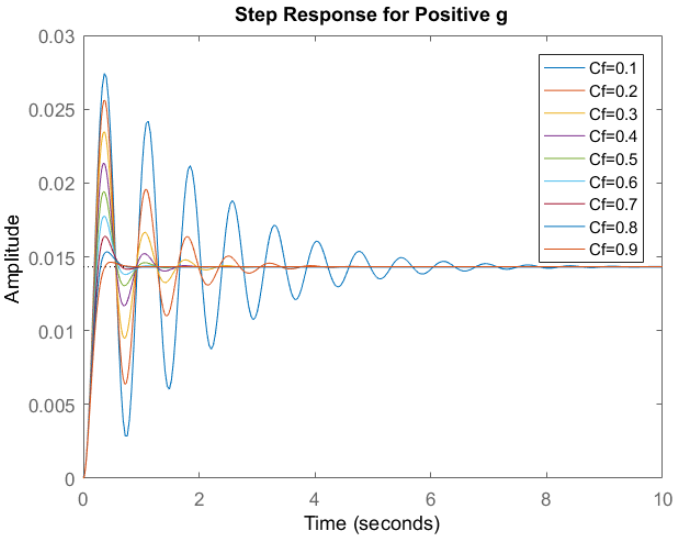

Figure 31: Acceleration & Velocity feedback step response for positive g

Since the damping is more in cases with positive g, that should be the preferred choice for future designs additionally it can be noted that negative gains are significantly larger in magnitude which is not practical.

Table 22: Acceleration & Velocity Feedback Data for ζc, wc/ws and positive g for different α

α	ζc	ω_f/ω_s	ω_c/ω_s	g	Settling Time (s)
0.1	0.33	1.19	1.41	0.21	2.74
0.2	0.34	1.16	1.35	0.21	2.79
0.3	0.34	1.13	1.29	0.21	2.84
0.4	0.35	1.11	1.23	0.21	2.90
0.5	0.36	1.08	1.17	0.21	2.96
0.6	0.37	1.06	1.12	0.20	3.01
0.7	0.38	1.04	1.08	0.18	3.06
0.8	0.38	1.02	1.05	0.17	3.11
0.9	0.39	1.01	1.02	0.16	3.43

The step responses for the above listed cases for α=0.1 and 0.9 are shown below.

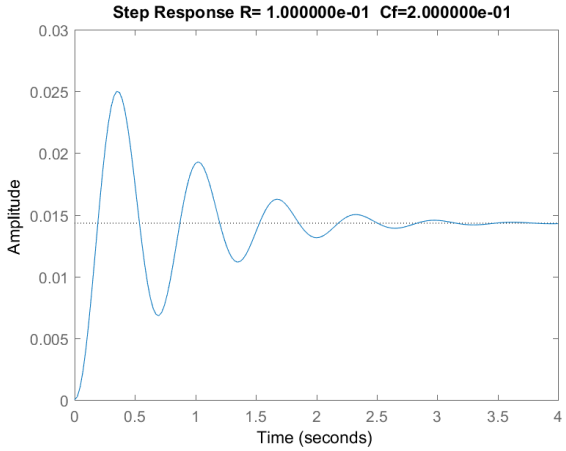

Figure 32: Acceleration & PPF Feedback Step Response for ζf=0.2 and α=0.1

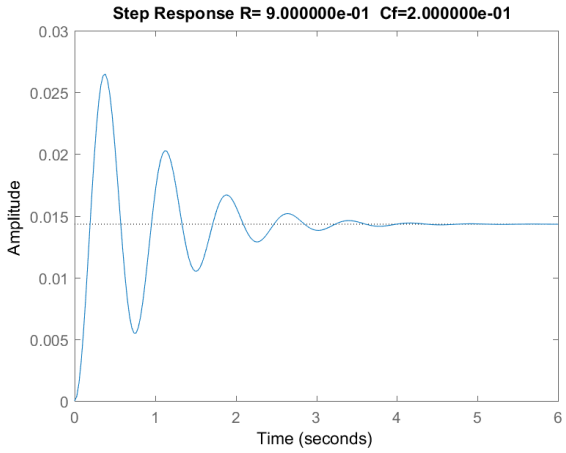

Figure 33: Acceleration & PPF Feedback Step Response for ζf=0.2 and α=0.9

4.2.3. Bode Plots

Studying the frequency domain behaviour of this system gives infinite gain and phase margins for all cases except for finite gain margins for positive gains for α=0.1, 0.2 and 0.3 and finite and high phase margins for large negative gains for α=0.7 through 0.9.

The following Table 23 lists the cases where the system shows non-infinite gain and phase margin. At first glance, it is clear that the gain margins are higher than the ideal and would therefore require an additional proportional gain to bring the margin down. While infinite phase margin in essence refers to a completely stable system, the higher phase margins would add in complications in physical implementation. From a controls perspective, the way to change the phase margin would be to introduce poles or zeroes however that would affect the stability of the system and is therefore not ideal.

Table 23: Settling Times, Gain and Phase Margin for Cases of Interest (Non infinite Gain and Phase Margins)

α	ζf	ζc	ω_f/ω_s	ω_c/ω_s	g	Settling time (s)	Gain Margin (dB)	Phase Margin
0.1	0.1	0.18	1.08	1.18	0.06	6.38	28.48	Inf
	0.2	0.33	1.19	1.41	0.21	2.74	36.45	Inf
	0.3	0.46	1.30	1.68	0.40	1.66	42.73	Inf
	0.4	0.56	1.41	1.99	0.61	1.04	48.30	Inf
	0.5	0.65	1.54	2.36	0.82	0.75	53.57	Inf
	0.6	0.72	1.66	2.77	1.00	0.50	58.91	Inf
	0.7	0.77	1.80	3.24	1.17	0.49	64.73	Inf
	0.8	0.82	1.94	3.76	1.33	0.30	72.51	Inf
0.2	0.1	0.18	1.07	1.15	0.06	6.42	30.55	Inf
	0.2	0.34	1.16	1.35	0.21	2.79	38.88	Inf
	0.3	0.47	1.25	1.57	0.42	1.71	46.23	Inf
	0.4	0.59	1.35	1.83	0.65	1.08	54.15	Inf
0.3	0.1	0.18	1.06	1.13	0.05	6.46	34.67	Inf
	0.2	0.34	1.13	1.29	0.21	2.84	43.77	Inf
0.7	0.7	8.83	0.15	0.02	-2514.73	7.42	Inf	135.46
	0.8	11.48	0.13	0.02	-4253.34	8.36	Inf	105.84
	0.9	14.48	0.12	0.01	-6772.53	8.53	Inf	93.75
0.8	0.1	0.35	0.52	0.27	-9.37	15.23	Inf	117.80
	0.2	1.20	0.31	0.09	-114.29	12.40	Inf	109.25
	0.3	2.59	0.21	0.05	-538.95	12.45	Inf	87.51
	0.4	4.53	0.16	0.03	-1657.34	12.11	Inf	72.21
	0.5	7.03	0.13	0.02	-3993.23	10.40	Inf	61.97
	0.6	10.08	0.11	0.01	-8220.05	12.30	Inf	54.96
	0.7	13.69	0.09	0.01	-15160.92	11.83	Inf	50.02
	0.8	17.85	0.08	0.01	-25788.58	13.38	Inf	46.44
	0.9	22.56	0.07	0.01	-41225.44	13.68	Inf	43.78
0.9	0.1	0.55	0.31	0.09	-103.98	26.67	Inf	45.44
	0.2	2.10	0.16	0.03	-1579.10	23.63	Inf	35.39
	0.3	4.69	0.11	0.01	-7907.13	24.61	Inf	28.35
	0.4	8.32	0.08	0.01	-24892.14	24.20	Inf	23.95
	0.5	12.98	0.07	0.00	-60659.89	20.85	Inf	21.18
	0.6	18.67	0.05	0.00	-125657.75	24.79	Inf	19.37
	0.7	25.41	0.05	0.00	-232654.77	23.83	Inf	18.15
	0.8	33.17	0.04	0.00	-396741.64	27.04	Inf	17.30
	0.9	41.98	0.04	0.00	-635330.68	27.63	Inf	16.68

If, observing the advantages of using positive gain from the step responses, we were to ignore the negative gain cases, only half the above listed cases are of importance. Therefore for $\alpha = 0.1$ through 0.3, the positive gain values do not result in infinite gain margin and while they are positive, implying stability, they are large in magnitude and therefore a proportional gain would be required to lower the gain margin for the physical system.

A few bode plots for cases of interest are listed below in Figure 34 through Figure 39.

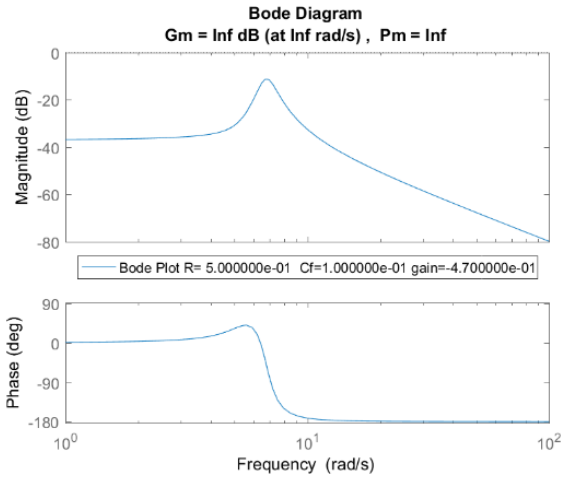

Figure 34: Acceleration & Velocity Feedback Bode Plots for $\zeta f=0.1$ $g<0$ $\alpha=0.5$

The figure illustrated below in Figure 35 displays a robust design with infinite gain and phase margin.

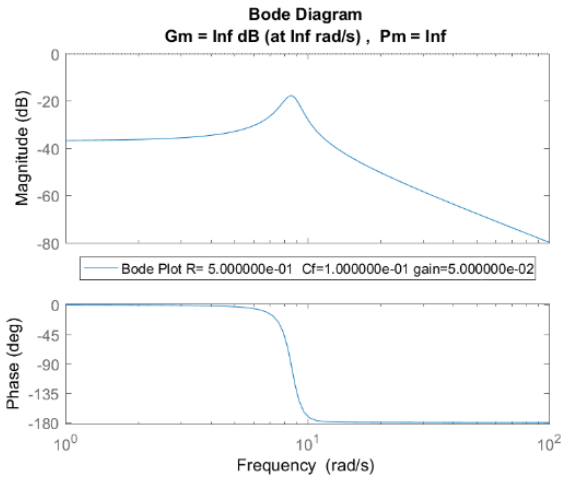

Figure 35: Acceleration & Velocity Feedback Bode Plots for ζf=0.1 g>0 α=0.5

Both cases with bode plots illustrated in Figure 35 and Figure 36 once again show robust designs with the listed gain and phase margins.

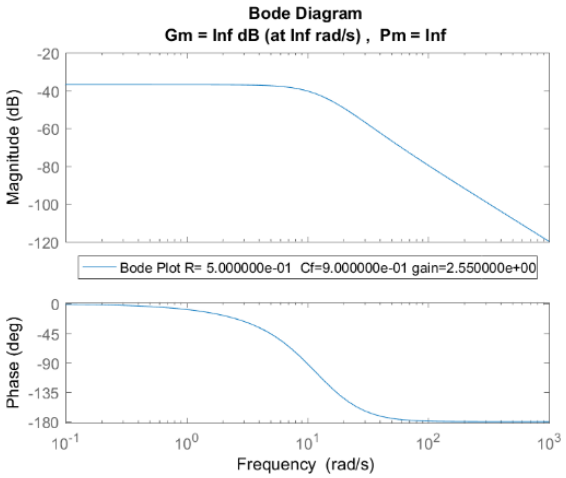

Figure 36: Acceleration & Velocity Feedback Bode Plots for ζf=0.9 g>0 α=0.5

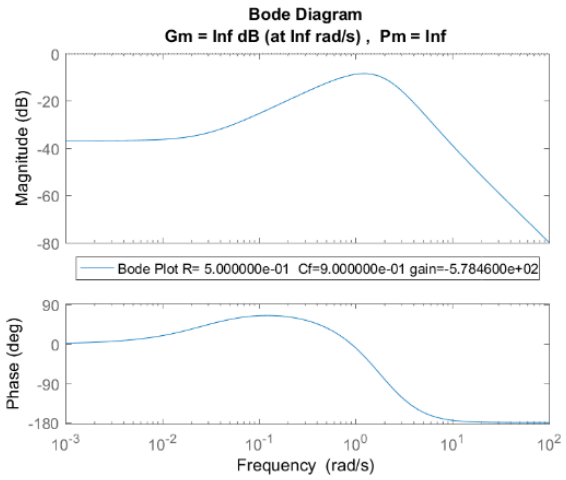

Figure 37: Acceleration & Velocity Feedback Bode Plots for ζf=0.9 g<0 α=0.5

While Figure 37 displays a robust design, Figure 38 still shows a positive gain margin within a reasonable range.

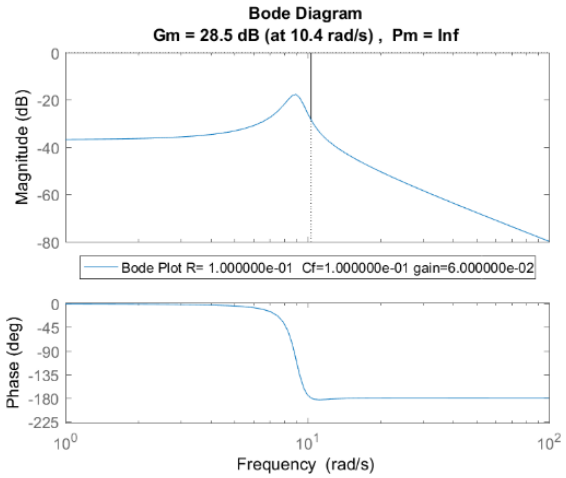

Figure 38: Acceleration & Velocity Feedback Bode Plots for ζf=0.1 g>0 α=0.1

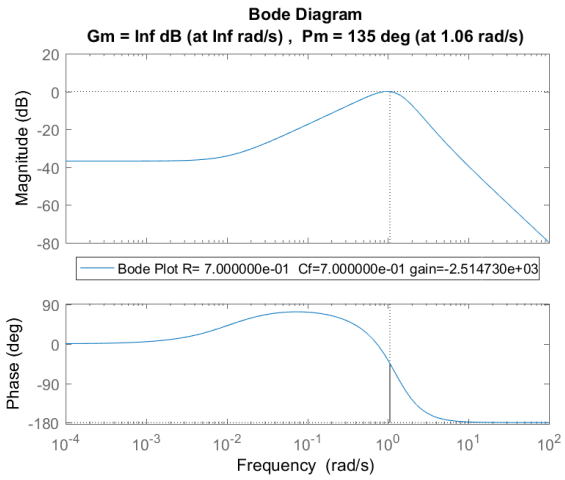

Figure 39: Acceleration & Velocity Feedback Bode Plots for ζf=0.7 g<0 α=0.7

For Varying values of α, i.e. the ratio between the 2 feedbacks, the results for ζf=0.2 and ζs=0.01 are as follows:

Table 24: Gain and Phase Margins for Different α

α	ζc	ω_f/ω_s	ω_c/ω_s	g	Settling Time (s)	Gain Margin (dB)	Phase Margin
	0.48	0.81	0.66	-0.54	4.68	Inf	Inf
0.1	0.33	1.19	1.41	0.21	2.74	36.45	Inf
	0.49	0.79	0.62	-0.74	4.83	Inf	Inf
0.2	0.34	1.16	1.35	0.21	2.79	38.88	Inf
	0.51	0.75	0.57	-1.08	5.05	Inf	Inf
0.3	0.34	1.13	1.29	0.21	2.84	43.77	Inf
	0.54	0.71	0.50	-1.76	5.38	Inf	Inf
0.4	0.35	1.11	1.23	0.21	2.90	Inf	Inf
	0.60	0.64	0.42	-3.30	5.92	Inf	Inf
0.5	0.36	1.08	1.17	0.21	2.96	Inf	Inf
	0.69	0.56	0.31	-7.49	6.84	Inf	Inf
0.6	0.37	1.06	1.12	0.20	3.01	Inf	Inf
	0.85	0.44	0.20	-22.87	8.58	Inf	Inf
0.7	0.38	1.04	1.08	0.18	3.06	Inf	Inf
	1.20	0.31	0.09	-114.29	12.40	Inf	109.25
0.8	0.38	1.02	1.05	0.17	3.11	Inf	Inf
	2.10	0.16	0.03	-1579.10	23.63	Inf	35.39
0.9	0.39	1.01	1.02	0.16	3.43	Inf	Inf
1	0.01000	0.02502	0.00063	-2.55E+06	NaN	-0.601	2.45

The bode plots and step responses for the above values are shown below for negative gains:

Therefore, we observe that all values of $\alpha<0.5$ yield better settling times and as the value of the ratio increases, i.e. as the acceleration feedback increases, the responses are more ideal.

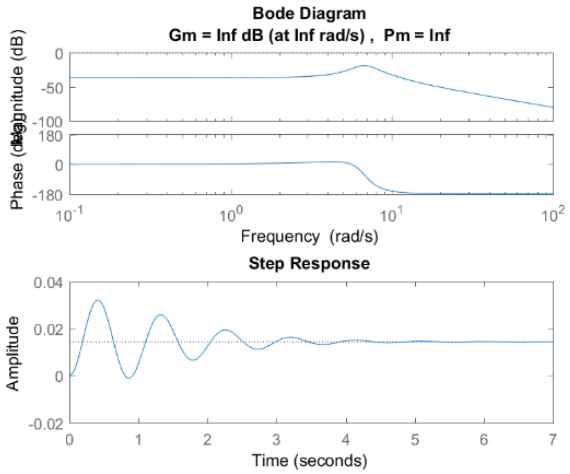

Figure 40: Acceleration and Velocity Feedback with Alpha = 0.1

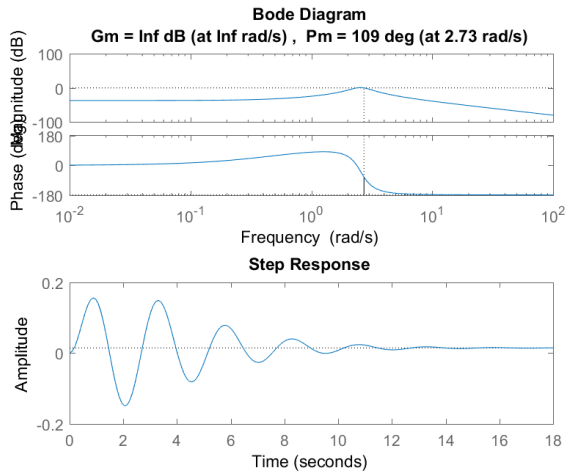

Figure 41: Acceleration and Velocity Feedback with Alpha = 0.8

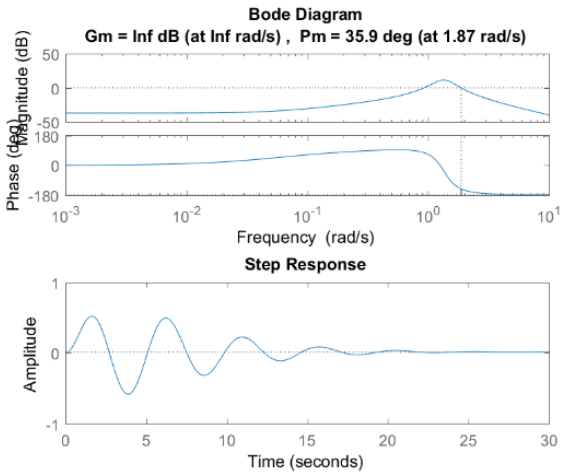

Figure 42: Acceleration and Velocity Feedback with Alpha = 0.9

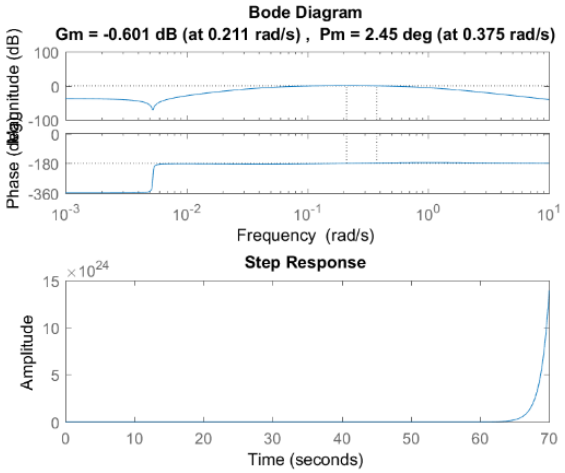

Figure 43: Acceleration and Velocity Feedback with Alpha = 1

4.2.4. Perturbations from coincident closed loop frequency

Following the same methodology as in Section 5.4. the following table lists the values obtained for applying perturbations.

Table 25: Acceleration & Velocity Feedback Values for Different Perturbations

δ	ω_c/ω_s	g	ζc	Settling Time (s)	Gain Margin	Phase Margin
0	0.4157	-3.2970	0.5964	5.9206	Inf	Inf
	1.1716	0.2056	0.3610	2.9576	Inf	Inf
0.1	0.4313	-3.0382	0.5859	8.6062	Inf	Inf
	1.1976	0.2291	0.3572	2.5935	Inf	Inf
0.2	0.4471	-2.7988	0.5758	12.9216	Inf	Inf
	1.2239	0.2513	0.3534	2.3193	Inf	Inf
0.3	0.4633	-2.5773	0.5661	22.6101	Inf	Inf
	1.2506	0.2722	0.3497	2.3843	Inf	Inf
0.4	0.4797	-2.3719	0.5567	60.7334	Inf	72.6575
	1.2775	0.2920	0.3461	2.4280	Inf	Inf
0.5	0.4964	-2.1814	0.5476	NaN	-4.3982	13.1723
	1.3047	0.3106	0.3425	2.4456	Inf	Inf

If the negative gain ‘g’ values are not considered, adding perturbations does not change the stability of the system and adding a perturbation of 0.2 yields the best result i.e. the least settling time about 0.6383 seconds faster than the case with no perturbation.

4.2.5. Energy Analysis

Possible errors due to the solution method and approximation can attribute to the values listed in the table below. While in general the positive gain g cases require less energy, further leading to the conclusion that choosing appositive gain is more suitable, the energy does not increase as expected. Possible solutions to this would be to perform experiments to test the results.

It can be noted that in Table 26 below, the negative gain g case dissipates more energy than the positive g, however it is more important to focus on the controller energy required.

Table 26: Energy Dissipated by the system

ζ_f	Energy Dissipated for positive g	Energy Dissipated for negative g
0.1	-0.00926	-0.12806
0.2	-0.01001	-0.01496
0.3	-0.00927	-0.0216
0.4	-0.00983	-0.03727
0.5	-0.00825	-0.06089
0.6	-0.006	-0.0991
0.7	-0.00553	-0.16791
0.8	-0.00579	-0.25504

At this stage, we can conclude that focusing on positive gains 'g' will be more fruitful. Focusing on the controller energy requirements for different values of the ratio α, we have the following results. Table 27: Controller Energy Required for Different α

α	Energy Required
0.1	1.277079
0.2	1.222735
0.3	**1.168391**
0.4	1.248379
0.5	1.689383
0.6	2.32228
0.7	3.019624
0.8	3.850375
0.9	4.873613

For the least amount of energy, the case for α=0.3 was perturbed and the energy results for those are as follows:

Table 28: Controller Energy Required for α=0.3 with perturbations

δ	Energy Required
0	0.00055825
0.1	0.00051080
0.2	0.00044892
0.3	0.00039566
0.4	0.00038296
0.5	**0.00037026**

Therefore, for a required damping ratio of 0.2, the acceleration and velocity feedback requires an α of 0.3 i.e. a dominant of acceleration feedback, with a perturbation of 0.5 for the most optimal controller with parameters:

$$\omega_c/\omega_s = \mathbf{1.42949}\text{ , g=0.2726, }\zeta\mathbf{c=0.32756}$$

4.3. COMBINED POSITIVE POSITION AND VELOCITY FEEDBACK

4.3.1. Formulation of Positive Position (PPF) and Velocity Feedback Controller

For a combined position and velocity compensator we have the compensator below

$$\ddot{\eta} + 2\zeta_c\omega_c\dot{\eta} + \omega_c^2\eta = \alpha\omega_s^2 a\xi + (1-\alpha)\omega_s a\dot{\xi} \tag{4.3.1.1}$$

When β=1, we have position feedback and when $\beta = 0$ we get velocity feedback but currently for the sake of a preliminary assessment, consider the ratio to be 0.5. Using the transfer function below:

$$\frac{\xi(s)}{Q_1(s)} = \frac{[s^2 + 2\zeta_c\omega_c s + \omega_c^2]}{[s^2 + 2\zeta_s\omega_s s + \omega_s^2][s^2 + 2\zeta_c\omega_c s + \omega_c^2] - abg\omega_c^2(\alpha\omega_s^2 + (1-\alpha)\omega_s s)} \tag{4.3.1.2}$$

To obtain the required variables from the given input; comparing the coefficients for the different powers of s gives rise to the following equalities:

S^3: $\mathbf{2(\zeta_c\omega_c + \zeta_s\omega_s) = 4\zeta_f\omega_f}$ (4.3.1.4)

S^2: $\boldsymbol{\omega_c^2 + 4\zeta_c\zeta_s\omega_c\omega_s + \omega_s^2 = 2\omega_f^2 + 4\zeta_f{}^2\omega_f^2}$ (4.3.1.5)

$$S^1: \boldsymbol{\omega_c \omega_s (2\zeta_s \omega_c + ab(-1+\alpha) g \omega_c + 2\zeta_c \omega_s) = 4\zeta_f \omega_f{}^3} \quad (4.3.1.6)$$

$$S^0: \boldsymbol{(1 - g\alpha) \omega_c{}^2 \omega_s{}^2 = \omega_f{}^2} \quad (4.3.1.7)$$

The values for ζc, wc/ws and g for different ζf were calculated using Mathematica and are listed below in Table 29. The following table lists the values of ζc, ω_f/ω_s, ω_c/ω_s, g and the settling time of the unit step response in seconds for different ζf, all at α=0.5.

Table 29: PPF and Velocity Feedback Data for ζc, wc/ws and g for different ζf

ζf	ζc	ω_f/ω_s	ω_c/ω_s	g	Settling time (s)
0.1	0.194	0.964	0.943	0.056	22.028
0.2	0.394	0.926	0.915	0.245	12.146
0.3	0.569	0.889	0.920	0.520	7.405
0.4	0.710	0.854	0.949	0.816	4.923
0.5	0.815	0.821	0.995	1.082	3.518
0.6	0.892	0.789	1.051	1.298	3.159
0.7	0.946	0.759	1.112	1.464	3.799
0.8	0.985	0.730	1.176	1.590	5.232
0.9	1.012	0.702	1.239	1.683	6.934

4.3.2. Step Input Responses

The Step Input Response for α=0.5 for ζf=0.1 and 0.9 are shown below in Figure 44 and **Error! Reference source not found.** respectively. There is a significant amount of damping though the behavior at higher damping ratios is not the common overdamped response. While there is no overshoot for large damping ratios, there is significant amount of oscillations that take place.

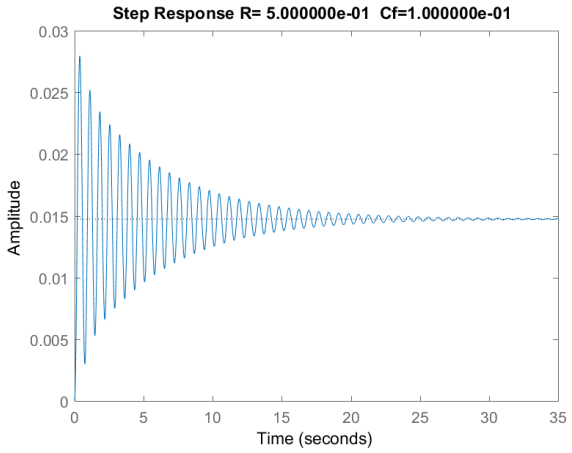

Figure 44: PPF & Velocity Feedback Step Response for ζf=0.1

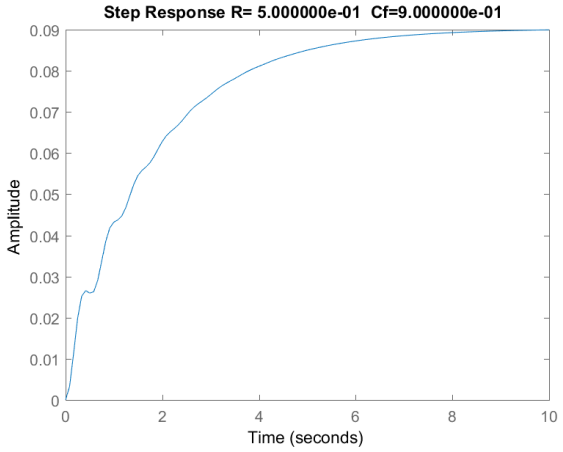

Figure 45: PPF & Velocity Feedback Step Response for ζf=0.9

The combined step responses are displayed below in Figure 46.

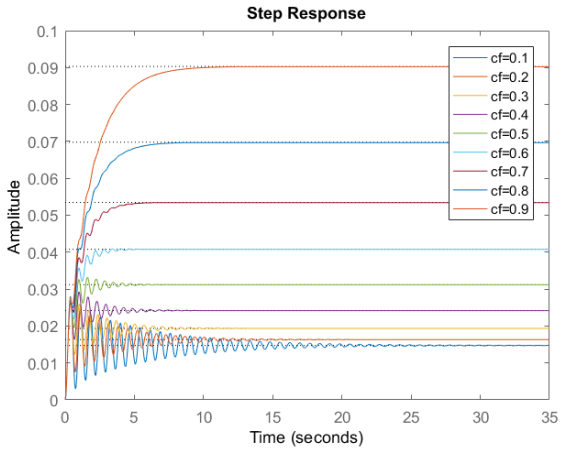

Figure 46: Position & Velocity Feedback combined step responses

Now, in order to observe how the ratio α, affects the step responses, the following table lists the values for ζf=0.2.

Table 30: PPF and Velocity Feedback Data for ζc, wc/ws and g for different α

α	ζc	ω_f/ω_s	ω_c/ω_s	g	Settling Time (s)
0.1	0.450	0.846	0.730	0.382	NaN
0.2	0.434	0.864	0.774	0.349	NaN
0.3	0.419	0.884	0.821	0.314	NaN
0.4	0.405	0.905	0.869	0.279	35.566
0.5	0.394	0.926	0.915	0.245	12.146
0.6	0.385	0.946	0.958	0.213	7.033
0.7	0.377	0.964	0.995	0.185	5.006
0.8	0.372	0.979	1.027	0.162	4.010
0.9	0.367	0.991	1.052	0.142	3.388

The step responses for α =0.1 and 0.9 are shown below.

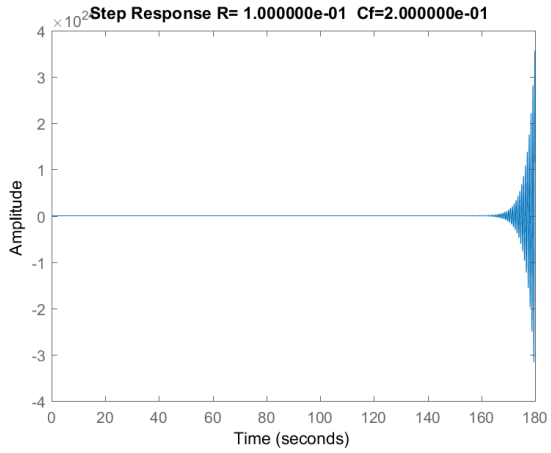

Figure 47: PPF & Velocity Feedback Step Response for α =0.1

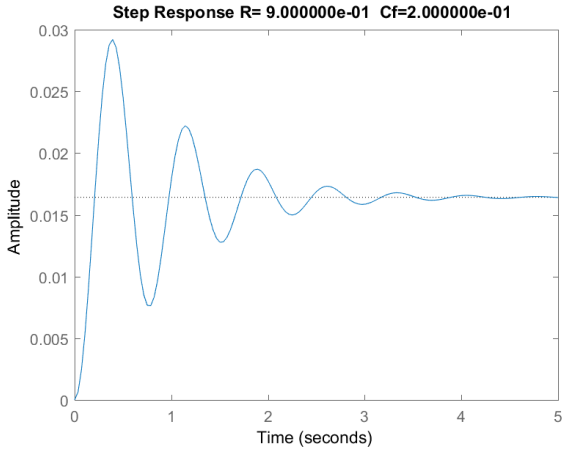

Figure 48: PPF & Velocity Feedback Step Response for α =0.9

4.3.3. Bode Plots

The following tables have data for the gain margin and phase margin for the various cases listed, all obtained from the bode plots.

Table 31: Gain and Phase Margin for Different ζf

ζf	Gain Margin (dB)	Phase Margin
0.1	Inf	Inf
0.2	36.438	Inf
0.3	38.076	Inf
0.4	40.079	Inf
0.5	41.905	Inf
0.6	43.455	Inf
0.7	44.781	Inf
0.8	45.917	Inf
0.9	46.871	Inf

Bode Plots (for cases of interest) are shown below, while the case with ζf=0.1 has infinite gain and phase margin and therefore inherent stability, the other cases still have positive gain margins which, as with the case of Chapter 6, are still large and would therefore require adding some proportional controller to reduce the gain margin.

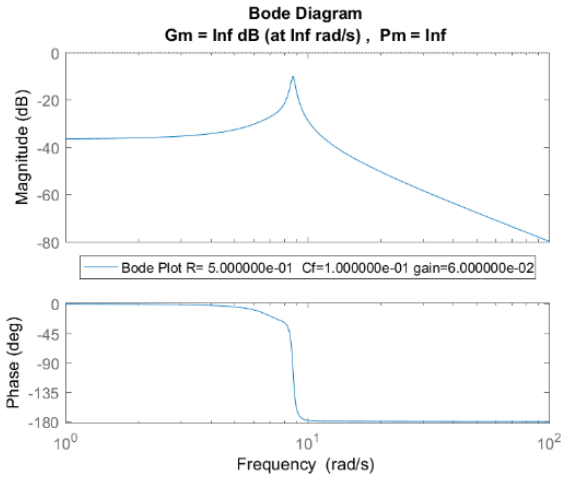

Figure 49: PPF & Velocity Feedback Bode Plot for ζf=0.1

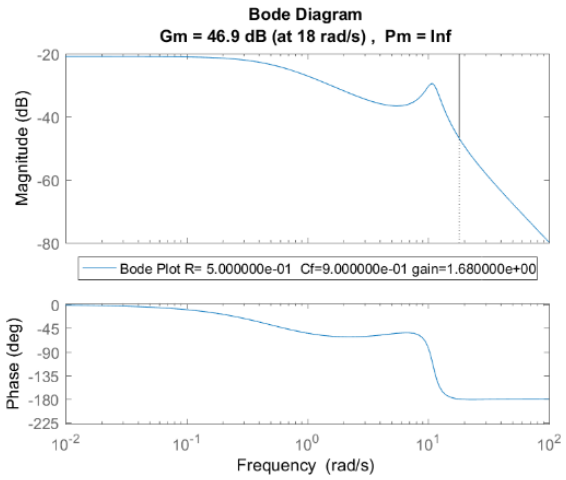

Figure 50: PPF & Velocity Feedback Bode Plot for ζf=0.9

Now, varying α with ζf=0.2 and observing the frequency responses gives the values listed in the following table.

Table 32: Gain and Phase Margin for Different α

α	Gain Margin (dB)	Phase Margin
0.1	55.100	Inf
0.2	54.114	Inf
0.3	52.730	Inf
0.4	24.503	Inf
0.5	36.438	Inf
0.6	Inf	Inf
0.7	Inf	Inf
0.8	Inf	Inf
0.9	Inf	Inf

We do observe that higher values of α give more robust and desirable systems with infinite gain and phase margin. Once again, the gain margins are larger than desired and should the cases be considered for implementation, proportional gains would have to be added to reduce the gain margin. The following figures illustrate the bode plots for few cases of interest.

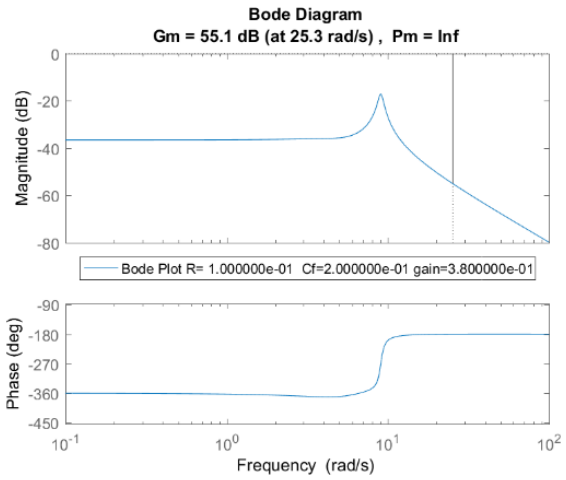

Figure 51: PPF & Velocity Feedback Bode Plot for α=0.1

Both gain margins listed in Figure 51 and Figure 52 are higher than the ideal and call for the use of a proportional gain to lower the margin during physical implementation. Figure 53 however shows a robust design.

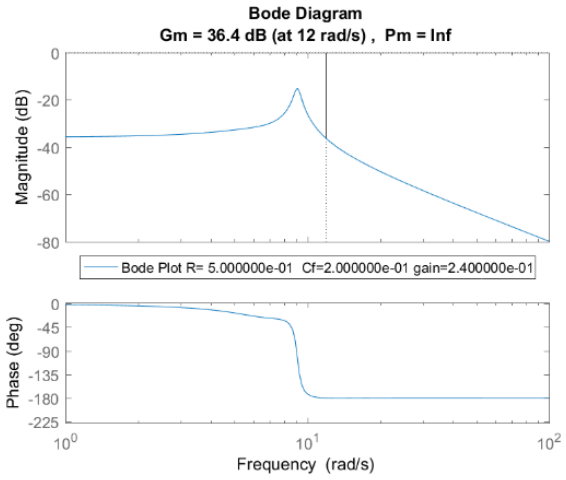

Figure 52: PPF & Velocity Feedback Bode Plot for α=0.5

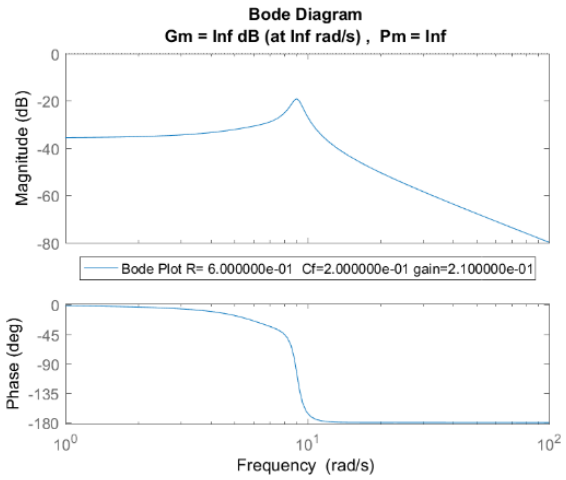

Figure 53: PPF & Velocity Feedback Bode Plot for α=0.6

4.3.4. Perturbations from coincident closed loop frequency

The following table displays the controller parameters we obtain from solving the equations, the settling times in seconds and the gain and phase margins of the resulting step response and bode plots respectively.

Table 33: PPF & Velocity Feedback Values for Different Perturbations

δ	ω_c/ω_s	g	ζc	Settling Time (s)	Gain Margin	Phase Margin
0	0.9151	0.2446	0.3938	9.7000	Inf	Inf
0.1	0.9410	0.2522	0.3881	8.2610	Inf	Inf
0.2	0.9665	0.2570	0.3828	7.1741	Inf	Inf
0.3	0.9916	0.2592	0.3779	6.1408	Inf	Inf
0.4	1.0164	0.2592	0.3734	5.4275	Inf	Inf
0.5	1.0410	0.2571	0.3692	4.7530	Inf	Inf

For the PPF and Velocity Feedback controller, adding perturbations improves the response as opposed to the 2 other designs discussed previously. Therefore, an optimal solution for the PPF and velocity feedback controller would be one with a 0.5 perturbation added.

4.3.5. Energy Analysis

Apart from the ζf=0.5 case, the energy dissipated increases as ζf increases, which, as with Chapter 5, is the expected and desirable condition.

Table 34: Energy Dissipated by the system

ζf	Energy Dissipated
0.1	-0.02373
0.2	-0.0268
0.3	-0.02786
0.4	-0.11299
0.5	-0.07548
0.6	-0.51749
0.7	-0.60941
0.8	-0.91186

Focusing on the controller energy requirements for different values of the ratio α, we have the following results.

Table 35: Controller Energy Required for Different α

α	Energy Required
0.1	**2.606401**
0.2	3.098777
0.3	3.631805
0.4	4.398517
0.5	5.258792
0.6	6.221204
0.7	7.302601
0.8	8.459555
0.9	9.395156

For the least amount of energy, the case for α=0.1 was perturbed and the energy results for those are as follows in Table 36 with the lowest case marked in bold.

Table 36: Controller Energy Required for α=0.1 with perturbations

δ	Energy Required
0	2.616847
0.1	2.722336
0.2	2.497848
0.3	2.456541
0.4	**2.315123**
0.5	2.35858

Therefore, for a required damping ratio of 0.1, the position and velocity feedback requires an α of 0.1 i.e. a dominant of velocity feedback, with 0.4 perturbation the most optimal controller with parameters:

$$\omega_c/\omega_s = \mathbf{0.73024}\text{ , g=0.38835, }\zeta\mathbf{c=0.44978}$$

5. COMPARISON & DISCUSSION

The following Table 37 displays the settling times for various cases listed previously.

Table 37: Settling Times

ζf	PPF	Acceleration	Velocity (-ve g)	Velocity (+ve g)	Acceleration + PPF	Acceleration + Velocity (-ve g)	Acceleration + Velocity (+ve g)	PPF + Velocity
0.1	6.8046	6.8292	7.8416	6.3296	7.136	9.7238	6.2985	22.0278
0.2	3.1912	3.4736	4.5686	2.6918	3.402	5.9184	2.9577	12.1455
0.3	2.1104	2.3439	3.1858	1.6191	1.733	4.552	1.8706	7.4051
0.4	1.4388	1.7196	2.5	1.0126	1.113	4.5178	1.2105	4.9228
0.5	1.1195	1.3925	2.2182	0.7225	0.764	3.7091	0.8879	3.5181
0.6	1.0606	1.0898	2.3859	0.4834	0.656	4.2375	0.8496	3.1589
0.7	0.8662	1.1022	2.1478	0.4712	0.567	3.9886	0.6009	3.7992
0.8	0.7916	0.8432	2.3065	0.2938	0.579	4.4411	0.6045	5.232
0.9	0.7591	0.9815	2.2593	0.3541	0.450	4.4924	0.5213	6.9336

Below in Figure 54, the settling times from the step responses of all the above listed cases can be viewed. The best possible solutions in comparison at this stage is the Acceleration & Velocity Feedback with positive gain (g) and the velocity feedback with positive g.

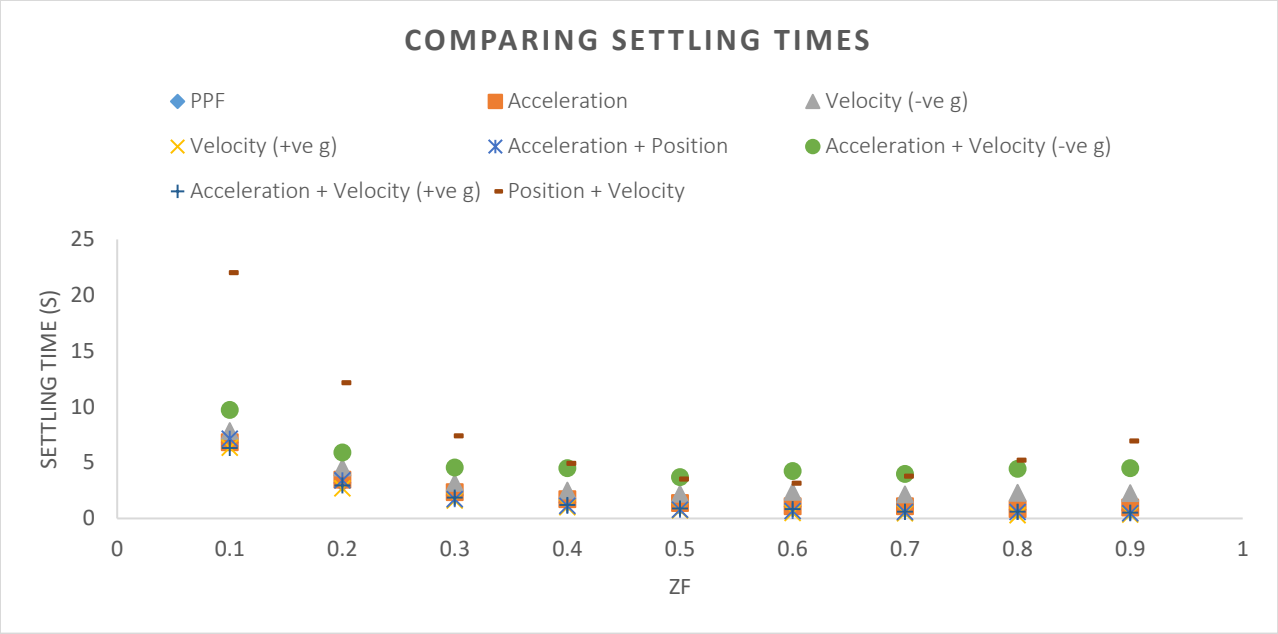

Figure 54: Comparison of Settling Times

Observing them at a closer range gives the following plot.

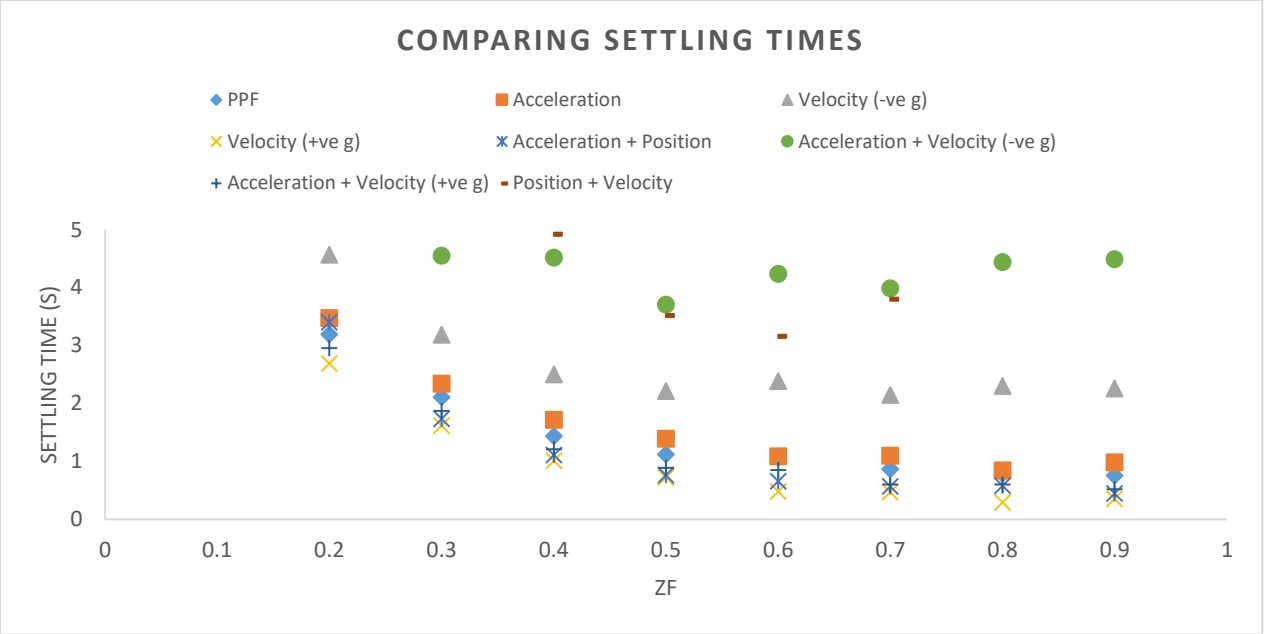

Figure 55: Comparison of Settling Times (Closer Range)

From the comparison above, we deduce that the responses are best for two types of feedback however, trying the cases with different combination ratios we get:

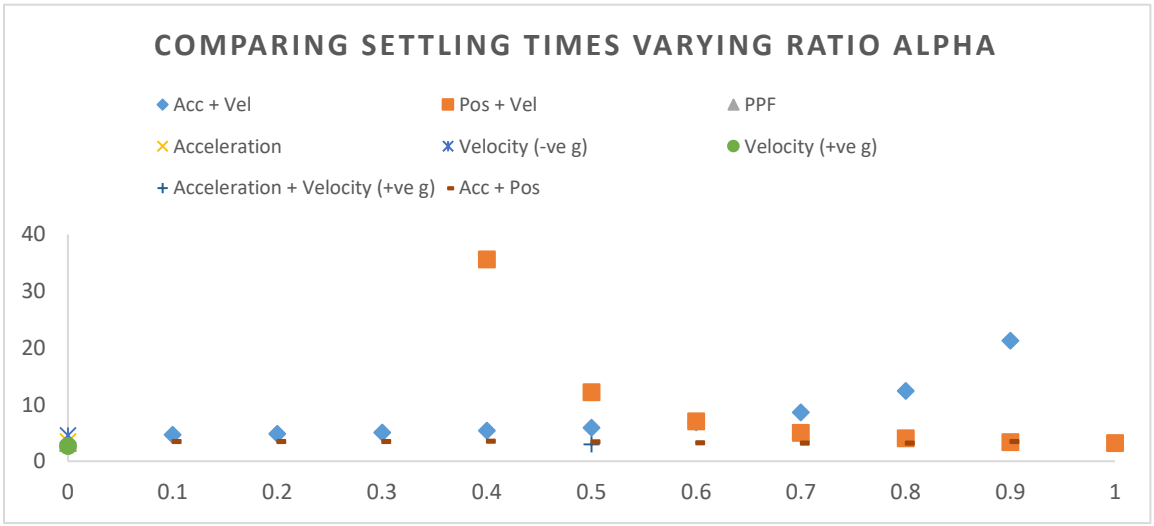

Figure 56: Combined Settling Times With varying feedback ratios

When we observe at a closer range we see

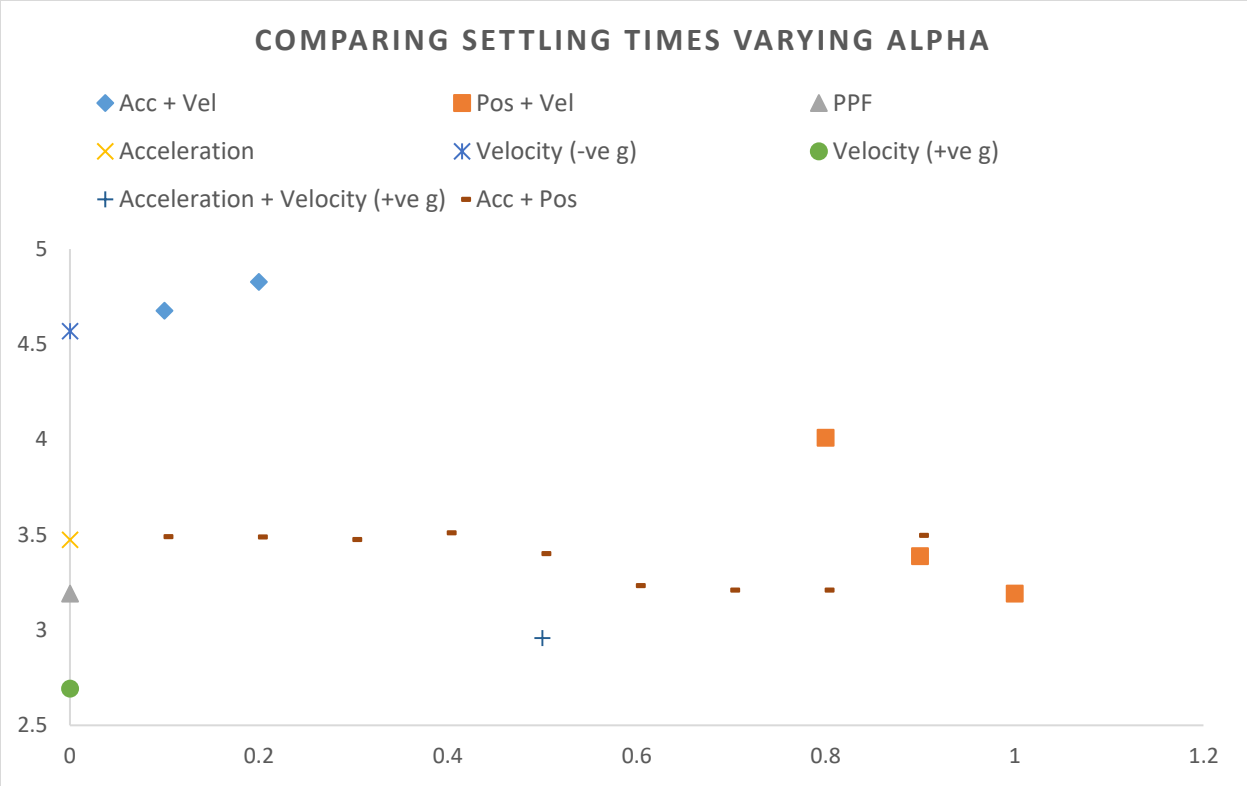

Figure 57: Combined Settling Times With varying feedback ratios (closer range)

Therefore, the best outcome still comes from the Velocity only feedback although it is closely followed by the Acceleration and Velocity combined feedback (with positive gain) and the PPF. Though the Acceleration and PPF feedback consistently shows fast damping.

Now, comparing the controller input energy required for different alpha values for closed loop damping ratio of 0.2 we get the plot shown in Figure 58.

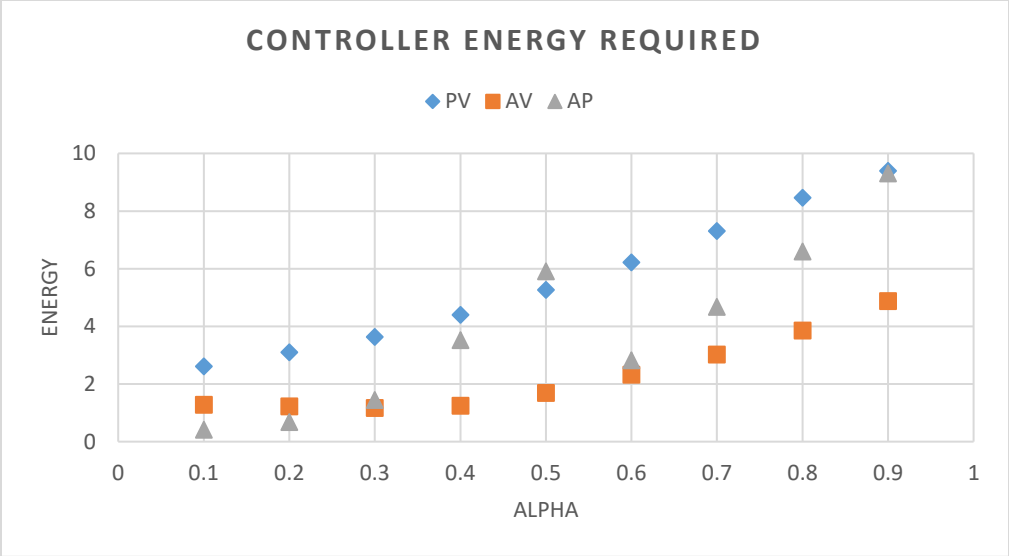

Figure 58: Comparing Controller Energy Required for different α

It is very clear that the acceleration and velocity feedback controller has the least energy requirement by a sizable margin. In order to obtain a visual representation of how the perturbations affect the best cases from varying the ratio of feedback, Figure 59 illustrates the trends. The behaviors of the controllers can be attributed to the elements that make up the combined feedback. Noting that the velocity feedback alone had the least energy requirement when compared to PPF feedback only which had the highest energy requirement, and acceleration feedback which fell in between, the behavior of the combined feedbacks as the ratio alphas are changed becomes understandable. Similarly, as the perturbation changes, the acceleration and position feedback shows a considerable range in energy requirements. This implies that when considering such controllers, it is very important to consider all the variables since small changes can affect the energy requirements.

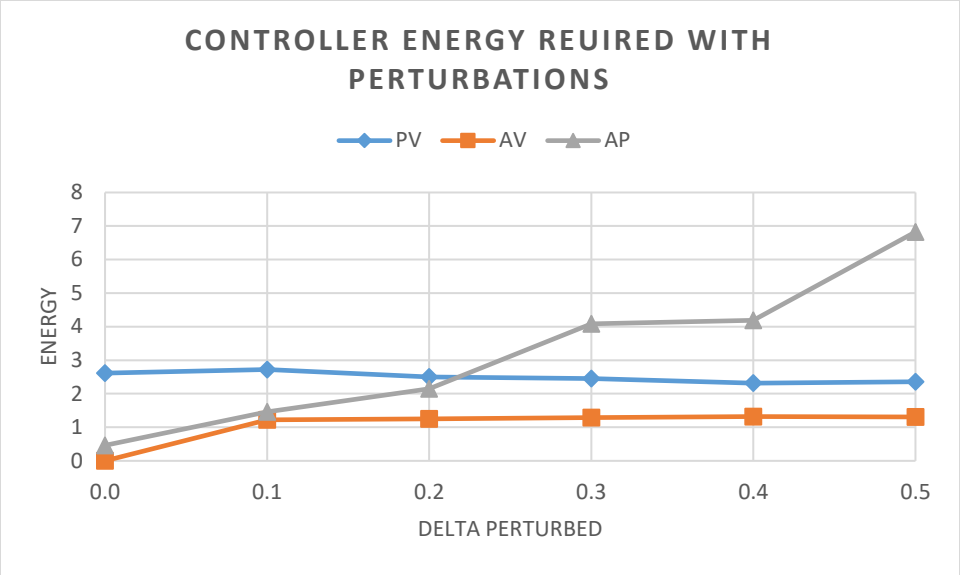

Figure 59: Controller Energy Required for perturbed solutions

We definitely notice the advantages and flexibility of combined feedback controllers. Out of all the simulated cases, the Acceleration and PPF combined feedback offers faster damping consistently however, it also has the highest energy requirement. The advantages of using a combined feedback include flexibility and the damping achieved is on par with the largest damping achieved with individual feedback. For the Acceleration and Velocity Controller, all cases resulted in stable solutions with either both infinite gain and phase margins or positive gain margins and infinite phase margins. It should also be noted that the combined cases perform well in terms of both energy required and settling times when compared to the individual inputs. That fact added to the large energy dissipated would affect the choice of implementing it.

Comparing all the alternatives shows that the best option is the *Acceleration and Velocity feedback* system with 0.3 acceleration feedback, and 0.7 velocity feedback and a perturbation of 0.5. This controller also offers a system which has all robust cases for all ratios and damping ratios, i.e.

offering more robust stable solutions and it has the lowest energy required and performs well in terms of damping the system fast.

The reason why this discussion focuses on combined feedback is because as mentioned in the background, there are errors that can arise with sensors collecting various data when operating under various situations. If the situations can be modeled according to operating conditions or system parameters, the ratio choosing how much feedback i.e. how much acceleration and velocity feedback is considered in the compensator, can be changed. The change can also be based on how much damping is required since that data also exists and data on the cases where certain combinations result in non-converging and unstable systems is also now available through this research. Multiple parameters and design constraints can potentially be added in via the ratio and knowing the stable range and the knowledge of how the system behaves to different inputs gives a lot of insight into the design of this versatile controller.

With flexibility offered and with solutions that offer high damping at faster speeds, it might be useful to consider the applications of these in non-linear conditions and different beam approximations and different boundary conditions.

6. CONCLUSION

With this thesis, several controllers were designed with multiple combined feedbacks; positive position & acceleration feedback, acceleration & velocity feedback and position & velocity feedback. This thesis thoroughly explored the stability, and stability ranges of the various systems in the frequency domain, concluding that the method used to determine combination controller parameters resulted in robust systems with infinite gain and phase margins implying inherently stable systems. The system responses were simulated for various required closed loop damping ratios and the cases were also tested for when the closed loop frequency was perturbed to find other optimal solutions. Since the optimal condition would depend on the application and feasibility itself in the real physical domain, a quick analysis shows how each system would behave to different types of combinations. It can be concluded that the *Acceleration and Velocity feedback* system with 0.3 acceleration feedback, and 0.7 velocity feedback and a perturbation δ of 0.5 is an optimal controller offering robust stability and high damping. The data in this thesis can be used a guide when designing compensators for damping systems modeled as simply supported Euler-Bernoulli beams since all the ranges provided can give a good estimate on what to expect. The next stage would be to consider experimentally verifying the data and considering non-linear applications to expand our knowledge on these active controllers. Therefore, in order to summarize the findings; this thesis presented 4 new elements:

1. Designed and studied the combinations of two feedbacks; Acceleration & Velocity, Position & Velocity and Acceleration & Position, which has not been previously explored at all. The controllers were designed using a new solution technique of equations transfer

function denominator coefficients of ‘s’, to yield single closed loop frequency for specified closed loop damping ratio and they were compared to the bode plot design to analyze stability in the frequency domain.

2. The design was also modified to include frequencies other than the single closed loop frequency by the perturbation method, where a perturbation about a single closed loop frequency ωf was introduced. The thesis research also simulated the settling time, gain margin and phase margin to visualize how the perturbations affect the time domain response. It was noted that the different controllers had different responses and behaviors to the perturbations.
3. The minimum controller energy to suppress and control vibrations was also calculated. In order of worst to best, i.e. most energy to least energy required, for a required damping ratio ζf of 0.2;
    - Combined Position & Velocity Feedback requires an α of 0.1 i.e. a dominant of Velocity Feedback, with a perturbation δ of 0.4 the most optimal controller with parameters:

$$\omega_c/\omega_s = \mathbf{0.73024}\text{ , g=0.38835, }\zeta\mathbf{c=0.44978}$$

    - Combined Acceleration & Position Feedback requires an α of 0.1 i.e. a dominant of Acceleration feedback, with no perturbation for the most optimal controller with parameters:

$$\omega_c/\omega_s = \mathbf{0.99, g=-0.18, }\zeta\mathbf{c=0.39}$$

- Combined Acceleration & Velocity Feedback requires an α of 0.3 i.e. a dominant of acceleration feedback, with a perturbation δ of 0.5 for the most optimal controller with parameters:

$$\omega_c/\omega_s = \mathbf{1.42949}\text{ , g=0.2726, }\zeta\mathbf{c=0.32756}$$

4. The best combination was found to be *Acceleration and Velocity feedback* system with 0.3 acceleration feedback, and 0.7 velocity feedback and a perturbation δ of 0.5 offering robust stability and high damping

APPENDIX A

A.1. 1. Acceleration & PPF feedback with varying closed loop damping ratio

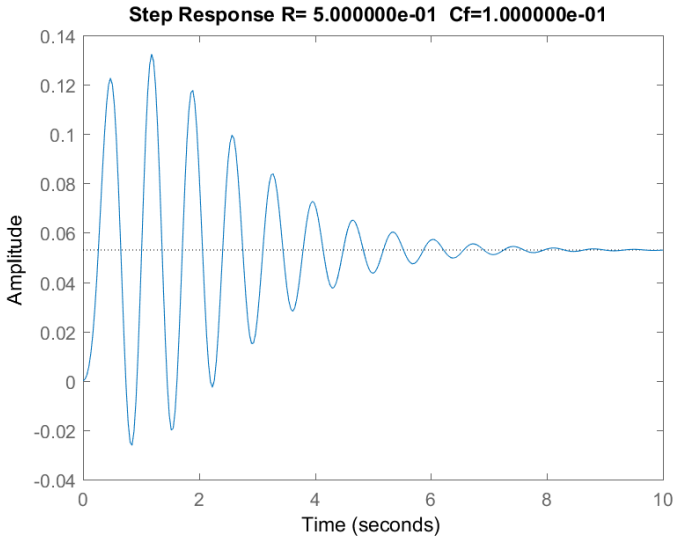

Figure 60: Acceleration & PPF for Alpha 0.5 and ζf=0.1

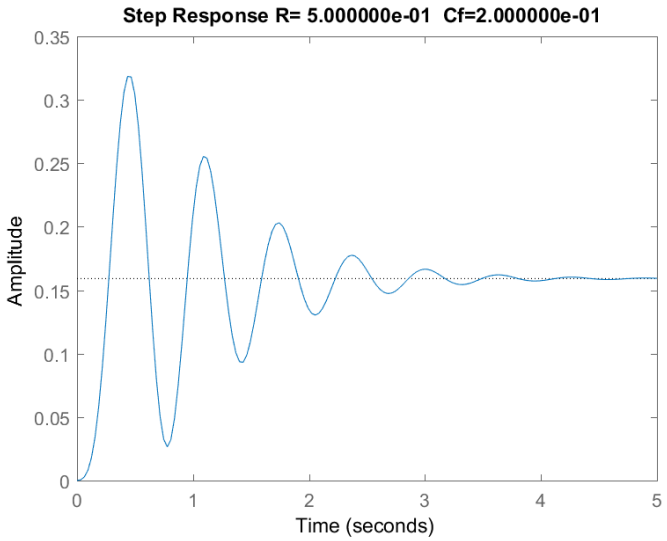

Figure 61: Acceleration & PPF for Alpha 0.5 and ζf=0.2

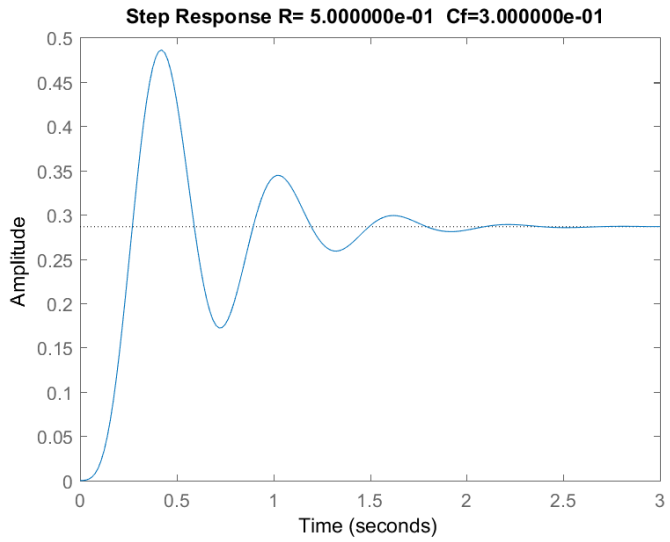

Figure 62: Acceleration & PPF for Alpha 0.5 and ζf=0.3

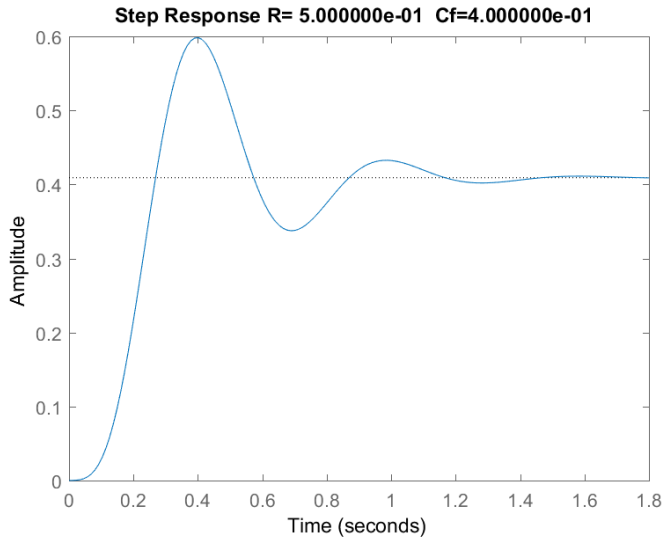

Figure 63: Acceleration & PPF for Alpha 0.5 and ζf=0.4

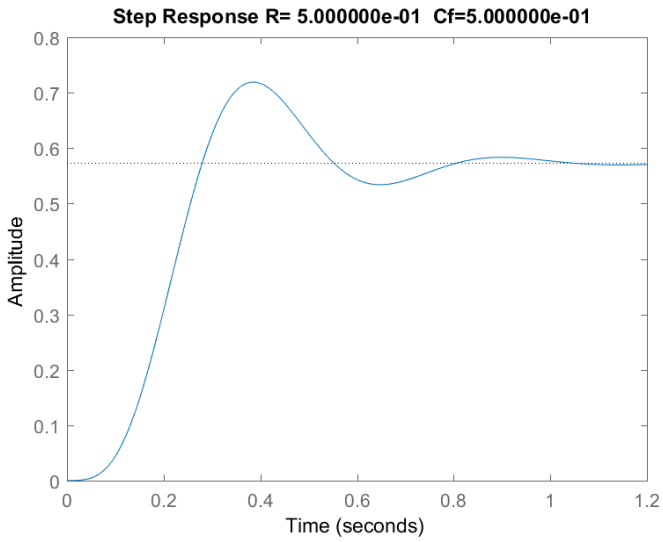

Figure 64: Acceleration & PPF for Alpha 0.5 and ζf=0.5

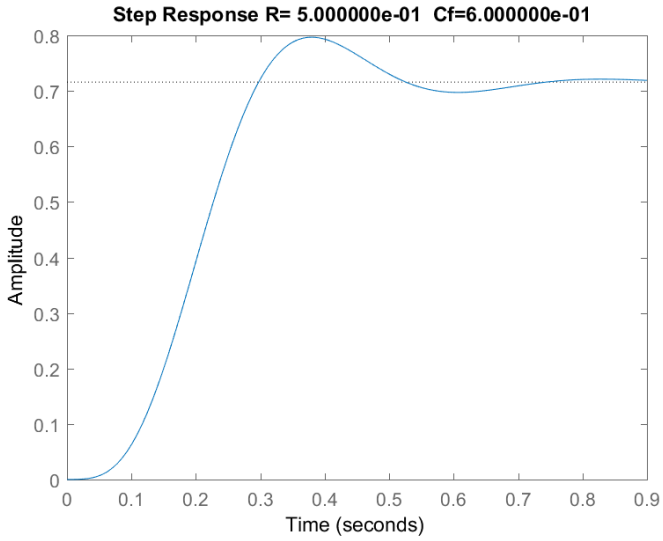

Figure 65: Acceleration & PPF for Alpha 0.5 and ζf=0.6

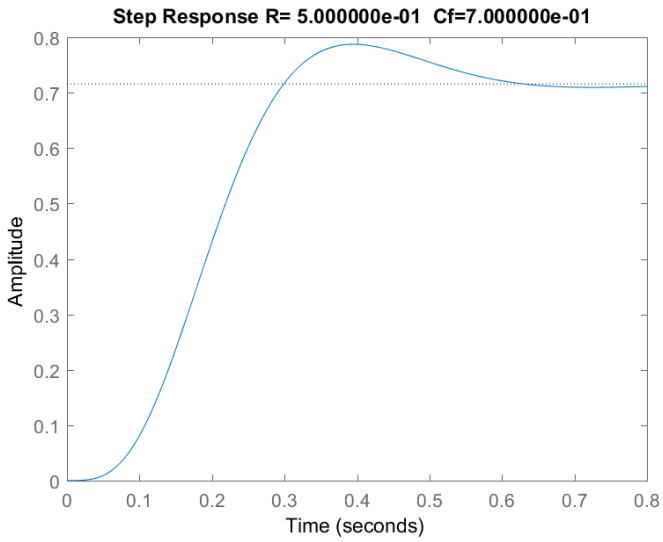

Figure 66: Acceleration & PPF for Alpha 0.5 and ζf=0.7

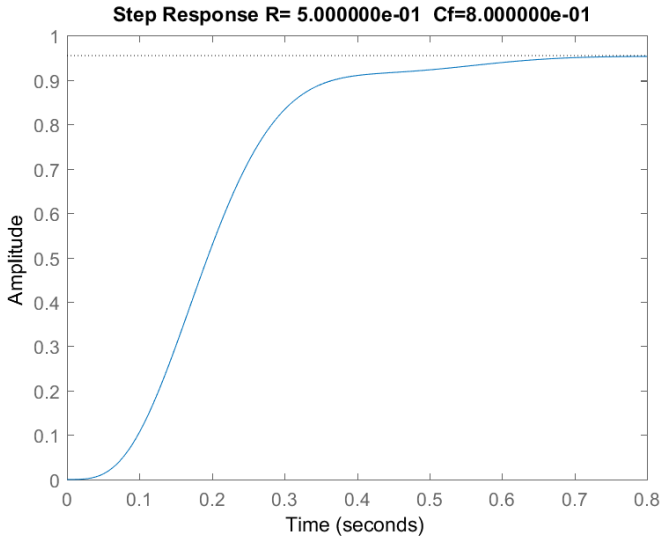

Figure 67: Acceleration & PPF for Alpha 0.5 and ζf=0.8

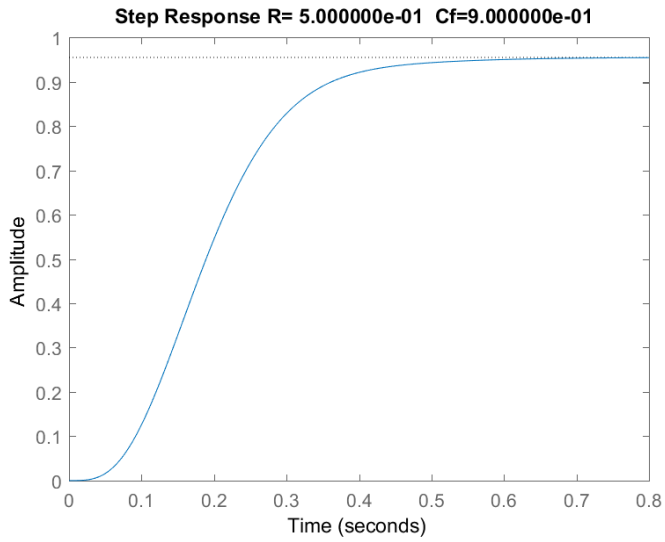

Figure 68: Acceleration & PPF for Alpha 0.5 and ζf=0.9

A.1. 2 Acceleration & PPF feedback with varying α ratio

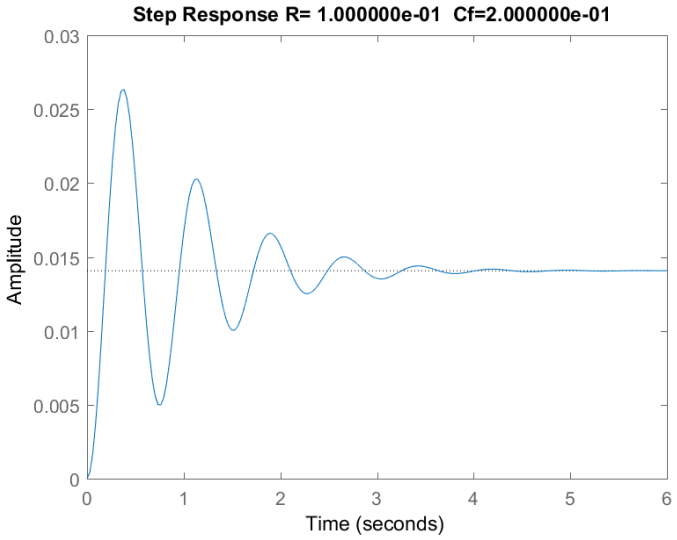

Figure 69: Acceleration & PPF for ζf=0.2 and α=0.1

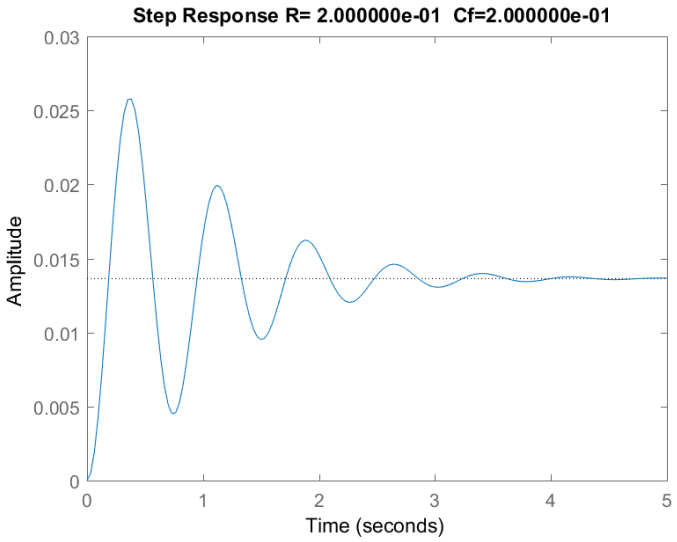

Figure 70: Acceleration & PPF for ζf=0.2 and α=0.2

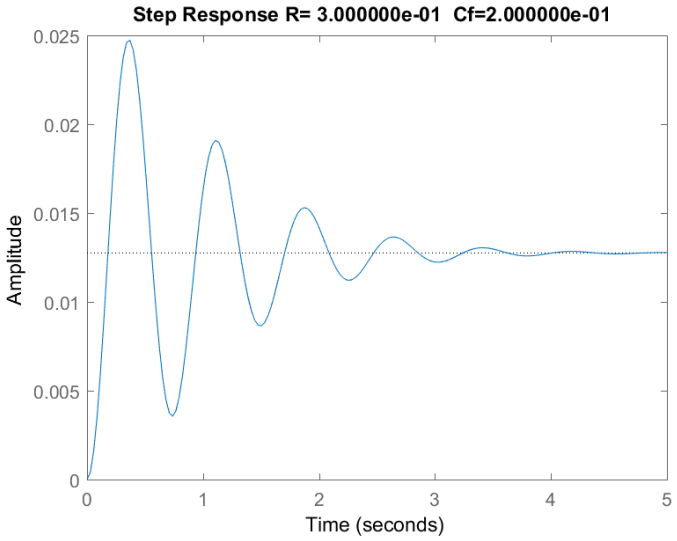

Figure 71: Acceleration & PPF for ζf=0.2 and α=0.3

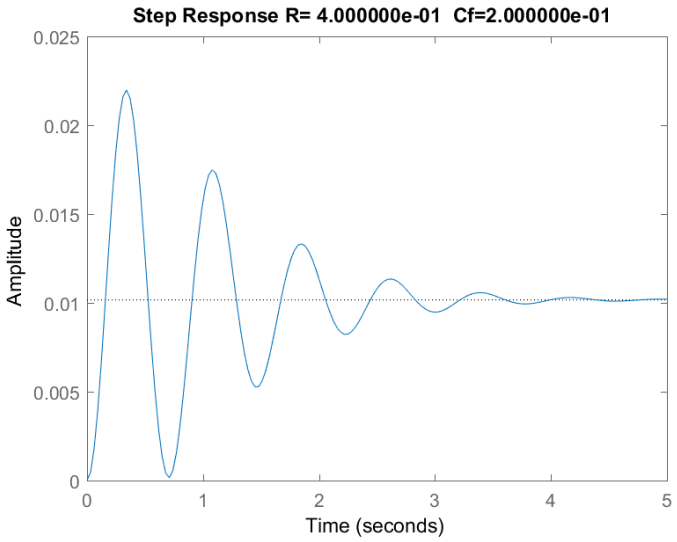

Figure 72: Acceleration & PPF for ζf=0.2 and α=0.4

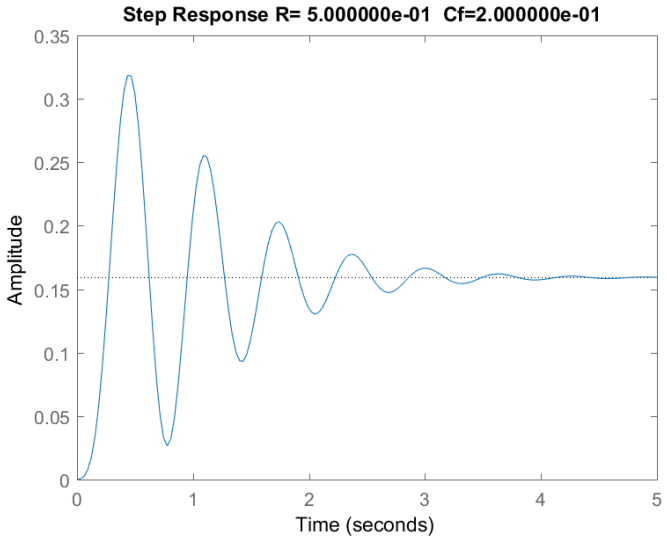

Figure 73: Acceleration & PPF for ζf=0.2 and α=0.5

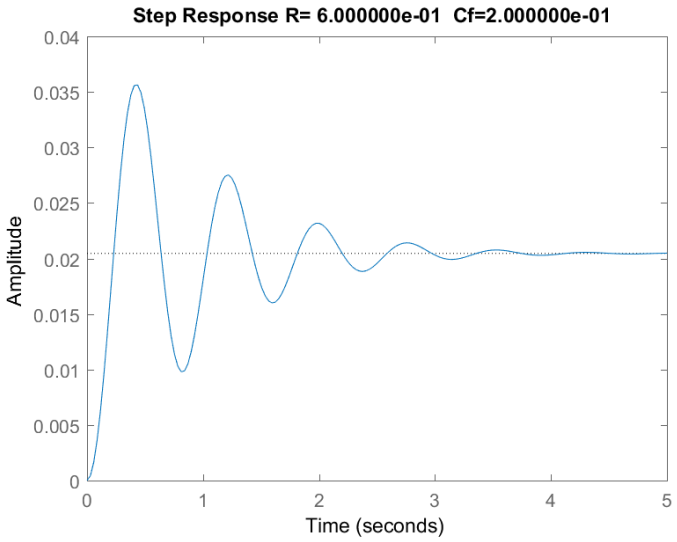

Figure 74: Acceleration & PPF for ζf=0.2 and α=0.6

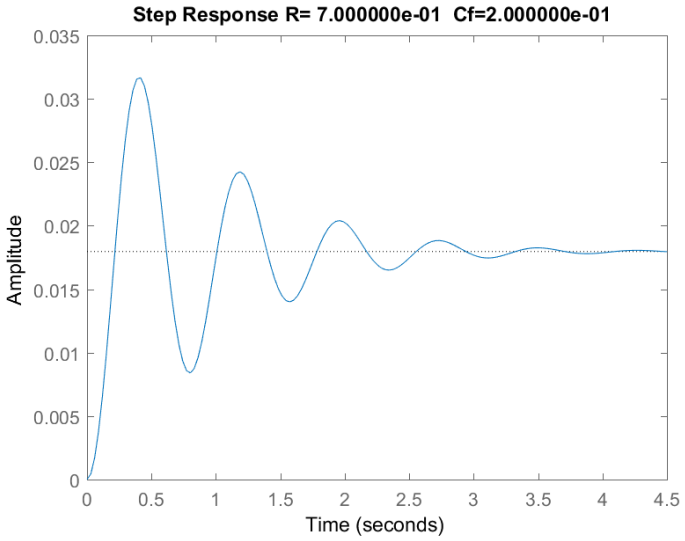

Figure 75: Acceleration & PPF for ζf=0.2 and α=0.7

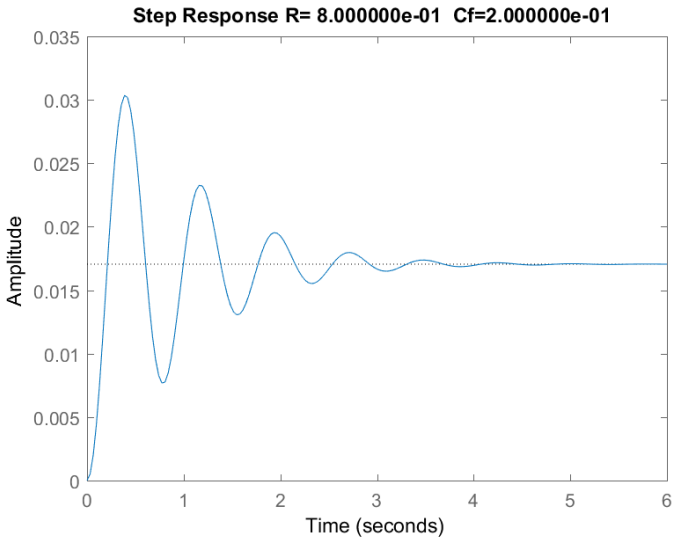

Figure 76: Acceleration & PPF for ζf=0.2 and α=0.8

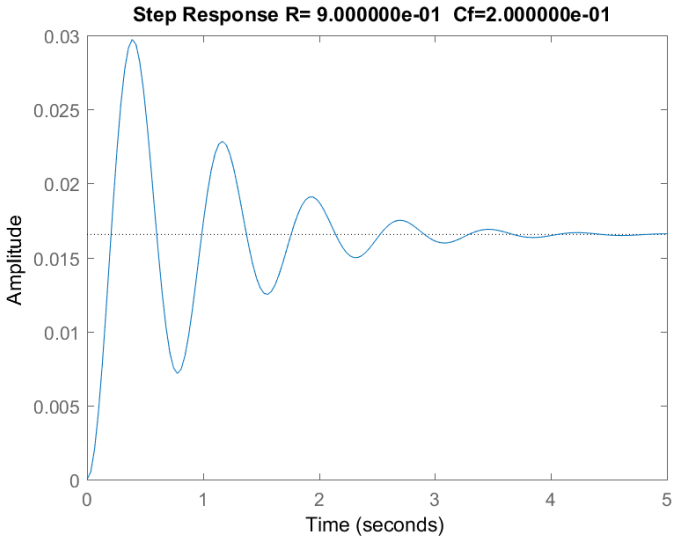

Figure 77: Acceleration & PPF for ζf=0.2 and α=0.9

A.2 Acceleration & PPF feedback with varying perturbations

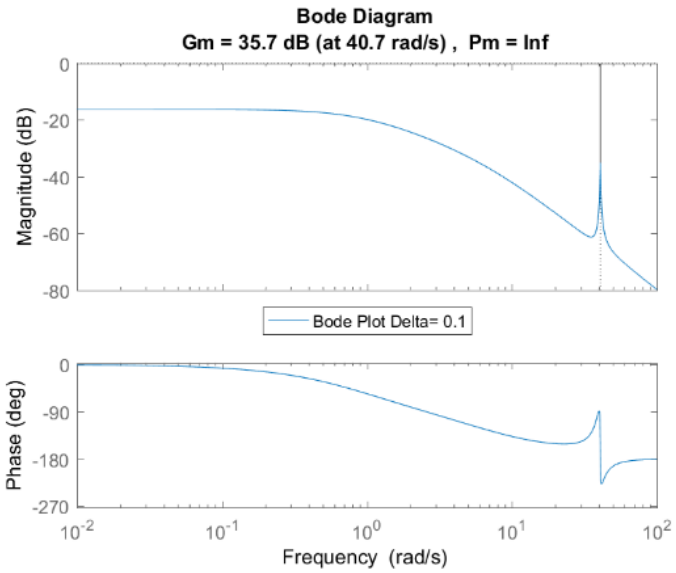

Figure 78: Acceleration & PPF Bode δ = 0.1

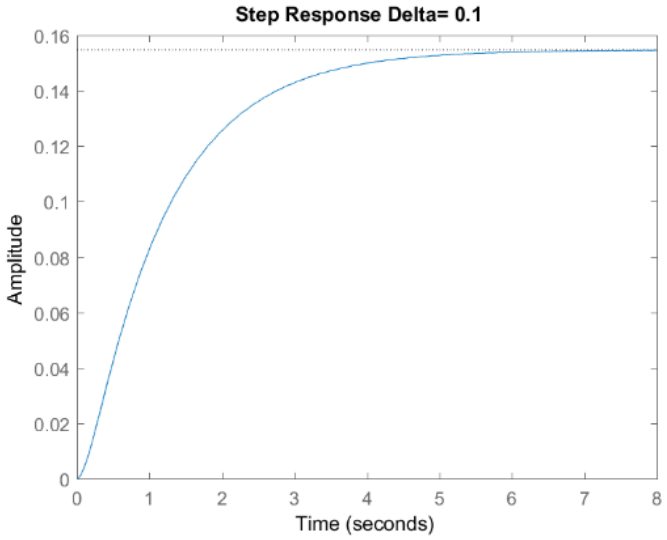

Figure 79: Acceleration & PPF Step δ = 0.1

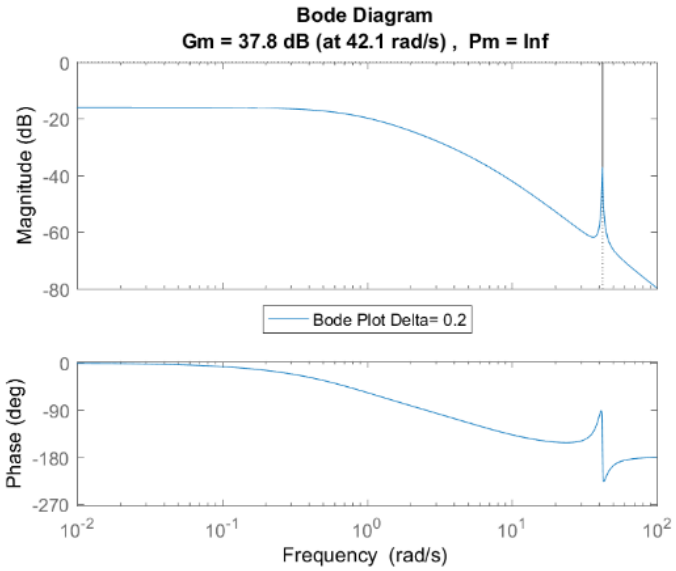

Figure 80: Acceleration & PPF Bode δ = 0.2

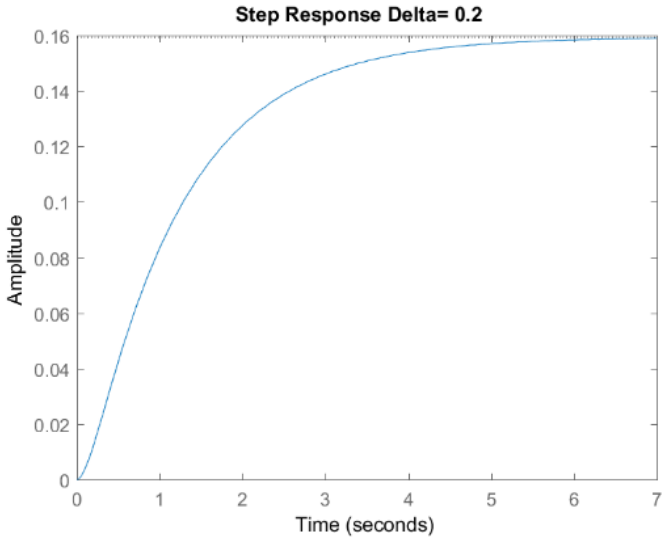

Figure 81: Acceleration & PPF Step δ = 0.2

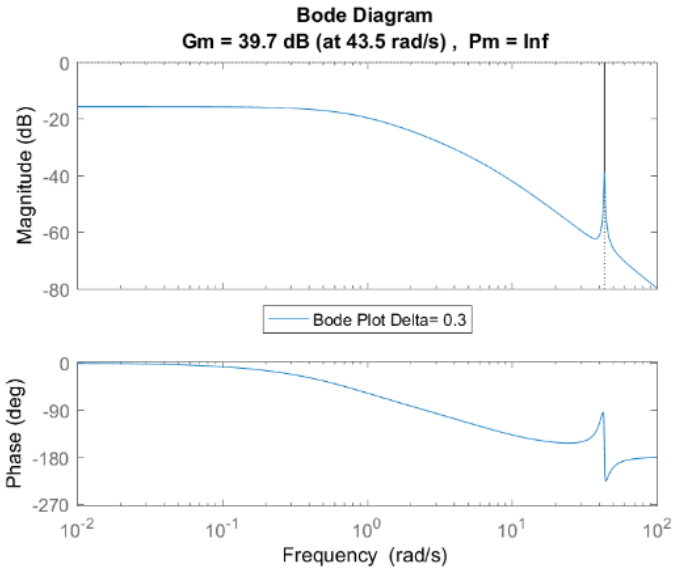

Figure 82: Acceleration & PPF Bode δ = 0.3

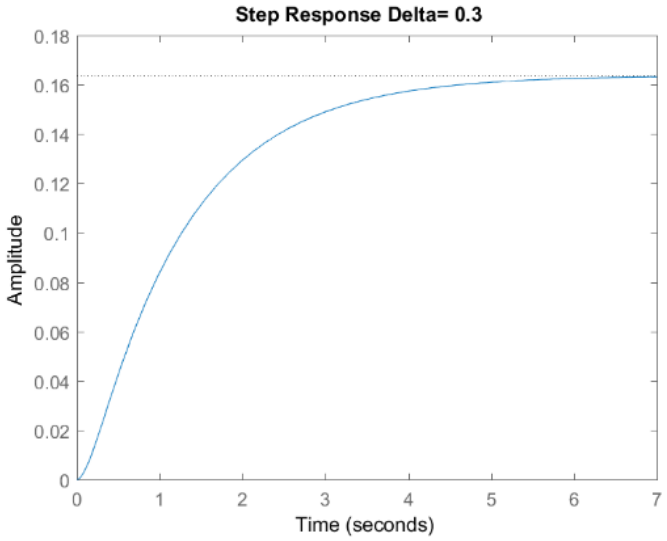

Figure 83: Acceleration & PPF Step δ = 0.3

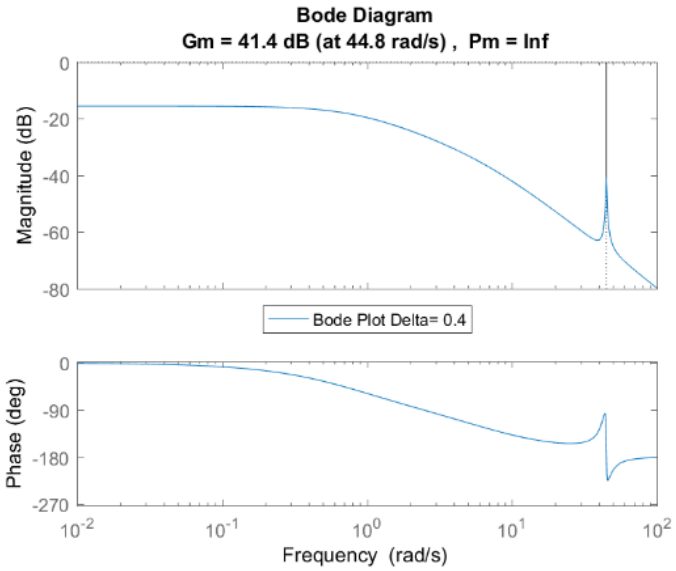

Figure 84: Acceleration & PPF Bode δ = 0.4

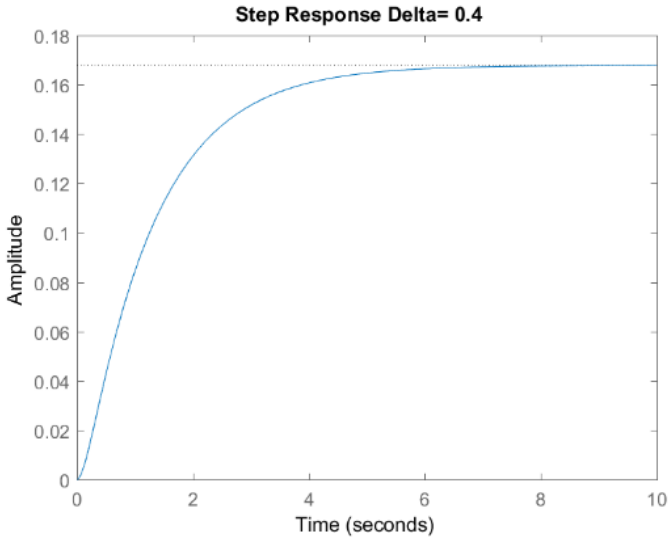

Figure 85: Acceleration & PPF Step δ = 0.4

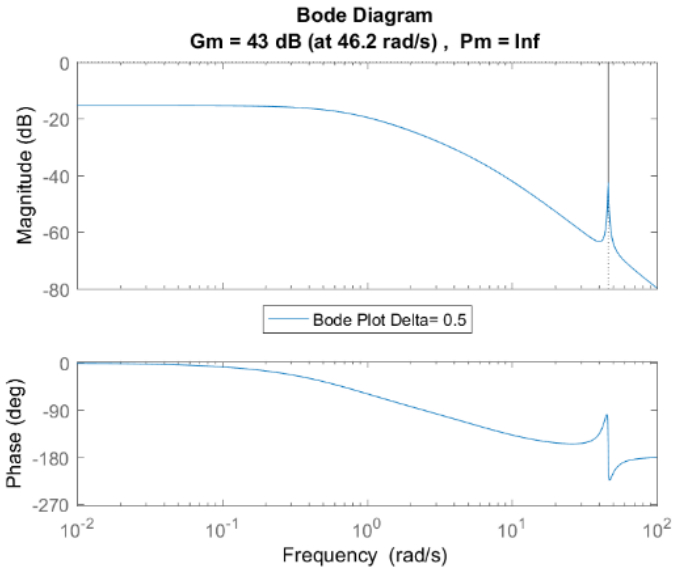

Figure 86: Acceleration & PPF Bode δ = 0.5

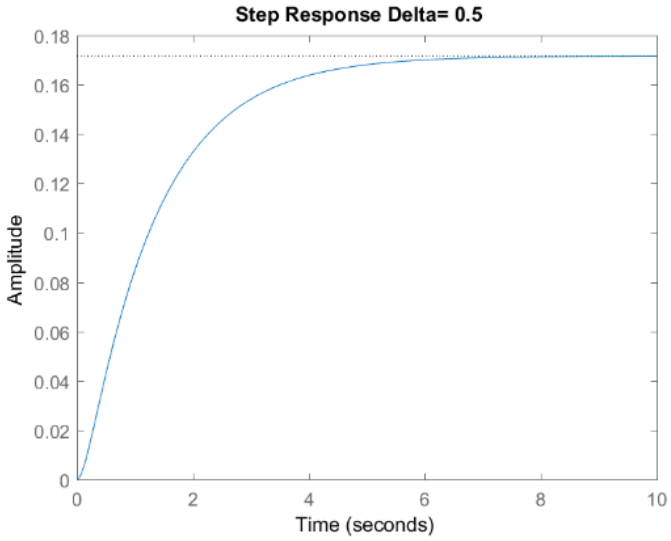

Figure 87: Acceleration & PPF Step δ = 0.5

A.2.1. Acceleration & velocity feedback with varying ratio α

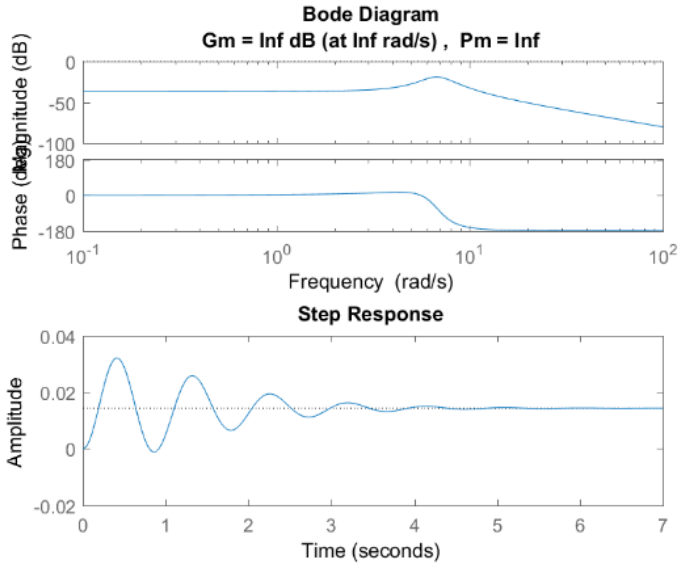

Figure 88: Acceleration and Velocity Feedback with ζf =0.2 ζs =0.01 and α = 0.1

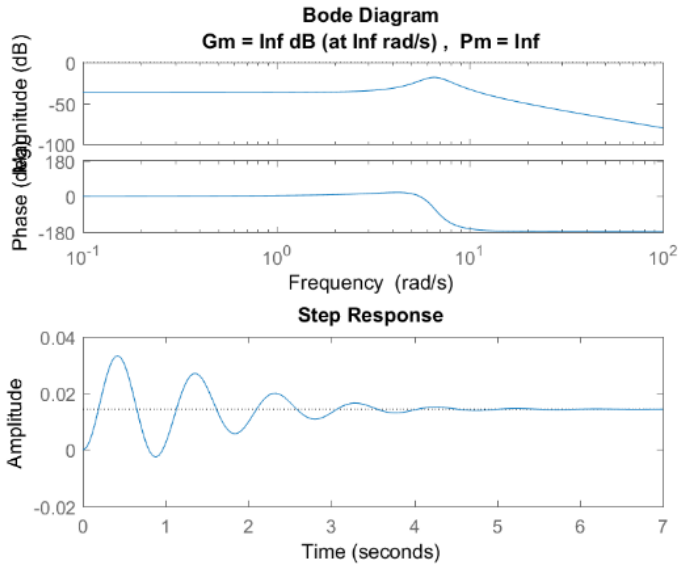

Figure 89: Acceleration and Velocity Feedback with ζf =0.2 ζs =0.01 and α = 0.2

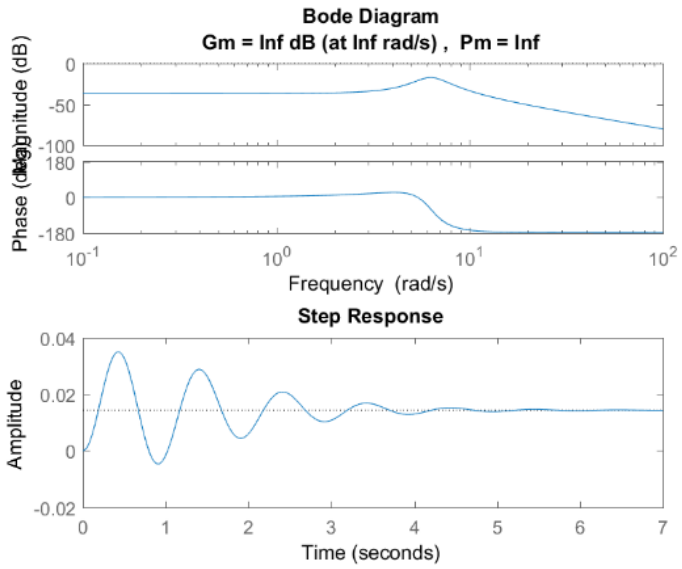

Figure 90: Acceleration and Velocity Feedback with ζf =0.2 ζs =0.01 and α = 0.3

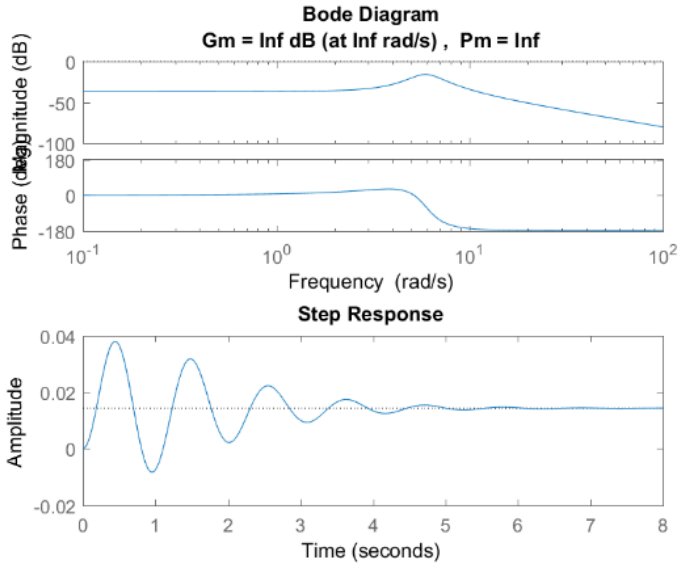

Figure 91: Acceleration and Velocity Feedback with ζf =0.2 ζs =0.01 and α = 0.4

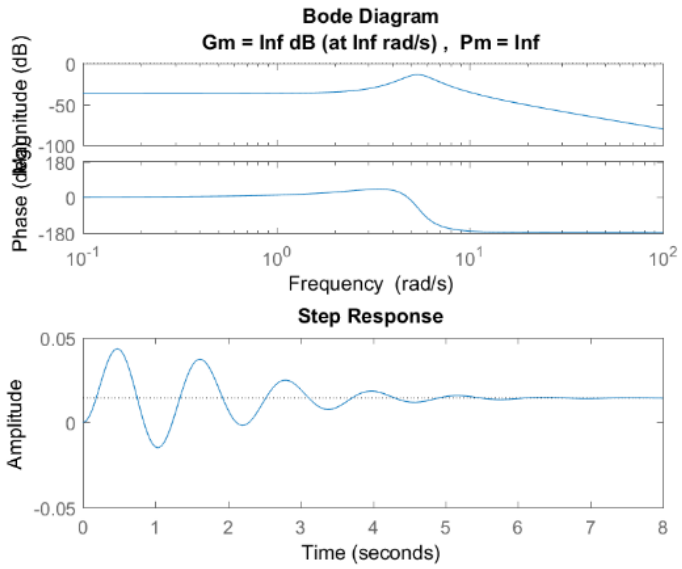

Figure 92: Acceleration and Velocity Feedback with ζf =0.2 ζs =0.01 and α = 0.5

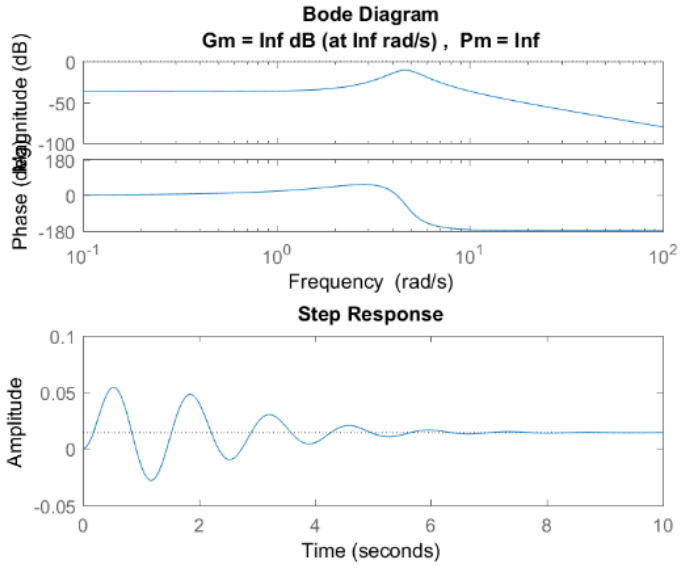

Figure 93: Acceleration and Velocity Feedback with ζf =0.2 ζs=0.01 and α = 0.6

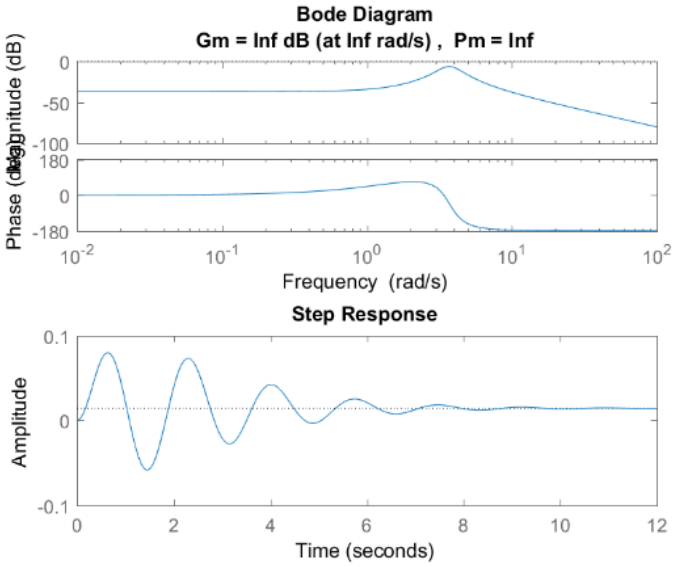

Figure 94: Acceleration and Velocity Feedback with ζf =0.2 ζs=0.01 and α = 0.7

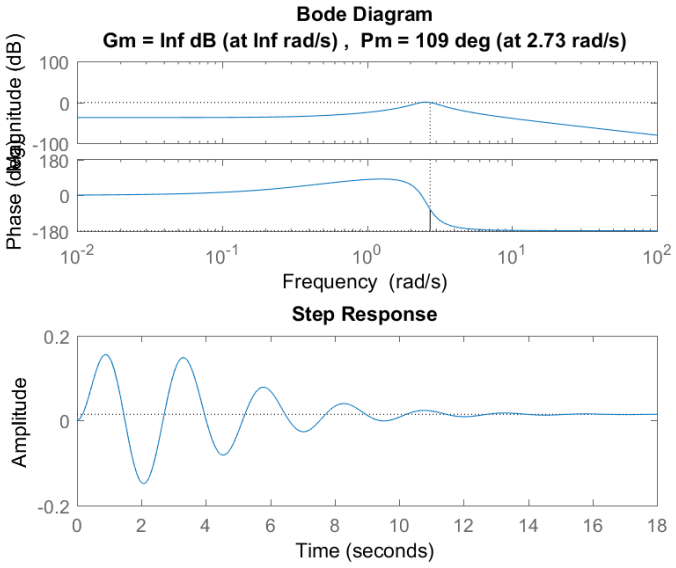

Figure 95: Acceleration and Velocity Feedback with ζf =0.2 ζs =0.01 and α = 0.8

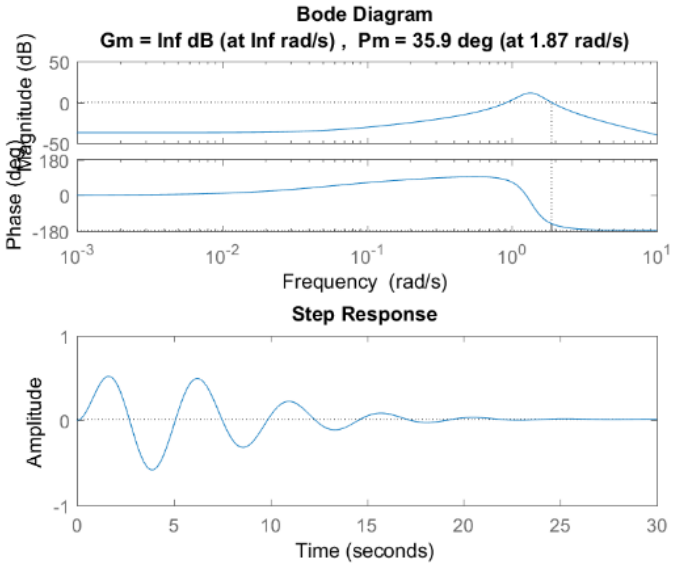

Figure 96: Acceleration and Velocity Feedback with ζf =0.2 ζs =0.01 and α = 0.9

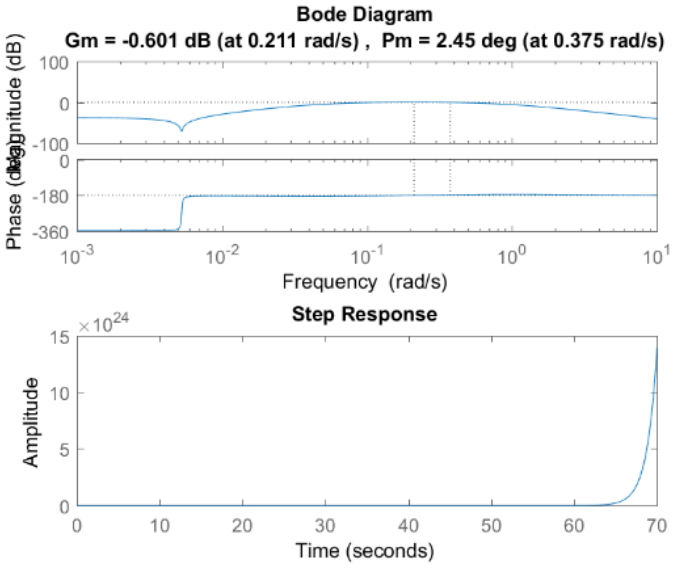

Figure 97: Acceleration and Velocity Feedback with ζf =0.2 ζs =0.01 and α = 1

A.3.1. Position & velocity plots

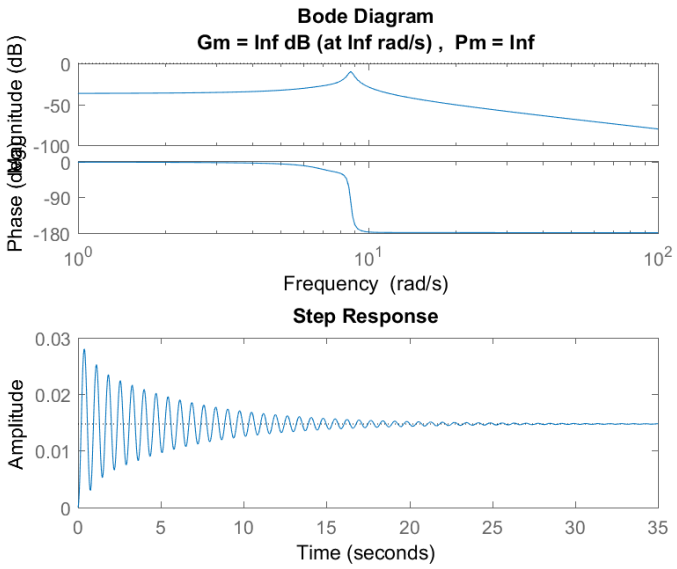

Figure 98: Position & Velocity Feedback Bode Plots and Step Response for ζf=0.1

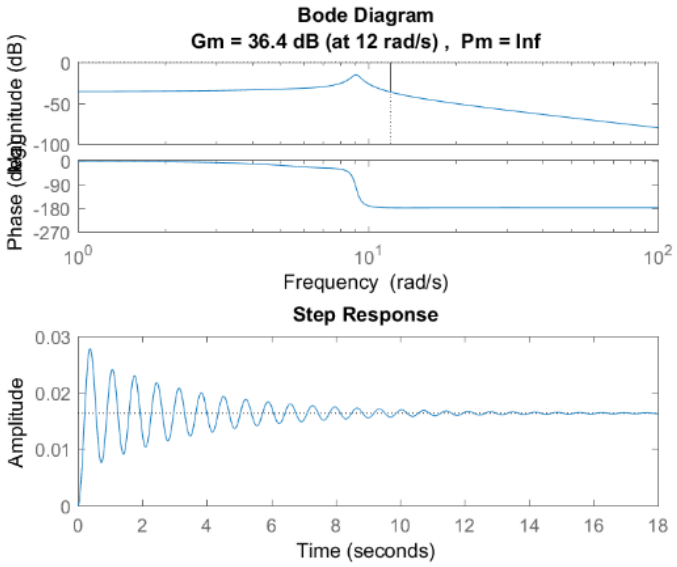

Figure 99: Position & Velocity Feedback Bode Plots and Step Response for ζf=0.2

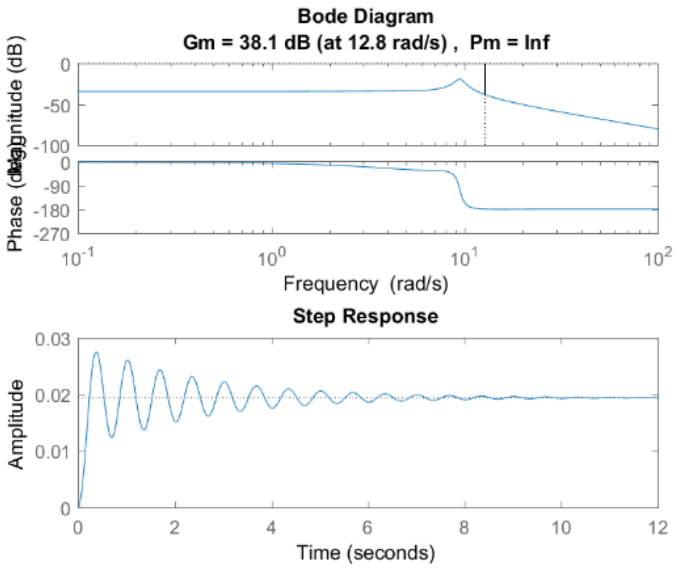

Figure 100: Position & Velocity Feedback Bode Plots and Step Response for ζf=0.3

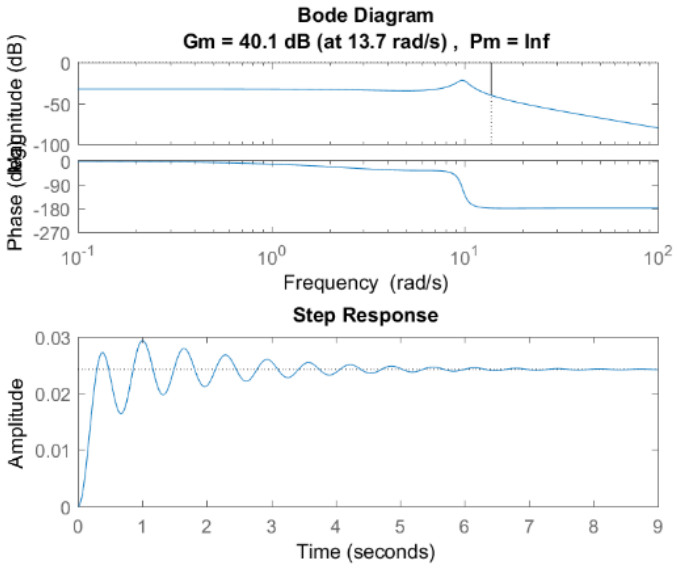

Figure 101: Position & Velocity Feedback Bode Plots and Step Response for ζf=0.4

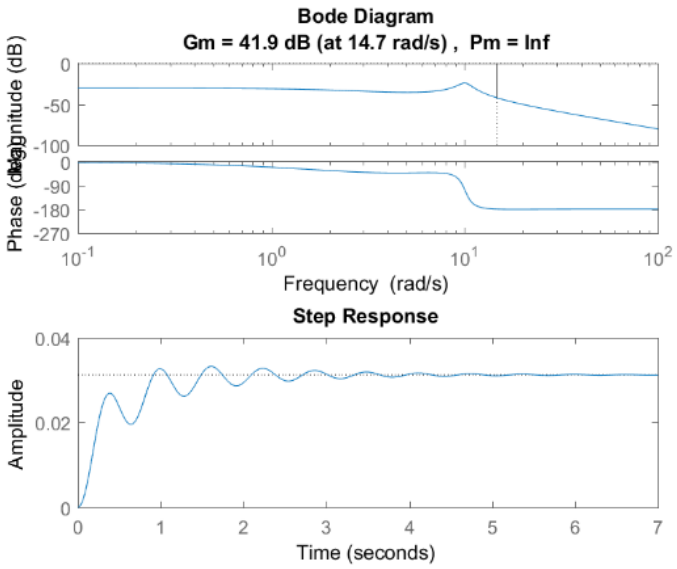

Figure 102: Position & Velocity Feedback Bode Plots and Step Response for ζf=0.5

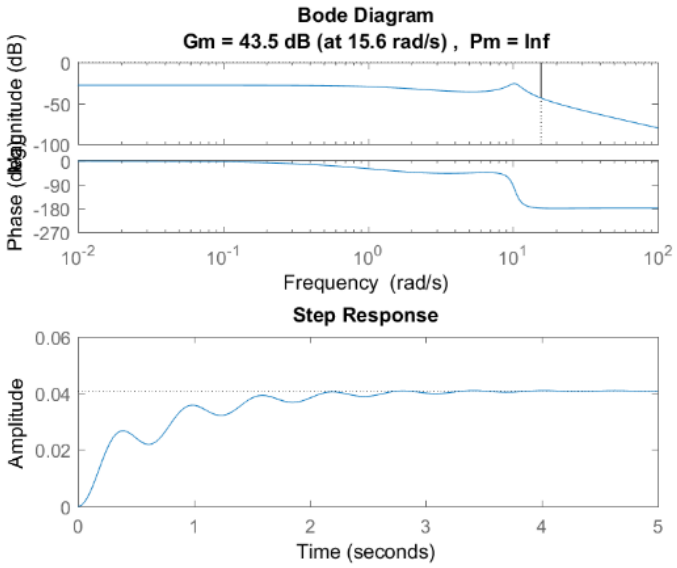

Figure 103: Position & Velocity Feedback Bode Plots and Step Response for ζf=0.6

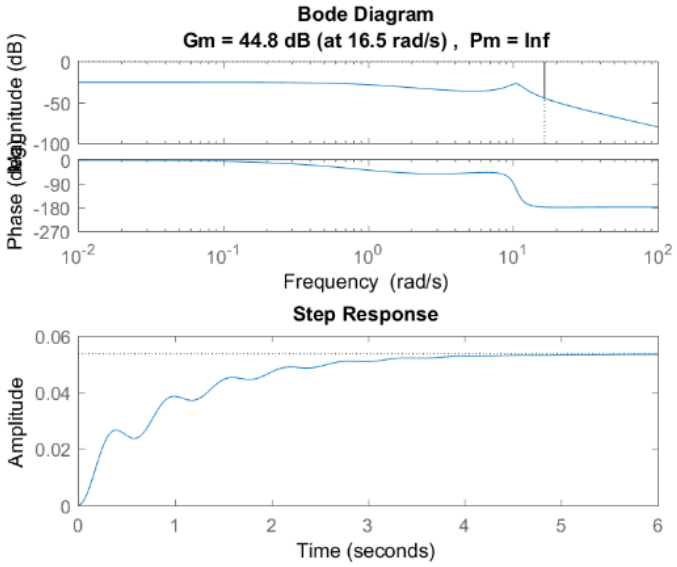

Figure 104: Position & Velocity Feedback Bode Plots and Step Response for ζf=0.7

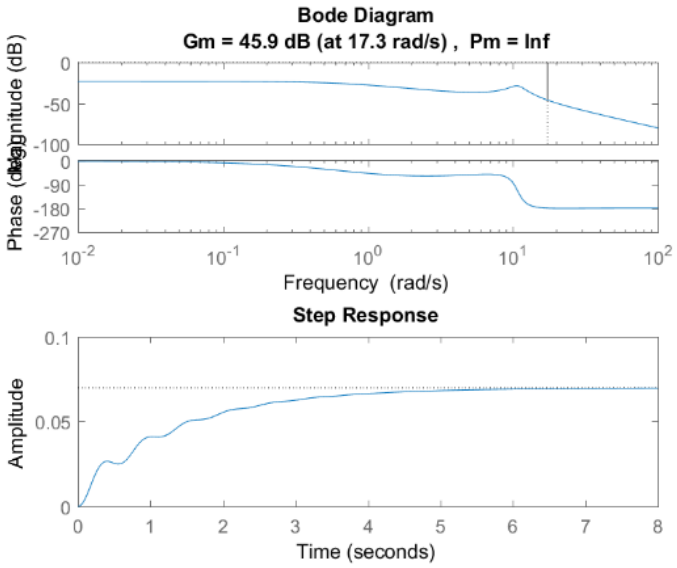

Figure 105: Position & Velocity Feedback Bode Plots and Step Response for ζf=0.8

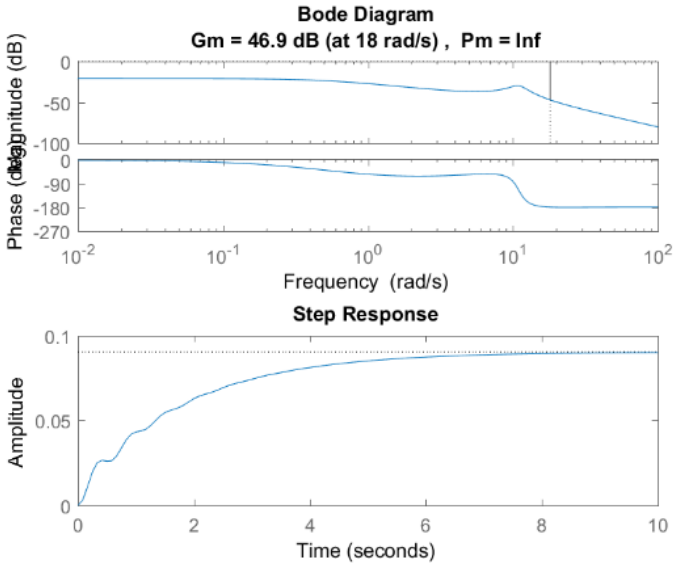

Figure 106: Position & Velocity Feedback Bode Plots and Step Response for ζf=0.9

REFERENCES

[1] M. P. Bayon de Noyer, P. J. Roberts and S. V. Hanagud, "Active Damping By Acceleration Feedback Control And Redistribution of Stresses in The Structure," *ASME,* 1999.

[2] E. Omidi, S. N. Mahmoodi and W. S. Shepard, "Vibration Reduction in Aerospace Structures via an optimized modified positive velocity feedback control," *Aerospace Science and Technology ,* vol. 45, pp. 408-415, 2015.

[3] C. J. Swigert and R. L. Forward, "Electronic damping of orthogonal bending modes in a cylindrical mast-theory," *Journal of Spacecraft and Rockets,* vol. 18, no. 1, pp. 5-10, 1981.

[4] K. Knipe, "Structural Analysis and Active Vibration Control of Tetraform Space Frame For Use in Micro-Scale Machining," Ohio State University , 2007.

[5] L. Wang, "Positive Position Feedback Based Vibration Attenuation For A Flexible Aerospace Structure Using Multiple Piezoelectric Actuators," IEEE, 2003.

[6] D. S. Bernstein, "Feedback Control: An invisible thread in the history of technology," *IEEE Control Systems Magazine,* pp. 53-68, 2002.

[7] B. d. Noyer, "Tail Buffet Alleviation of High Performance Twin Tail Aircraft using Offset Piezoceramic Stack Actuators and Acceleration Feedback Control," Georgia Institute of Technology , 1999.

[8] P. J. Roberts, "An Experimental Study of Concurrent Methods For Adaptively Controlling Vertical Tail Buffet In High Performance Aircraft," Georgia Institute of Technology, 2007.

[9] S. Hanagud, M. W. Obal and A. J. Calise, "Optimal Vibration Control by the Use of Piezo Ceramic Sensors and Actuators," in *AIAA/ASME/ASCE/AHS Structural Dynamics and Materials Conference*, 1987.

[10] S. Hanagud and G. L. Nagesh Babu, "Smart Structures in the Control of Airframe Vibration," *Journal of The American Helicopter Society* , 1994.

[11] H. F. Olsen, "Electronic Control of Mechanical Noise, Vibration Reverberations," *Journal of Acoustical Society of America,* 1956.

[12] R. Alkhatib and M. F. Golnaraghi, "Active Structural Vibration Control: A Review," *The Shock and Vibration Digest*, vol. 35, no. 367, 2003.

[13] J. V. R. Prasad and S. V. Hanagud, "Vibration Control of a Smart Structure Using Fixed Order Ddynamic Compensation," *Journal of Intelligent Materials, Systems and Structures*, vol. 3, pp. 501-518, 1992.

[14] S. Khot, N. P. Telve, R. Tomar, S. Desai and S. Vittal, "Active vibration control of cantilever beam by using PID based output feedback controller," *Journal of Vibration and Control,* vol. 18, no. 3, pp. 366-372, 2011.

[15] Y. Aoki, P. Gardonio and S. J. Elliott, "Modelling of a piezoceramic patch actuator for velocity feedback control," *Journal of Smart Materials and Structures,* vol. 17, 2008.

[16] K. Zhang, G. Scorletti, M. Ichchou and F. Mieyeville, "Robust active vibration control of piezoelectric flexible structures using deterministic and probabilistic analysis," *Journal of Intelligent Material Systems and Structures* , vol. 25, no. 6, pp. 665-679, 2014.

[17] L. Iorga, H. Baruh and I. Ursu, "A Review of H infinity Robust Control of Piezoelectric Smart Structures," *Applied Mechanics,* vol. 61, 2008.

[18] S. Gosh, A. Sahu and P. Bhattacharya, "Observer-Bbased H2-Robust Controller for Active Vibration Control of a Laminated Composite Plates with an Optimally Placed IDE-PFC Actuator," *Journal of Aerospace Engineering,* Vols. ISSN 0893-1321, 2016.

[19] Z.-c. Qiu, J.-d. Han, X.-m. Zhang, Y.-c. Wang and Z.-w. Wu, "Active vibration control of a flexible beam using a non-collocated acceleration sensor and piezoelectric patch actuator," *Journal of Sound and Vibration,* vol. 326, pp. 438-455, 2009.

[20] P. Bhattacharya, H. Suhail and P. K. Sinha, "Finite element analysis and distributed control of laminated composite shells using LQR/IMSC approach," *Aerospace Science and Technology,* vol. 6, pp. 273-281, 2002.

[21] K. Ma and M. N. Ghasemi-Nejhad, "Adaptive Simultaneous Precision Positioning and Vibration Control of Intelligent Composite Structures," *Journal of Intelligent Material Systems and Structures,* vol. 16, pp. 163-175, 2005.

[22] T. Bailey and J. E. Hubbard Jr. , "Distributed Piezoelectric-Polymer Active Vibration Control of a Cantilever Beam," *Journal of Guidance,* vol. 8, no. 5, pp. 605-612, 1985.

[23] C. Y. Chee, L. Tong and G. P. Steven, "A review on teh Modelling of Piezoelectric Sensors and Actuators Incorporated in Intelligent Structures," *Journal of Intelligent Material Systems and Structures* , vol. 9, 1998.

[24] J. L. Fanson, "Positive Position Feedback Control for Large Space Structures," in *AIAA Dynamics Speacialist Conference,* Monterey, CA, 1987.

[25] E. Pereira and S. S. Aphale, "Stability of positive-position feedback controllers with low-frequency restrictions," *Journal of Sound and Vibration,* vol. 332, pp. 2900-2909, 2013.

[26] S. N. Mahmoodi, Mohammad Rastgaar Aagaah and Mehdi Ahmadian, "Active Vibration Control of Aerospace Structures Using a Modified Positive Position Feedback Method," in *American Control Conference*, St. Louis, 2009.

[27] S Nima Mahmoodi and Mehdi Ahmadian, "Modified acceleration feedback for active vibration control of aerospace structures," *Smart Materials and Structures,* vol. 19, 2010.

[28] A. Ezratty, "Vibration control, Design of the parameters based on the crossover point," Georgia Institute of Technology, Atlanta, 2013.

[29] S. D. Gennaro, "Output Stabilization of Flexible Spacecraft With Active Vibration Suppression," Universita di L'Aquila , 2003.

[30] M. H. E. H. M. E.-S. S. A. El-Serafi, "Comparison Between Passive and Active Control of a Non-Linear Dynamical System," *Japan J. Indust. Appl. Math.*, vol. 23, pp. 139-161, 2006.

[31] Z. Wu, "Multi-mode Active Vibration Control Using H8 Optimization MIMO Positive Position Feedback Based Genetic Algorithm," Flinders University , Adelaide, 2014.

[32] Michael I Friswell and Daniel J Inman, "The relationship between positive position feedback and output feedback controllers," *Smart Material Structures,* vol. 8, pp. 285-291, 1999.

[33] J. Shan, H.-T. Liu and D. Sun, "Slewing and vibration control of a single-link flexible manipulator by positive position feedback (PPF)," *Mechatronics,* vol. 15, pp. 487-503, 2005.

[34] M. O. Tokhi and M. A. Hossain, "Self-tuning active vibration control in flexible beam structures," *Journal of Systems and Control Engineering* , vol. 208, pp. 263-278, 1994.

[35] G. Ma and Q. Hu, "Spacecraft Vibration Suppression Using Variable Structure Output Feedback Control and Smart Materials," *Journal of Vibration and Acoustics,* vol. 128, pp. 221-230, 2006.

[36] R. R. Orszulik and J. Shan, "Active vibration control using genetic algorithm-based system identification and positive position feedback," *Journal of Smart Materials and Structures,* vol. 21, 2012.

[37] C. J. Goh and T. K. Caughey, "Analysis and Control of Quasi Distributed Parameter Systems," California Institute of Technology , Pasadena, California, 1983.

[38] W. K. Gawronski, Dynamics and Control of Structures, New York: Springer, 1998.

[39] W Shields, J Ro and A Baz, "control of sound radiation from a plate into an acoustic cavity using active piezoelectric-damping composites," *Smart Materials and Structures*, vol. 7, 1998.

[40] R. G. Loewy, "Recent developments in smart structures with aeronautical applications," *Smart Materials and Structures*, vol. 6, 1997.

[41] Y. A. Wang and D. J. Inman, "Comparison of Control Laws for Vibration Supression Based on Energy Consumption," *Journal of Intelligent Material Systems and Sstructures,* vol. 22, pp. 795-810, 2011.

[42] Maxime P. Bayon de Noyer and Sathya V. Hanagud, "A comparison of H2 Optimized design and cross-over point design for acceleration feedback control," *American Institute of Aeronautics and Astronautics*, 1998.